CODEN:LUTEDX/(TEIE-5306)/1-108(2013)

Industrial Electrical Engineering and Automation

Model Calibration of a Vertical Wind Power Plant using Dymola/Modelica

Stefan Andersson
Jonatan Strömner

Division of Industrial Electrical Engineering and Automation
Faculty of Engineering, Lund University

Model Calibration of a Vertical Wind Power Plant using Dymola/Modelica

Stefan Andersson & Jonatan Strömner

January 30, 2013

Abstract

Wind energy has been used by mankind since ancient times and the last decades have seen large technological advancements in the field of wind turbines. One technology, although not very common, for harnessing the energy in the wind is the vertical axis wind turbine (VAWT). These types of turbines have not been as successful as the horizantal axes wind turbines (HAWTs) regarding efficiency and commercialization. There are however indications that the VAWTs are favorable for some applications.

For researchers and developers, identifying and assessing losses occurring in a wind turbine or in any electricity generating device is important for finding potential improvements. The losses can be dependent on a range of parameters. A method has been developed in this project, focusing on vertical axis wind turbines, with the purpose to assess and quantify these parameters using Dymola. Models of the different components of a wind turbine have been developed to be used for calibration, that is, assessing the parameters. The calibration has been conducted by using the calibrate function in the Design Library in Dymola.

Some of the models are based on previous master thesis work and these were translated from the SPOT library to the Electric Power Library. The data collected for the calibration were mainly synthetic data taken from a Dymola model of the entire wind turbine system, an approach using real measurement data from an AC/DC/AC-converter was also attempted. The synthetic data were used with and without added noise to check the sensitivity of the calibration process. The real measurement data were filtered to be suitable for calibration.

The methodology for calibration of the parameters is shown to be functional for the rotor and generator component. The calibration of the converter is troublesome since only one parameter is affecting the outputs. Calibration using synthetic data is performed, however no calibration using real data were finalized.

Acknowledgements

During the time we have been working on this project we have received help, encouragement and constructive inputs from a number of kind people. Many thanks to all friendly people on Modelon AB who have welcomed us to their working place and for all advice they have given us during the course of this project. The project has partly been based on another master thesis written by Joel Petersson and Pär Isaksson, we are very thankful for the inputs this has given us. Hans-Jürg Wiesmann, the author of the Electric Power Library used in Dymola, has given us some vital support during times of trouble. For this, we are very grateful. Thanks to Måns Andersson and Aleksandar Stojkovic who offered us some of their valuable time to help us with data measurements in the laboratory.

Our supervisors deserves special thanks. They are Jens Pålsson and Johan Ylikiiskilä at Modelon AB and Jörgen Svensson at the department of Industrial Engineering and Automation (IEA), Faculty of Engineering, Lund University. They have continuously given us support and encouragement during the whole period, for this, they deserve special thanks.

Contents

Nomenclature

α	Power law exponent
β	Pitch angle
$\dot{x}(t)$	Deravative of variable in model, chapter 4
ϵ	Error function
ϵ_F	Filtered error function
λ	Tip speed ratio
ω_m	Mechanical angular speed
ψ	Magnetic flux
ρ	Air density
σ_E	Eddy current loss coefficient
σ_H	hysteresis loss coefficient
τ_0	Shear stress at surface
θ	Parameter vector for model, chapter 4
θ_e	Electrical angle
A	Area
AC	Alternating Current
B	magnetic flux density
B_0	Nominal magnetic flyx density
C_1-C_6	C_p equation coefficient
C_d	Drag coefficent
C_l	Lift coefficent
C_t	Resulting force coefficient in tangential axis
D_M	Set of values that defines θ in a specific model
D_S	Duty cycle
DC	Direct Current
E	Internal voltage
E_0	Nominal internal voltage
E_S	Energy loss over swiching period
f	Frequency
F_{switch}	Switching frequency converter
f_{sw}	Switching frequency
HSW_{nom}	Switching loss
i_C	Collector current
i_d	active current
i_q	reactive current
i_{di}	active current iron
i_{dm}	active current magnetization

i_{qi} reactive current iron
i_{qm} reactive current magnetization
K_b Bearing loss parameter
K_w Windage loss parameter
k_w Winding coefficient
L Lift force
l Length
M Model structure
M^* Model structure with restrictions on parameters
P_b Ball bearing loss
P_c Copper loss in generator
P_n Rated power output
P_s Stray load loss
P_w Windage loss
$P_{D,cond}$ Conduction power loss
$P_{D,rr}$ Reverse recovery power loss
$PMSM$ Permanent Magnet Synchronous Machine
Q_f Charge
Q_{rr} Reverse recovery loss
r Radius
r Resistance
r_a Stator winding resistance
R_D Diode resistance
R_s Resistance
r_s self reactance
snr Signal to noise ratio
T_{sw} Switching period
U Wind speed
u^* Friction velocity
u_{CE} Satureation voltage
u_{GE} Gate-emitter voltage
V_a Voltage in phase a
V_b Voltage in phase b
V_c Voltage in phase c
V_N Scalar function used to minimize error
V_n Forward threshold-voltage
V_{D0} Diode threshold voltage
V_{DC} DC link voltage
V_{norm} Three phase voltage norm
V_{S0} Forward voltage at no current
w Number of turns in the coil
$x(t)$ Internal variables in a model, chapter 4
$y(t)$ Output from model, chapter 4
z Height above ground
Z^N Data set including inputs and outputs
C Chord length

EPL Electric Power Library

Chapter 1

Introduction

1.1 Background

Wind power is growing increasingly important for the world´s electricity generation. This is mainly due to that environmental policies and technological developments have made wind power more economically feasible. Additionally, the price volatility and the awareness of the finiteness of fossil fuels have boosted the rapid growth. In some countries in Europe, wind power will contribute to the replacement of electricity generated from nuclear and fossil fuels and also to meet an increase in electricity demand. The world´s demand for electricity is projected to increase from 17 200 TWh in 2009 to over 31 700 TWh in 2035 and 44 % of this increase is believed to come from renewable sources, dominated by wind and hydro [1].

Wind turbines can be divided into two categories, vertical axes wind turbines (VAWTs) and horizontal axes wind turbines (HAWTs). Up until now the large expansion of constructed wind turbines has consisted of HAWTs, VAWTs have so far not been able to compete. However, VAWTs have a potential market, especially for smaller sized turbines. Some advantages of vertical systems are independence of wind direction, lower noise and they handle strong and gusty winds better than horizontal systems. Additionally, the design of VAWTs is more simple and robust which reduces investment and maintenance costs[2][3].

Modeling of various physical systems is one of the major activities concerning engineering science. Examples of physical models are seen everywhere and have greatly shifting complexity. Ranging from assuming that the weather on one day will be similar to the weather on the next day, to advanced modeling of human cells or the climate system of the earth. All models have in common that they try to predict a systems reaction to specific conditions.

Modeling, simulations and model calibration are important to optimize and improve different products. Modeling and simulating complex systems are a cost effective way to get experiences and insights in how a system performs and reacts, this is especially important in product development. Simulations can be used as a complement to the construction of prototypes. Model calibration is the process where parameters are calculated (parameter estimation) so that

the simulation result corresponds to measured data from a real device. A model describing a physical system usually contains parameters that are not explicitly known and calibration of the model makes it possible to determine the magnitude of these parameters[4].

1.2 Motivation

The aim of this project is to develop test bench models of a vertical axis wind turbine and its mechanical and electrical components, adapt them for calibration and then perform the calibrations of these test bench models. The modeling and calibration is done using Dymola, which is a tool based on the Modelica language, see section 1.3.1 and 1.3.2. Dymola contains, among others, model libraries which are used to build and calibrate models of the wind turbine and its components. Two important Modelica Libraries used are the Electric Power Library (former SPOT Library) and the Design Library (calibration package). Models of the components of a wind turbine will be calibrated and verified to real data from a prototype 2 kW VAWT that is mounted on the "M-building" at Lund University, Faculty of Engineering. The components that will be calibrated are the rotor, the generator and the converter.

The models considered all contain parameters that are unknown for the modeled system but they can be estimated from measurement data. Even if the parameters cannot be measured per se, the measurement data shows the behavior of the system which allows parameter estimation[5].

Prior to the start of this project, a master thesis project developed models and control of a wind turbine based on the Modelica SPOT Library[2]. Parts of the work presented in this thesis are based on this work.

1.2.1 Project Goals and Limitations

The project is limited to the objectives listed below.

- Existing wind turbine models using the SPOT library will be translated into the Electric Power Library.
- Develop test benches for the entire turbine as well as of the rotor, generator and converter.
- Develop a method of how to calibrate parameters in wind turbine components.
- Calibrate the models of the wind turbine and the rotor, generator and converter to synthetic data (optionally do the same for the whole wind power system).
- Calibrate the component models to real measurement data.
- Conduct a performance test of the 2kW wind turbine.

1.3 Modeling Language and Tools

1.3.1 Modelica

Modelica is a free, object-oriented and equation based language introduced in 1996 and is the most wide-spread modeling language for component-based modeling[5]. It was developed for modeling of complex and dynamic physical systems and is increasingly used by the industry, especially in the automotive, aerospace and energy sectors. Modelica is developed by the non-profit Modelica Association and can be used with several simulations tools, one of them is Dymola.

The modelica language contains constructs for defining equations and components. Components can be connected to create larger systems and the language also gives the possibility for a graphical representation of components. Modelica needs an implementation of the language to be able to use for modeling and simulations. Dymola is a Modelica interpreter.

1.3.2 Dymola

Dymola, Dynamic Modeling Laboratory, is a commercial Modelica based tool designed for dynamic modeling and simulation of complex systems. It can be applied within various engineering fields, such as mechanical, thermodynamic, electric and control systems and combinations of the fields. The tool is developed by Dassault Systèmes and can be used with a number of different model libraries. It is also possible to create your own equation based models. Dymola has a graphical interface for modeling where models can be built and modified[6][2].

1.3.3 JModelica.org

JModelica.org, developed and maintained by Modelon AB, is an open-source platform which uses the Modelica language and is used for simulation and optimization of complex dynamic systems.

1.3.4 Matlab

MATLAB (matrix laboratory), developed by MathWorks, is a high-level programming language and numerical computing environment for a wide range of application fields. Allows for example analysis of data, graphical presentations and development of algorithms.

1.4 Outline of the report

The first part of the report contains some background information about wind power in general. Details concerning VAWTs, HAWTs and components commonly used in wind turbines are presented in chapter 2. The prototype tur-

bine at LTH is described in section 3, it also contains information about the translation to EPL (from SPOT). Some important differences between the two libraries are also treated. Theory concerning modeling and model calibration is presented in section 4. The developed method, test benches used for calibration as well as results are presented in section 5. A final discussion of the project can be found in section 6.

Chapter 2

Wind Power Theory

Wind energy has for a long time been used by humans for energy, in the past it was used for e.g. water pumping, grinding grain and sawing wood. Wind lost its importance with the rising popularity of coal during the industrial revolution. Coal was a superior energy source with its transportability and its quality that it could be used whenever needed, unlike the unpredictable wind. Wind energy increased in importance again during the 1990´s, when more efficient and megawatt sized wind turbines were introduced to the market.

A major difference between the windmills of the past and the wind turbines of today is that the mechanical power from the wind in modern turbines is converted into electrical energy. By connecting the turbines to the electrical grid the problem with the transportability is overcome. However, since the electric energy cannot be stored in an efficient manner and the rate of production is dependent of the wind currently blowing, the problem of supply and demand is still present[7]. In order to make better use of wind energy and other unreliable renewable sources, much work is currently being done in the area of smart grids. The basic idea is to alter the energy demand in order to match the supply and in that way make better use of the energy available.

In the following chapter the basics about wind characteristics, some technical aspects concerning wind power in general and the difference between VAWT and HAWT specifically will be presented. In addition, details concerning the most important components of a VAWT will be presented.

2.1 Wind Characteristics

All the wind resources of the earth originate from the sun and its uneven heating of the earth by solar radiation. This creates convective cells in the lower layers of the atmosphere, these circulations are greatly influenced by the seasonal variations of incoming solar radiation as well as the rotation of the earth. The uneven distribution of solar radiation creates variations in the atmospheric pressure field, causing air to blow from high to low pressure.

The mass flow rate in the wind can be expressed with the mass conservation equation 2.1.

$$\frac{dm}{dt} = \rho \cdot A \cdot U \tag{2.1}$$

Where $\frac{dm}{dt}$ is the mass flow of air flowing through an area A with the velocity U and density ρ.

The kinetic power of the flow can be expressed by:

$$P = \frac{1}{2} \cdot \frac{dm}{dt} \cdot U^2 = \frac{1}{2} \cdot \rho \cdot A \cdot U^3 \tag{2.2}$$

The mean wind speed increases and turbulence decreases with height above ground, thus giving benefits for wind turbines with high towers. There are two dominating mathematical models that are used to predict the vertical wind profile over areas with flat terrain. The first model is the logarithmic profile, also known as the log law, derived from boundary layer flow in fluid mechanics and atmospheric research. The second model, used by many wind energy researches, is the power law profile. Both these models have uncertainties due to the complexity of turbulence[7].

Logarithmic wind profile

$$U(z) = \frac{u^*}{k} \cdot ln(\frac{z}{z_0}) \tag{2.3}$$

$$u^* = \sqrt{\frac{\tau_0}{\rho}} \tag{2.4}$$

Where U is the horizontal component of velocity, u^* is defined as the friction velocity, τ_0 is the shear stress value at the surface, ρ is the air density, z is the height and z_0 is the surface roughness length which characterizes the roughness of the terrain. k is the von Karman´s constant, often assumed to equal 0.4. The log law can conveniently be used to extrapolate wind speed from a reference height to other heights[7].

Power Law Profile

$$\frac{U(z)}{U(z_r)} = (\frac{z}{z_r})^{\alpha} \tag{2.5}$$

$U(z)$ is the wind speed at height z, $U(z_r)$ is the reference wind speed at height z_r and α is the power law exponent, which depends on parameters such as elevation, time of day, season, terrain characteristics, wind speed and temperature[7].

2.2 Technology

Wind power turbines can be divided into two groups, vertical axis wind turbines (VAWT) and horizontal axis wind turbines (HAWT). Most of the components are similar and they serve the same purpose of converting the kinetic energy in the wind to the more useful electric energy. There are some other interesting techniques, e.g. turbines involving high altitude kites[8].

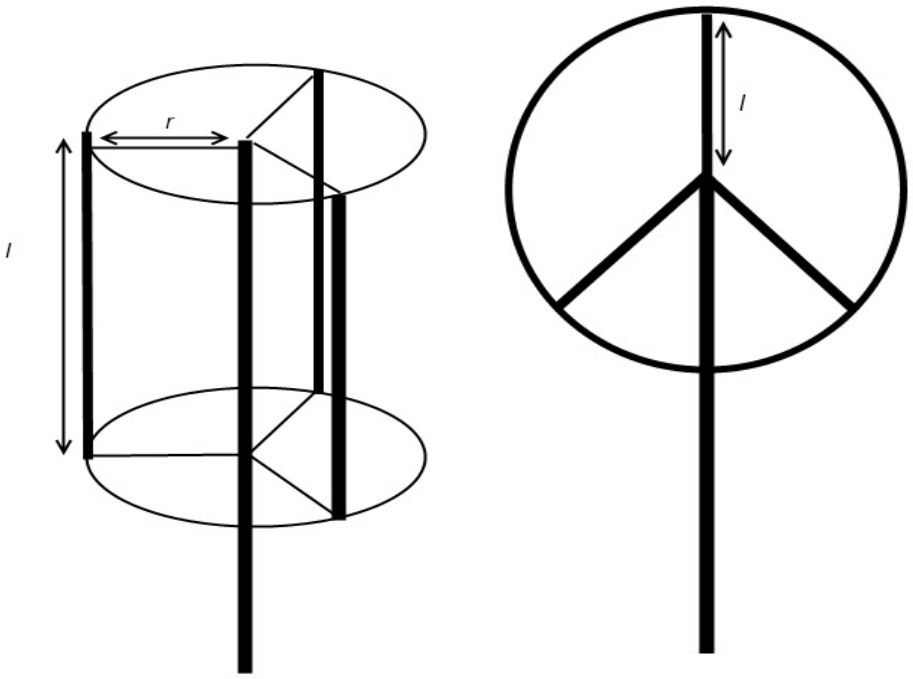

(a) Schematic picture of a VAWT **(b)** Schematic picture of a HAWT

Figure 2.1

The mechanical energy extracted by the rotors from the wind results in a decreased kinetic energy and thus a lower air flow velocity behind the wind turbine. This applies when the mass flow through the rotor is unchanged. The extracted power can be expressed as

$$P = \frac{1}{2} \cdot \dot{m}(v_1^2 - v_2^2) \tag{2.6}$$

where v_1 is the air flow velocity before passing through the rotor and v_2 is the air flow velocity after passing through the rotor. From equation 2.6, it appears as if maximum power extraction would occur when v_2 equals zero,

which means that the air flow would be brought to a complete stop at the rotor. If this would be true, the air flow through the converter would also be zero. Instead, the maximum extractable power occurs at a certain v_2/v_1 ratio[9]. This theoretical limit for power conversion from the wind is commonly refered to as the *Betz Limit* and states that the maximum power conversion is 59.26%[10]. The Betz limit derives from linear moment theory assuming an ideal turbine rotor and two-dimensional flow.

The swept area, A, for a VAWT and a HAWT respectively, are calculated as shown below

$$A_{VA} = 2 \cdot r \cdot l \tag{2.7}$$

$$A_{HA} = l^2 \cdot \pi \tag{2.8}$$

Where l is the length of the blades and r is the radius of the blades in the VAWT case, as illustrated in figures 2.1a and 2.1b.

The ratio between the mechanical power extracted by the turbine and the available power contained in the undisturbed air stream is known as the power coefficent, C_p[7].

$$C_p = \frac{\texttt{Rotor power}}{\texttt{Power in the wind}} = \frac{P_{rotor}}{\frac{1}{2} \cdot \rho \cdot A \cdot U^3} \tag{2.9}$$

C_p is often expressed as a function of the tip speed ratio (TSR), λ. The tip speed ratio is the tangential velocity of the rotor blades tip in relation to the undisturbed wind velocity. TSR can be expressed with equation 2.10

$$\lambda = \frac{\texttt{Blade tip speed}}{\texttt{Wind speed}} = \frac{\omega \cdot R}{U} \tag{2.10}$$

ω is the angular velocity of the rotor and R is the radius of the rotor. For low to medium wind speeds, the control system of the turbine aims to set an optimum λ to maximize power extraction. For wind speeds above the rated winds speed of the turbine, the tip speed ratio is decreased to maintain a constant power extraction.

Modern HAWTs can achieve power coefficents of almost 0.5 which far exceeds older wind wheels operated on aerodynamic drag. Older wind wheels could only reach power coefficients of 0.3. It has been seen that wind turbines using the aerodynamic lift principle are much more efficient than turbines using aerodynamic drag[9]. Lift driven rotors creates a difference in pressure between the two sides of the blades, similar to the wings of aircrafts, the resulting force drives the rotor (see figure 2.2. The drag driven rotors are simply pushed by the wind, similar to cup anemometers commonly used to measure wind speed.

The major disadvantage of a drag driven machine is that the rotor surface cannot move faster than the wind. This causes the relative velocity between the wind and the rotor to be small. This is not the case for lift machines,

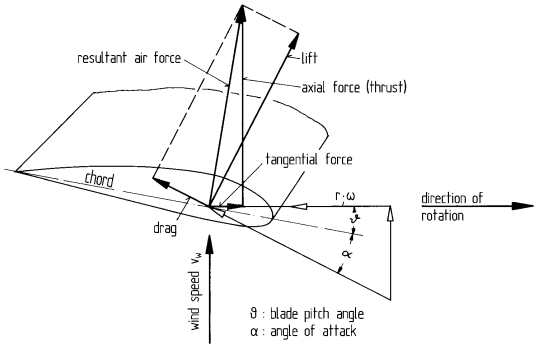

Figure 2.2: Airfoil cross-section of a blade element with the aerodynamic forces and flow velocities [10]

giving them an advantage since the forces developed are a function of the relative wind speed in square[7]. Modern VAWTs have been able to reach power coefficients of 0.37[11].

Pitch and stall control

In high wind speeds, usually around 14 m/s, control is needed to avoid too high loads on the turbine. Control is also needed if the grid connection is lost and consequently the generator can not extract any energy from the rotor. The most effective way this can be done is to use pitch control. Pitch control is when the pitch angle of the rotor blades are adjusted mechanically to alter the aerodynamic angle of attack, see figure 2.2 and 2.3. The pitch angle and angle of attack are often confused, a difference is that the pitch angle is a design parameter and the angle of attack is an aerodynamic parameter[10]. When the angle of attack is adjusted, input power to the rotor is changed. Pitch control makes it possible for the turbine to always operate at maximum C_p.

When the angle of attack exceeds a certain critical aerodynamic value, a stall effect occurs. This is when there is separation of the air boundary layer on the surface of the blade which causes wake effects, increased drag and reduced lift. Sometimes stall is used to regulate the rotor power at high wind speeds. This is not common for modern wind turbines since it put heavy loads on the rotor and the whole turbine. The advantage of stall control is the fact that it is self-regulating and passive, without adjustment of the rotor pitch angle, aerodynamic stall will occur at higher wind speeds[7][9].

2.2.1 Vertical Axis Wind Turbine

VAWT has a vertical rotational axis as can be seen in figure 2.4. VAWTs can be designed to work with either lift or drag as the main driving force. When looking at turbines for production of electricity they are predominantly lift driven since they generally have a higher total efficiency. In locations with low wind speeds however, e.g. a rooftop in the city, the drag design can be favorable [12]. The blades can either be straight or curved towards the rotating

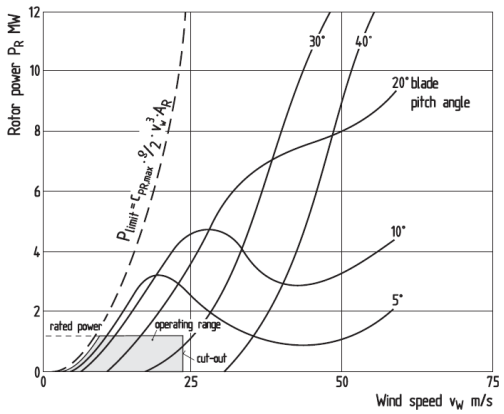

Figure 2.3: Example of rotor power for different wind speeds at different pitch angles [10]

shaft (Darrieus type). Turbines with straight blades can be pitched but this is uncommon since it makes the construction more complex.

One major difference between VAWTs and HAWTs is that VAWTs have the ability to accept wind from any direction. This is an important advantage, especially at sites with gusty and turbulent winds and where the direction of the wind changes frequently and rapidly. VAWTs, as opposed to HAWTs, do not experience power losses during these temporary wind gusts from directions other than the main wind direction. These characteristics give VAWTs an advantage over HAWTs in mountainous and urban areas. Additionally, an omni-directional wind turbine does not require a yaw system, which is the system that orientates the rotor towards the wind. This enables a more simplistic design and erases costs for the equipment, installation, operation and maintenance of such a system.

The generator and gearbox of a VAWT can be located at ground level. Such design reduces the loads on the foundation and tower, allowing them to be constructed lighter. The absence of a nacelle eases the erection of the turbine and makes maintainence more easier. The blades of a VAWT can be attached to the tower at several points (see figure 2.4), this reduces the loads on the blades but the support structures add extra weight to the turbine. The blades of a HAWT are only attached at the root and thus are the blades required to be self-supporting. A characteristic for the blades of most of the VAWTs is that the tangential speed is the same for all the segments of the rotor. This gives that the tip speed ratio will roughly be the same over the length of the blade, thus the shape of the blade can be the same from top to bottom, making low cost manufacturing possible. The blades of H-rotor VAWTs (see figure 2.4a) experience large bending moments due to the centripetal acceleration. This effect decreases with increasing turbine radius, when the speed of the blade is assumed to be constant. The reduction of the effect comes from that larger turbines has a lower angular speed, compare equation 2.10 for a given TSR[14].

VAWT experiences a changing torque on the blades due to the changing angle of attack between the blades and the apparent wind. This uneven torque

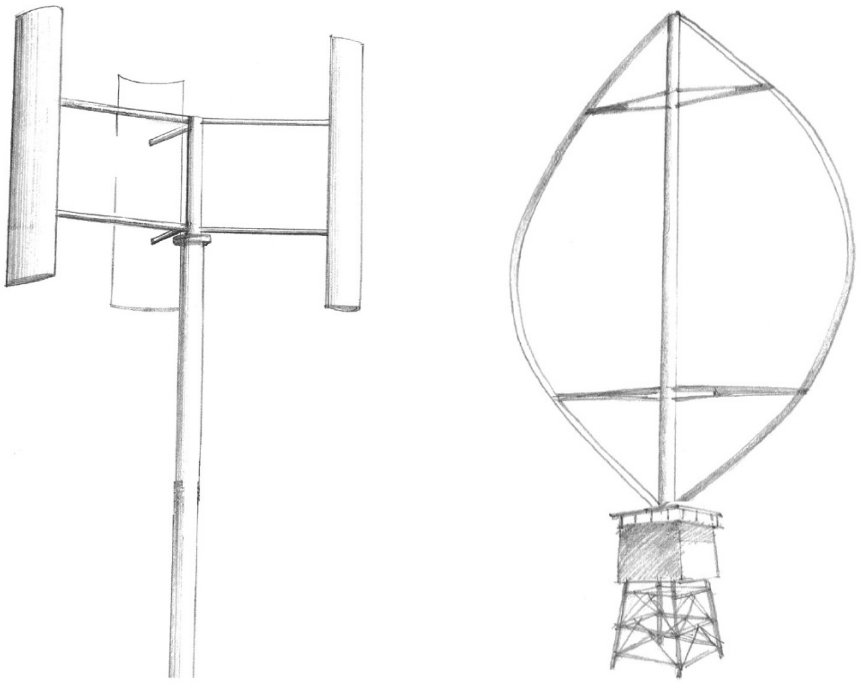

(a) A darrieus H-rotor VAWT [13] **(b)** Darrieus VAWT with curved blades [13]

Figure 2.4

affects the lifetime of the drive train components and reduce the quality of the power output. This effect is decreased by increasing the number of blades, see section 2.3.1. Another disadvantage of VAWTs, is that they have poor starting torque and many turbines are not able to start rotating in low wind speeds. This can be remediated by using the generator as a motor to accelerate the rotor to a speed where it can extract more power[14].

The land area occupied by a wind turbine is dependent on noise, needed security distance and possible guy wires. A VAWT emits less noise and needs shorter security distance than a HAWT but needs for the most part relatively long guy wires[14]. The noise emitted by a wind turbine can be separated in two parts, aerodynamic noise from blade tips and mechanical noise from drive train components. An increase in tip speed of a blade increases the aerodynamic noise. VAWTs have a tip speed which is approximately half the tip speed of HAWTs, hence making VAWTs less noisy than HAWTs. Since the drive train components of a VAWT are situated at ground level, mechanical noise from a VAWT propagates less than turbines with the drive train components positioned on the top of the tower.

Cons with VAWTs

- The change of the wind direction throughout the revolution makes the structural loads on the blades vary greatly causing fatigue damages. It is difficult to build high VAWT which makes it harder to reach the best

wind locations[7].

- The rotor of a VAWT has an oscillating resulting force on the tower. This force vector changes direction and size with the rotation of the rotor, guy wires are thus needed to stabilize the tower of smaller turbines. This oscillating force makes high VAWT towers disadvantageous to construct since they require a very solid construction and long guy wires[15].

- The power coefficient for VAWTs is usually considerably lower than for HAWTs. Some researchers claim that this is due to the fact that most research and development the last 20 years have been focusing on HAWTs. On rooftops, however, an H-rotor VAWT was shown to have superior power coefficient compared to a HAWT. [14].

2.2.2 Horizontal Axis Wind Turbine

As mentioned, most of the modern wind turbines are of horizontal type. This means that the axis of rotation is parallel to the ground. The horizontal turbines have many variations. The turbine can be of upwind (the rotor is facing the wind) or downwind (the rotor is facing away from the wind) type, the orientation can be teetering (not fixed) or rigid. The rotor control can be of pitch or stall type and the number of blades can vary where three is the most common[7].

Pros

- The main reason why HAWT has become the dominant technique is that it manages convert a larger part of the energy in the wind compared to the VAWT.
- Building a large HAWT requires less material per sweeping area than a large VAWT [3].
- HAWTs can more easily be designed with pitch control compared to VAWTs, pitching allows the turbine to be effective in all wind speeds[14].

Cons

- As an effect of having a horizontal rotational axis, the generator, gearbox and break has to be installed in the nacelle at the top of the tower. This makes maintenance and construction more challenging.
- Different parts of the blades are rotating at different speeds, the same angular frequency but at different radius from the center. As a consequence of this, a lot of work has to be done in order to find a good design for the blade profile.

2.3 Components in a Wind Turbine

Regardless if working with a VAWT or a HAWT most of the components are similar. In this section the main components used in wind power are presented. Important components of a HAWT can be seen in figure 2.8.

2.3.1 Rotor

The rotor is considered to be the first part of the turbine since it starts the energy conversion of a wind turbine by converting wind energy to mechanical energy. Equation 2.2 describes the energy in the wind, however all of that energy can not be caught which is decribed in section 2.2.

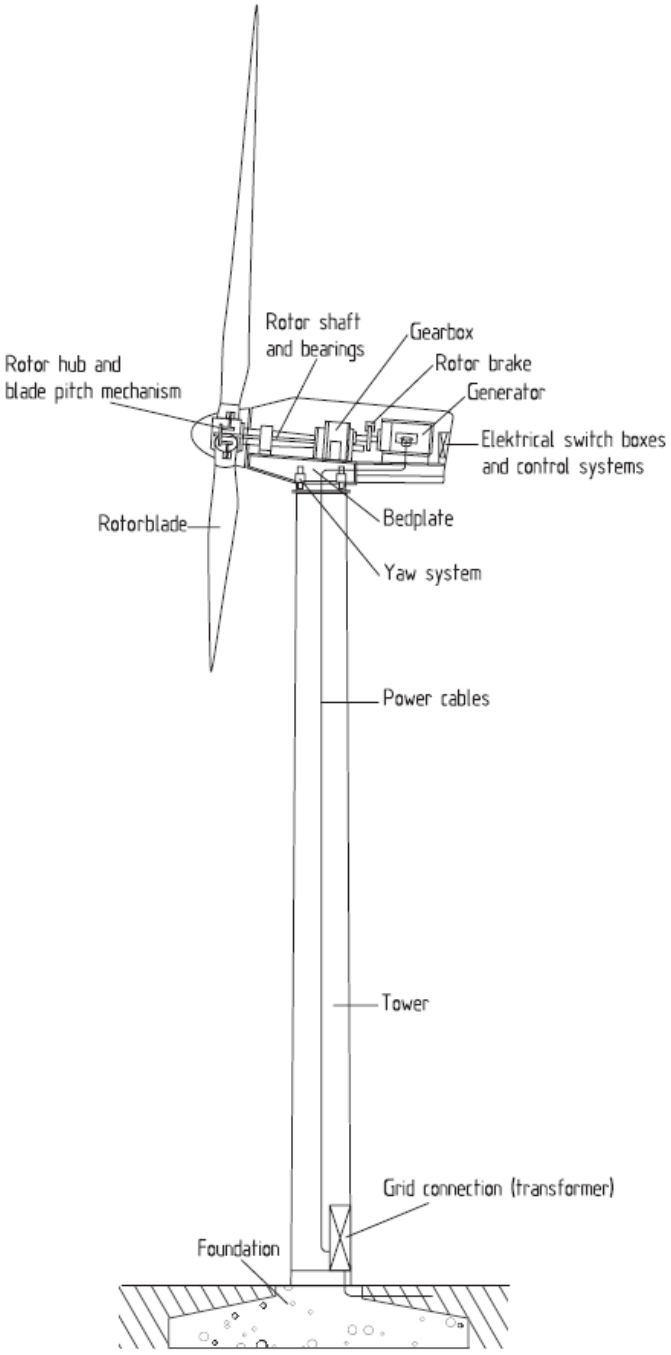

Figure 2.5: Components of a HAWT [9]

Mathematical description of straight-bladed vertical rotors

In this section the main features of how vertical straight-bladed rotors work are presented as well as how to calculate the power extraction.

The relative velocities between the wind and the blades will vary during the revolutions. The wind speed seen by the rotor blade can be expressed in two vectors, V_n and V_c. V_n is the normal vector that is aligned with the normal to the blade and V_c is the chord vector that is parallel with the chord of the

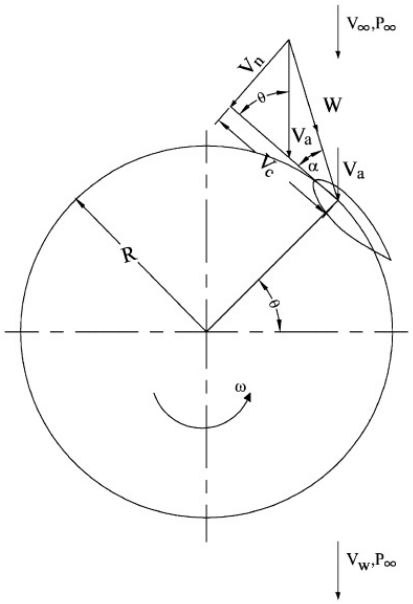

Figure 2.6: Flow velocities of a straight bladed rotor [13]

blade as ilustrated in figure 2.6.

$$V_c = R \cdot \omega + V_a \cdot cos(\theta) \tag{2.11}$$

$$V_n = V_a \cdot sin(\theta) \tag{2.12}$$

where V_a is the air velocity in the rotor area, ω is the rotational speed, R is the radius and θ is the azimuth angle as shown in figure 2.6

The angle α in the figure is referred to as the angle of attack and can be expressed as

$$\alpha = tan^{-1}(\frac{V_n}{V_c}) \tag{2.13}$$

By dividing 2.11 and 2.12 with V_∞, which is the undisturbed wind speed, a dimensionless expression is obtained. These expressions can then be inserted into 2.13 and the following relation is obtained,

$$\alpha = tan^{-1}\left[\frac{sin(\theta)}{(R\omega/V_\infty)/(V_a/V_\infty) + cos(\theta)}\right] \tag{2.14}$$

If a blade pitch angle, γ, is introduced the angle α becomes,

$$\alpha = tan^{-1}\left[\frac{sin(\theta)}{(R\omega/V_\infty)/(V_a/V_\infty) + cos(\theta)}\right] - \gamma \tag{2.15}$$

The relative flow velocity, W, the velocity of the wind in reference to the blade can be expressed as,

$$W = \sqrt{V_c^2 + V_n^2} \tag{2.16}$$

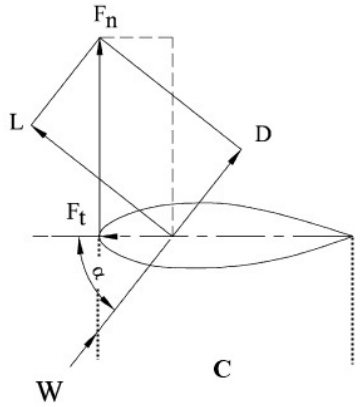

Figure 2.7: Force diagram of a blade profile [13]

The air flow around the blade creates lift and drag forces on the blade. The shape of the blade defines the lift coefficient, C_l and the drag coefficient C_d. The lift force is here denoted by L and the drag force is denoted by D, the tangential force coefficient, C_t is defined as the resulting force coefficient in tangential axis. The normal force coefficient, C_n is in a similar way described by the difference in normal forces. This can be written as

$$C_t = C_l \cdot sin(\alpha) - C_d \cdot cos(\alpha) \tag{2.17}$$

$$C_n = C_n \cdot cos(\alpha) - C_d \cdot sin(\alpha) \tag{2.18}$$

The actual forces can then be found as

$$F_t = C_t \cdot \frac{1}{2} \cdot \rho \cdot C \cdot l \cdot W^2 \tag{2.19}$$

$$F_n = C_n \cdot \frac{1}{2} \cdot \rho \cdot C \cdot l \cdot W^2 \tag{2.20}$$

where ρ is the density, C is the chord length (see figure 2.7) and l is the blade length[13].

Since α and W is known at all azimuth angles through the equations 2.11, 2.12, 2.15 and 2.16, the average tangential force throughout the revolution can be expressed as

$$F_{ta} = \frac{1}{2\pi} \int_0^{2\pi} F_t(\theta) d\theta \tag{2.21}$$

The total torque, Q, can be expressed as

$$Q = N \cdot F_{ta} \cdot R \tag{2.22}$$

where N is the number of blades and R is the radius as shown in figure 2.6. The power output, P is then

$$P = Q \cdot \omega \tag{2.23}$$

The theory above is summarized from [13] for more details the reader is refered to the reference.

2.3.2 Shaft

The shaft is a fairly simple component usually made of rigid steel. The purpose of the shaft is to connect the rotor to a generator, sometimes through a gearbox depending on what drive train solution that is used.

2.3.3 Brake

All wind turbines need to have a brake in order to be able to hold the rotor at a standstill during maintenance and repairs. The brake should also be able to stop the rotor if the other systems fail, but should not be used to control the speed of the rotor during operation.

2.3.4 Gearbox

Gearboxes are used in wind turbines to increase the rotational speed of the generator´s input shaft. This is done because most wind turbine rotors turn at a lower speed than is required by electrical generators and thus the rotational speed needs to be increased. In recent years manufacturers have started to design wind turbines without gearboxes, using power electronics that allows the rotor to have a varying speed instead. Gearboxes have a tendency to break down over time, leading to costly repairs and loss of production[7].

2.3.5 Generator

The generator converts mechanical energy to electrical energy. In the generator, electromagnetic induction creates an electrical voltage. In the wind power unit the shaft is connected to a magnetized rotor which, when rotating, induces a voltage in the windings.

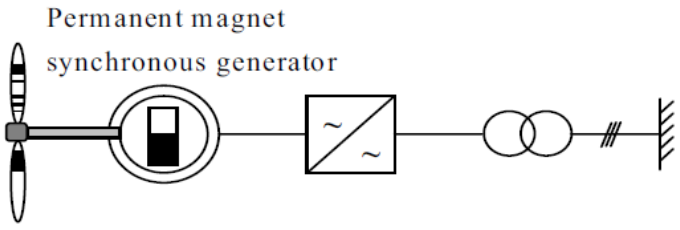

Figure 2.8: Wind turbine system with permanent magnet synchronous generator[16]

Asynchronous motors have been the most used motor for wind energy applications, however, the permanent magnet synchronous machine (PMSM) is

getting more and more common. This is due to the increased popularity of gearless i.e. direct-driven wind turbines, avoiding expensive gearboxes that need much maintenance. The PMSM is usually constructed with a rotor with permanent magnets and a stator with a three phase winding. Without a gearbox, the rotational speed of the shaft becomes low which is a drawback for electric generators since they need a high torque to generate desired power. The solution for this is to use generators with large rotor diameter, thus increasing the torque. The generator also needs a high number of poles for obtaining a suitable frequency. A multi-pole asynchronous generator would demand a high current for the magnetization of the poles, this is not needed for PMSMs since they provide their own magnetization which makes them more efficient than asynchronous generators. A PMSM can reach an efficiency of 96% [17][18][19][20].

Generator Losses

There are four main sources of losses in the generator; there are copper, iron, stray load and mechanical loss[21]. The total loss in the generator can be expressed by using equivalent circuits in the d-q reference frame, see figure 2.9. The dq0 transformation, also called Park tranformation, is a commonly used mathematical transformation used to decouple variables. It is often used to simplify the analysis of three-phase AC systems. A transfered three-phase AC system is represented by DC quantities, making calculations easier[22]. The d-axis circuit describes active currents and voltages while the q-axis circuit describes the reactive currents and voltages. The i_d and i_q currents in figure 2.9 are divided into two currents each, a magnetizing part and an iron loss part. The magnetizing part consists of i_{dm} and i_{qm} and the iron loss part consists of i_{di} and i_{qi}[21][2].

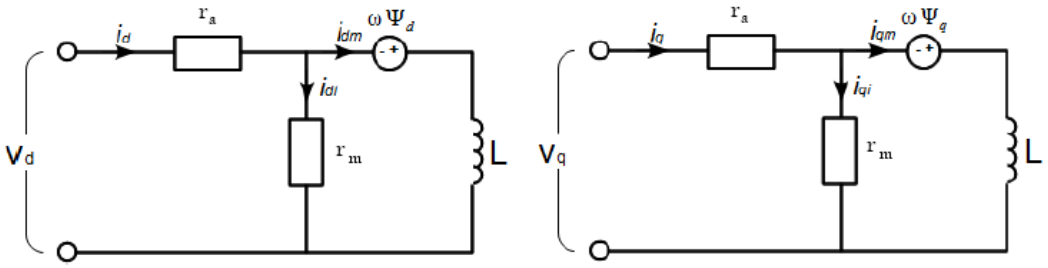

Figure 2.9: d-axis and q-axis equivalent circuits of a PMSM[2]

Copper loss The copper loss, P_c, occurs in the stator coil and can be estimated using the stator winding resistance r_a. Equation 2.24 gives the copper loss[21].

$$P_c = r_a(i_d^2 + i_q^2) \tag{2.24}$$

Mechanical loss The mechanical losses can be divided in two parts, ball bearing and windage loss, referred to as P_b and P_w. Both are friction losses due to the rotation of the rotor. The ball bearing loss can be expressed with equation 2.25, where K_b is a parameter which takes the generator rotor weight, the diameter of the axis and the rotational speed of the axis into account. The windage loss arises from the friction between the rotor and the air. This loss can be approximately estimated by equation 2.26 where ω_m is the mechanical angular speed and the K_w parameter concerns rotor shape and length as well as its rotational speed. Since the rotational speed of gearless PMSM wind turbine systems is very low, the mechanical losses in the generator are small[21].

$$P_b = K_b \cdot \omega_m \tag{2.25}$$

$$P_w = K_w \cdot \omega_m^2 \tag{2.26}$$

Stray load loss Stray load loss, P_s, occurs under loading conditions and originates from eddy currents that arise in the conductors, the iron core and the adjacent metallic parts due to leakage flux. The stray load loss can be estimated with equation 2.27, where P is the generated output and P_n is the rated power output[21].

$$P_s = 0.005 \cdot \frac{P^2}{P_n} \tag{2.27}$$

Iron loss Iron loss originates in the iron core of the stator and depends on the magnetic flux density in the core. The iron loss consists of two parts, eddy current loss and hysteresis loss, both of which arise due to the change in the magnetic field. Since the magnetic flux is of different magnitudes in different parts of the iron core also the losses will be of different magnitudes in the different sections of the core. The total iron loss, per kg, can be expressed with equation 2.28

$$p_f = B^2 \left\{ \sigma_H (\frac{f}{100}) + \sigma_E \cdot d^2 (\frac{f}{100})^2 \right\} \tag{2.28}$$

where B is the magnetic flux density, σ_H is the hysteresis loss coefficient, σ_E is the eddy current loss coefficient, f is the frequency and d is the thickness of the iron core steel plate. The magnetic flux density can be obtained with equation 2.30, however, in this equation the internal voltage E is needed. The internal voltage relates to magnetic flux described by equation 2.29

$$E = 4.44 \cdot f \cdot k_w \cdot w \cdot \psi \tag{2.29}$$

where k_w is the winding coefficient, w is the number of turns in the coil, f is the frequency and ψ is the magnetic flux. E_0 and B_0 are nominal values. The magnetic flux density, B, can be calculated with equation 2.30 and be used in equation 2.28[21].

$$B = B_0 \cdot \frac{E}{E_0} \tag{2.30}$$

2.3.6 Converter

Inverters(DC to AC) and rectifiers (AC to DC) are both types of converters and are important parts of many electrical devices including wind turbines. They make it possible to control and alter the voltage and current in an efficient manner. The power electronic converter is created by using, diodes, transistors, inductors and capacitors in an elaborate way. In this chapter the basics of how converters work will be explained in order to show where the losses occur and identify which parameters to tune in the model. A three phase inverter usually consists of three pairs of semiconductor transistor, two for each phase, and an equivalent number of diodes. As transistors, insulated gate bipolar transistors (IGBTs) are commonly used, see figure 2.10. Ideally, when turned on, an IGBT conducts a collector current i_C at a negligable saturation voltage $u_{CE} \approx 0$. When turned off, the IGBT will block a voltage u_{CE} with negligable leakage current $i_C \approx 0$. A diode should only conduct current in one direction, however there is a small current in the opposite direction which is called leakage current. The mode of operation, whether the switch is on or off, is determined by the gate-emitter voltage, u_{GE} [23].

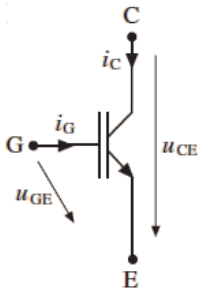

Figure 2.10: IGBT with terminals: C - collector, E - emitter and G - gate [23]

Pulse Width Modulation

Pulse width modulation (PWM) is a method used for inverters to convert DC to DC or AC. It is achieved by switching the DC on and off for very short periods, in pulses. This is done by using a transistor as a switch, for example an IGBT (see figure 2.10). The switching frequency is in the kHz range, in our project a switching frequency of 4.883kHz was used. The DC is switched in a way that the integral of the pulse is equivalent to the level of the desired sine wave, at that actual instant. The subsequent pulse is then adapted to the new

level of the desired sine wave, see figure 2.11. After filtering the output of an inverter using PWM, an almost perfect sine wave is formed. The technology has a relatively high efficiency, inverters using PWM have an efficiency of up to 96%[24].

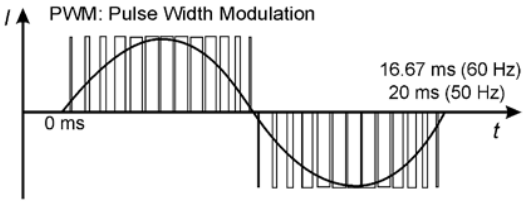

Figure 2.11: Pulse Width Modulation[24]

The Buck converter

The Buck DC-to-DC converter is the simplest version of transistor converter. The Buck converter manages to give a DC voltage output equal to or lower than the input DC voltage. This is done by using a semiconductor switch to change the transistor T_1 in figure 2.12 between its on-state and off-state. By controlling the ratio between the amount of time the transistor is on and off the average output is determined. In order to prevent sharp changes in the current the inductance L_{L1} in figure 2.12 is introduced[17].

During the time the transistor is conducting, energy is stored in the inductor. When the transistor is turned off the inductor will try to keep the current in the circuit constant and releases some of the energy stored, preventing the voltage over the load to drop significantly. During this stage the current will flow through the diode D_2.

Boost converter

The boost converter is similar to the buck converter introduced earlier, but instead of producing an output voltage lower than the input voltage the output voltage is higher than the input voltage. The boost converter is realized by the circuit described in figure 2.13. The output voltage level can be controlled by connecting a PWM to the transistor T_2.

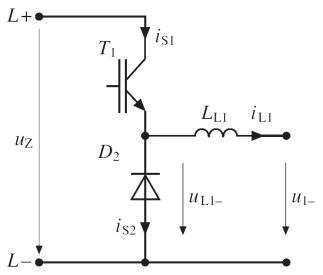

Figure 2.12: Buck converter[23]

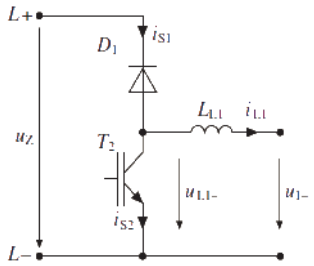

Figure 2.13: Circuit diagram of boost converter[23]

Buck-boost converter

By combining a buck and a boost converter as in figure 2.14 the buck-boost converter also referred to as a "'phase leg"' is created. D_1 and D_2 in the figure are referred to as antiparallel diodes. They allow current to flow in both directions and voltage over the load, u_{1-} to be positive and negative limited in amplitude by $L-$ and $L+$. By combining several Buck boost converters as in figure 2.15, a three phase AC/DC converter is realized. More details on this can be found in [23].

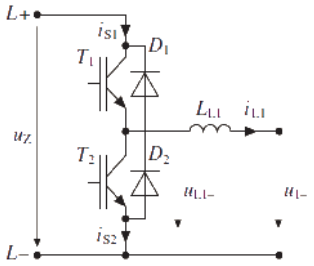

Figure 2.14: Circuit diagram of buck boost converter (phase leg)[23]

Converter Losses

Power electronic converters generally have high efficiency, but never the less there are losses that need to be considered. The losses of a converter needs to be evaluated since the heat the losses generates has to be taken into consideration when designing a cooling system for a converter. There are two main types of losses in a converter, switching and conduction losses[17].

Ideally, a transistor in a converter is in one of two modes.

- The transistor is conducting a large current with no voltage drop.
- The transistor is not conducting any current, resulting in a large voltage drop.

In both these modes the losses are equal to zero, this since in both modes the current or the voltage will be equal to zero. However, during the transition between the on and off mode of the switch, this is not the case. Switching losses

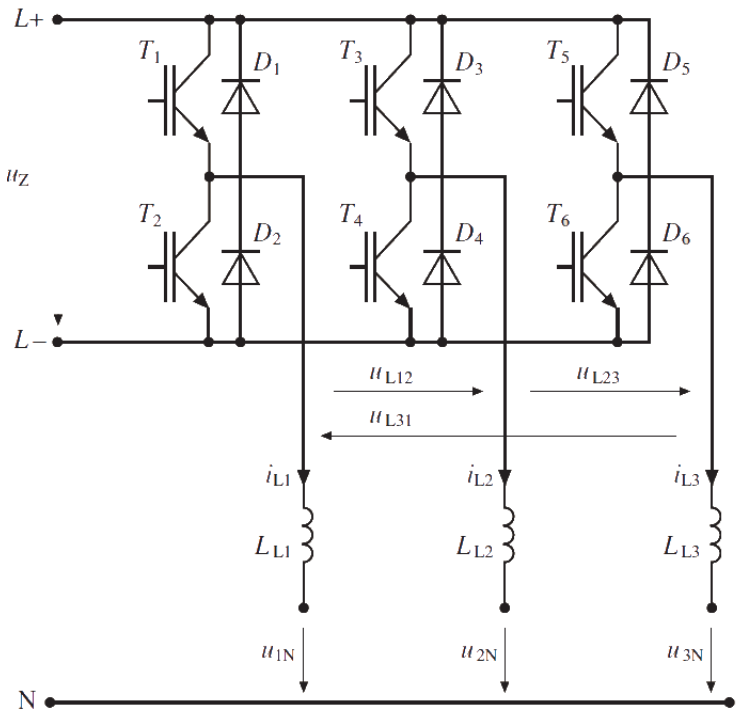

Figure 2.15: Circuit diagram of a three phase converter with IGBTs and diodes [23]

originates from when the switch is transitioning from its on-mode to its off-mode, and vice versa. The switching losses are thus dependent on the switching frequency. The higher frequency, the more times the switch is changing mode per second.

The losses occurring at one instant can be assessed by multiplying the instantaneous voltage across the switch with the instantaneous current through the switch. The losses are close to zero when the switch is off. When the switch is on, there are considerable conduction losses due to the fact that the voltage across the switch is never zero. In the upper diagram of figure 2.16, the switching waveforms for a switch with an inductive load can be seen. When switching an inductive load and the switch is turned off, the inductor will create a voltage to maintain the continuity of current through it[17].

There are three phases where the losses occur; turn-on, on-state and turn-off phase. They can be seen in figure 2.16 in the bottom diagram. The total energy loss, E_S, over one switching period is the instantaneous power loss integrated over the switching period, T_{sw}, see equation 2.31. The highest instantaneous power loss takes place during the switching events, this is due to the fact that there is a high voltage drop across the switch as well as a high current through the switch, see upper diagram in figure 2.16.

$$E_S(T_{sw}) = \int_{T_{sw}} p_S(\tau)d\tau = E_{S,on}(T_{sw}) + E_{S,cond}(T_{sw}) + E_{S,off}(T_{sw}) \quad (2.31)$$

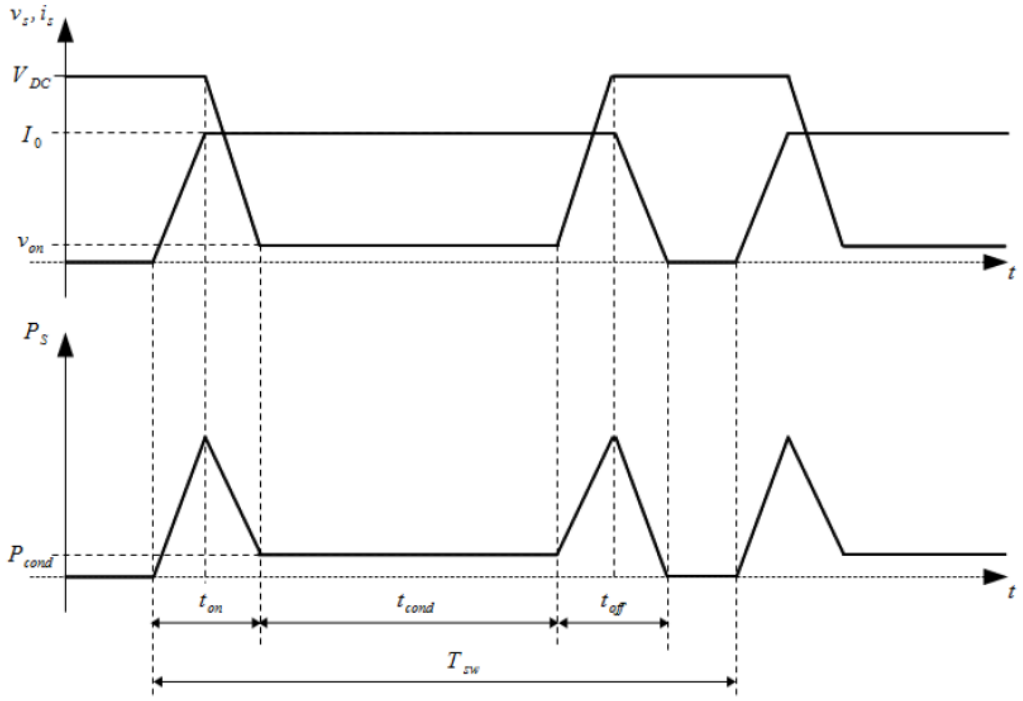

Figure 2.16: Approximate switching waveforms.
Top: Voltage drop across the transistor and current flowing through the transistor.
Bottom: Instantaneous power losses [17]

$$E_{S,on}(T_{sw}) = \int_{t_{on}} p_S(\tau)d\tau = V_{DC} \cdot I_0 \cdot \frac{t_{on}}{2} \tag{2.32}$$

$$E_{S,off}(T_{sw}) = \int_{t_{off}} p_S(\tau)d\tau = V_{DC} \cdot I_0 \cdot \frac{t_{off}}{2} \tag{2.33}$$

Conduction losses occur when the switch or the diode are conducting current and they arise due to the resistance in the transistor. The result is a small voltage drop across the transistor. The conduction losses can be even greater than the switching losses. Conduction losses in converters are duty cycle (the fraction of time the component is in its active state in relation to the total time) dependent. For conduction losses in a switch, this is the relative part of the switching period the switch is conducting current[25]. The diode conduction loss and the transistor conduction loss can be calculated in the same way. The total conduction energy loss can be calculated by integrating the instantaneous conduction loss over the conduction time, see equation 2.34[17][2].

$$E_{S,cond}(T_{sw}) = \int_{t_{cond}} p_S(\tau)d\tau = V_{S(on)} \cdot I_o \cdot t_{cond} \tag{2.34}$$

Where $V_{S(on)}$ is current dependent and can be described as

$$V_{S(on)} = V_{S0} + R_s \cdot I_0 \tag{2.35}$$

where V_{S0} is the forward voltage at no current and R_S is the resistance, which often is temperature dependent[17]. To calculate the average power loss the energy losses are divided by the switching time period, T_{sw}, see equation 2.36.

$$P_S(T_{sw}) = \frac{E_S(T_{sw})}{T_{sw}} = P_{S,on}(T_{sw}) + P_{S,off}(T_{sw}) + P_{S,cond}(T_{sw}) \tag{2.36}$$

$$P_{S,on}(T_{sw}) = \frac{E_{S,on}(T_{sw})}{T_{sw}} = E_{S,on}(T_{sw}) \cdot f_{sw} = \frac{V_{DC} \cdot I_0 \cdot t_{on}}{2} \cdot f_{sw} \tag{2.37}$$

$$P_{S,off}(T_{sw}) = \frac{E_{S,on}(T_{sw})}{T_{sw}} = E_{S,off}(T_{sw}) \cdot f_{sw} = \frac{V_{DC} \cdot I_0 \cdot t_{off}}{2} \dot{f}_{sw} \tag{2.38}$$

$$P_{s,cond}(T_{sw}) = \frac{E_{S,cond}(T_{sw})}{T_{sw}} = V_{S(on)} \cdot I_0 \cdot \frac{t_{cond}}{T_{sw}} = V_{S(on)} \cdot I_0 \cdot D_S \tag{2.39}$$

In equation 2.39 the parameter D_S denotes the duty cycle and f_{sw} denotes the switching frequency. Many properties of semiconductors are temperature dependent, therefore the operating temperature of a device should be considered for the balance of losses[23]. The total switch loss can be obtained by adding the turn-on and turn-off switch losses. This can be expressed with equations 2.37 and 2.38 resulting in equation 2.40.

$$P_{S,sw}(T_{sw}) = P_{S,on}(T_{sw}) + P_{S,off}(T_{sw}) \tag{2.40}$$

To calculate $P_{S,sw}(T_{sw})$, t_{on} and t_{off} have to be known. This is rarely the case since t_{on} and t_{off} varies with DC-link voltage. However, often given in data sheets are the turn-on and turn-off energies, $E_{on,n}$ and $E_{off,n}$. These parameters also take into account the voltage rise and fall times. The energies are given at a specific DC-link voltage ($V_{DC,n}$) and load condition ($I_{0,n}$). To use this data for other magnitudes of $V_{DC,n}$ and $I_{0,n}$, the data are to be scaled to make them more accurate, see equation 2.41 and 2.42[17]. The switching loss can consequently be calculated.

$$E_{S,on}(T_{sw}) = \frac{E_{on,n}}{V_{DC,n} \cdot I_{0,n}} \cdot V_{DC} \cdot I_0 \tag{2.41}$$

$$E_{S,off}(T_{sw}) = \frac{E_{off,n}}{V_{DC,n} \cdot I_{0,n}} \cdot V_{DC} \cdot I_0 \tag{2.42}$$

Diode losses

The power loss in the diodes consists of a conduction loss ($P_{D,cond}$) and a reverse recovery loss ($P_{D,rr}$). The conduction loss can be expressed with the equation

$$P_{D,cond}(T_{sw}) = V_{D(on)} \cdot I_0 \cdot D_D \tag{2.43}$$

where the forward voltage drop across the diode,$V_{D(on)}$, can be calculated with equation 2.44. The duty-cycle of the diode, D_D, can be approximated with equation 2.45.

$$V_{D(on)} = V_{D0} + R_D \cdot I_D \tag{2.44}$$

$$D_D \approx 1 - D_S \tag{2.45}$$

V_{D0} is the diode threshold voltage, which also can be refered to as the diode knee voltage. R_D is the resistance of the diode. As can be seen in the equations above, minimizing conduction losses in both the transistor and the diode can be done by lowering the forward voltage drops across the components. This is hard to achieve since the leakage current tends to increase with lower voltage drops[23].

The reverse recovery loss in the diode occurs due to excess carriers stored in the interior of the diode. These carriers have to be swept away and causes a reverse current. As can be seen in figure 2.17, there will be a high diode current at the same time there is a large voltage drop across the diode, resulting in losses. To determine the losses, the charge Q_f has to be estimated. Most often, Q_f is not given by manufacturers, instead the total reverse recovery loss, Q_{rr}, is given.

$$Q_f \approx \frac{1}{S+1} \cdot Q_{rr} \tag{2.46}$$

$$S = \frac{t_{rr1}}{t_{rr2}} \tag{2.47}$$

The reverse voltage across the diode will at the time interval t_{rr2} be equal to the DC link voltage, V_{DC}. For every switch period, there is one reverse recovery. This gives the equation for the reverse recovery loss.

$$P_{D,rr} = V_{DC} \cdot Q_f \cdot f_{sw} \tag{2.48}$$

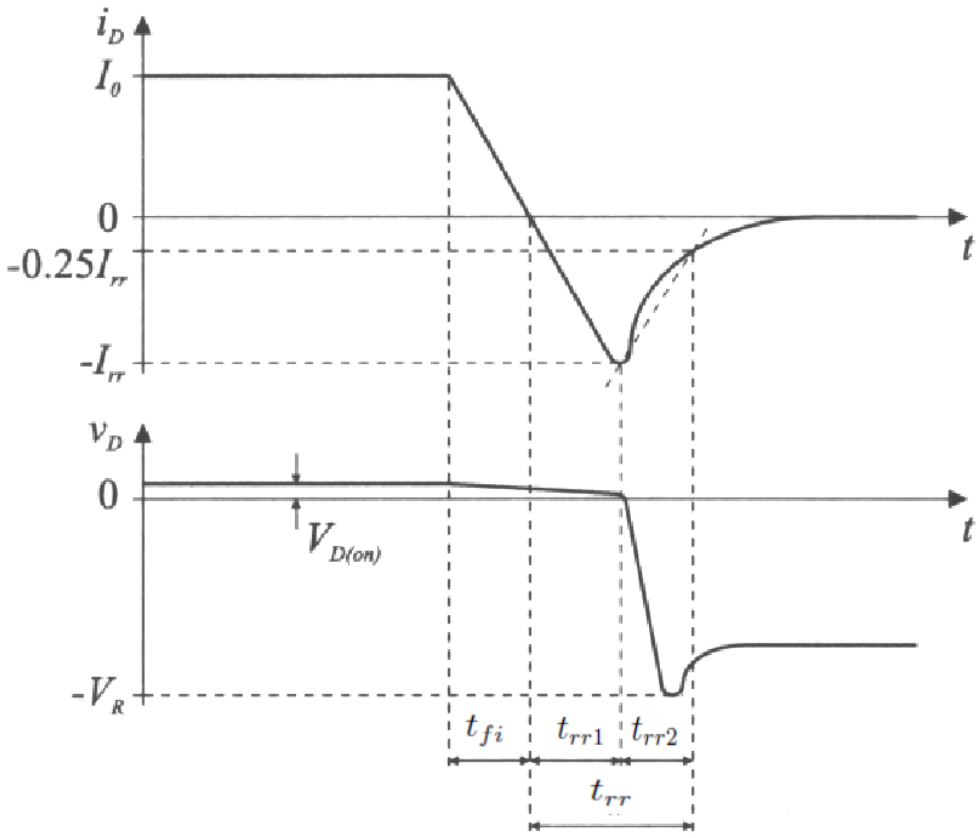

Figure 2.17: Diode during turn-off.

Chapter 3

LTH Wind Power Test Unit

In a collaboration between local businesses and Lund University a test unit for vertical wind power has been constructed. Work has previously been put into constructing and mounting the unit, a wind measurement system has been installed and work on a control system is in progress. A model of the power plant has previously been made in Dymola. This chapter includes a short summary of the test unit. It also summarizes the model of the unit that was previously made and our translation of that model into the new library EPL.

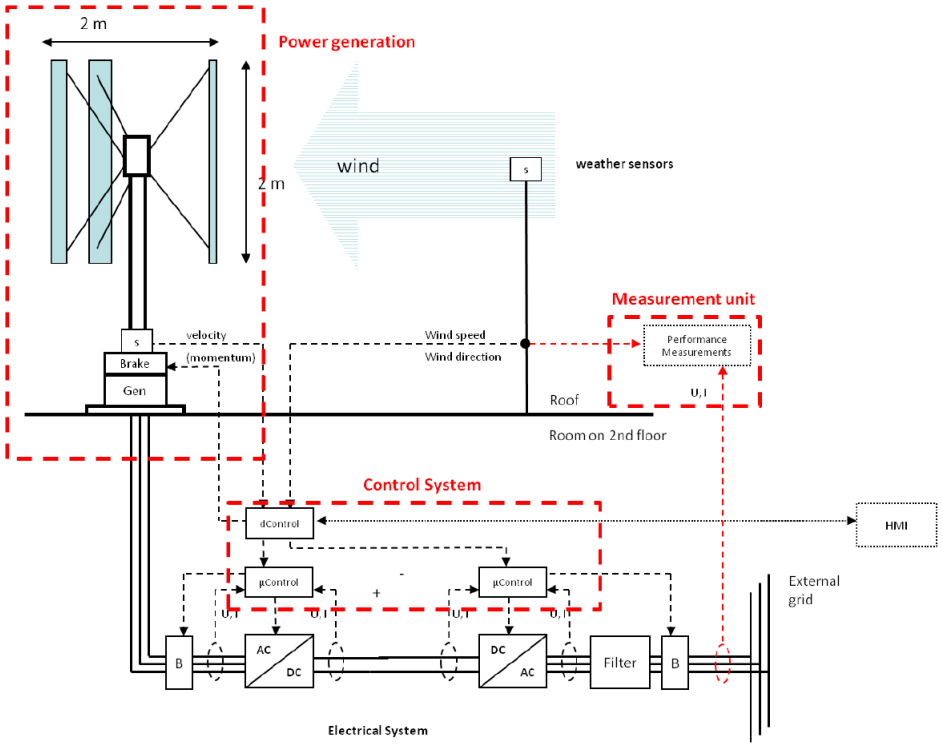

Figure 3.1: Overview of the layout [26]

3.1 Components and Layout

Test unit layout

The test unit is mounted at the roof of the university, has a rated electrical power of 1.8 kW[26] and is described in figure 3.1. The test unit includes the power generation, a control system, electrical system and a measurement unit. When writing this the power generation unit is at place, a lot of work has been put into the electrical and control system and it will soon be up and running. When the other parts are complete the measurement unit should be implemented shortly after.

Rotor

The rotor has three straight blades that are 2 m long. The diameter of the rotor is 2 m. The pitch angle of the blades is 10 degrees. The tower is 6 m high. The rotor is believed to have a rated wind speed of 12 m/s and a rotor speed range of 0-240 rpm.[26]

Generator

Unfortunately the exact model of the generator mounted on the test unit is not known. It is known that it is a PMSM.

Converter

In the wind power test unit, three phase AC from the generator is connected to the converter unit where it is rectified and then converted back to three phase AC. The converter used in the test unit is a SEMISTACK IGBT. The controllers for the converter are written in the programming software LabVIEW (Laboratory Virtual Instrumentation Engineering Workbench) developed by National Instruments and commonly used for e.g. instrumental controls. The actual controls are of CompactRIO type which is a reconfigurable embedded control and acquisition system, also developed by National Instruments.

3.2 Modeling

Modeling is the production of equations and algorithms that can predict the behavior of systems. For small and simple models, equations that describe the system can be written down. This approach is too time consuming and demanding if larger systems are defined. The problem can be solved by having parts of the system already modeled and using them to build a system. This is called component-based modeling. The idea is that common components are modeled and stored in a model library which later can be used to build up larger systems. The parameters in the models can be specified manually or estimated statistically to correspond to special characteristics of a unique system[5].

In a previous master thesis work a model of a similar wind power plant including a proposal of a control system was developed using the component library, SPOT and external C++ code. For details see [2]. Since then a new enhanced library, EPL (Electric Power Library) has been released. As a first part of our work those models were translated into EPL.

Figure 3.2: The layout of the SPOT based model

The model was structured as shown in figure 3.2 including components, experiments, pictures and tests. Most components in EPL and SPOT are almost identical in the way they work but are located in new folders and some of them have new names. Other components have new features or are built in another way. The components that in our experience have been changed the most are the converters, generator and the DC-link. These components will therefore be described in more detail. In addition, some results from tests as well as some experiments using the old SPOT models and the new EPL

models will be shown in order to provide a verification that the two set-ups provide the same results.

Before going into some details about the electrical components, some comments are needed concerning the wind power and control components located in the components package in figure 3.2. The components in the wind power package were written using the standard Modelica Library, no translation of the components are needed since the library is unchanged.

Worth mentioning is the rotor component which transfers the power in the wind to the rotor,

$$\begin{cases} C_p(\lambda,\beta) = C_1\left(C_2\lambda_i - C_3\beta - C_4\right)e^{-C_5\lambda_i} + C_6\cdot\lambda \\ \\ \lambda_i = \dfrac{1}{\lambda + 0.08\cdot\beta} - \dfrac{0.035}{\beta^3+1} \end{cases} \tag{3.1}$$

$C_1 - C_6$ are parameters to tune the curve to the aerodynamics of a specific rotor, β is the pitch angle and λ is the tip speed ratio, the equation is a commonly used way of modeling C_p-curves for VAWTs[2].

The controls were written using C++ code and the standard Modelica Library, this means that no modifications are needed to use the same controllers with the EPL version. However the controls written in C++ have to be copied into the source folder of Dymola.

3.2.1 Challenging components

Converter

The converter in SPOT are divided into two separate models, the average model which is a simpler converter that is faster to simulate and a more advanced switched model that is heavier to simulate but are closer to the reality. Both these models have two input ports, the two blue triangles in figure 3.3. The triangle to the left has two inputs, the reference voltage (determining the absolute voltage on the AC-side) and the phase of the AC-voltage. The triangle to the right is for the frequency of the AC-voltage. The red square is a heat port to handle heat losses, the heat port of the average model has a vector length of one and the heat port of the switched model has a vector length of three, one for each phase. In figure 3.3, the top left model is the default EPL inverter model and the top right is the same EPL model but with added ports enabling additional inputs to the model. The bottom models are from the SPOT library, the bottom left the simpler average model and bottom right the more advance model with roughly the same graphical design.

The average model of the converter is modeled as a voltage source where the amplitude, frequency and phase of the voltage is determined by the inputs. For the more advanced converter model the component consists of two parts, a modulator that creates control signals to the second part, the converter, which can have different settings. The modulator part has multiple modes, it can be set for synchronous PWM where the switching frequency is determined by the frequency of the connected AC-voltage. Another modulator mode is the

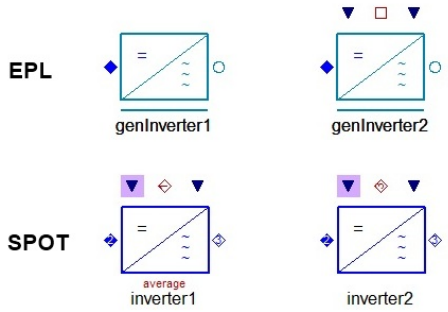

Figure 3.3: Inverters in SPOT (bottom) and EPL (top)

asynchronous where the switching frequency has a fixed value. The converter part has three modes where the first two uses diode equations to model the converter. The control signals from the modulator determines whether the "diode" should be conducting or not. The simpler one of them neglects the anti parallel diode and the second one does not. The most advanced model of the converter uses transistor models and anti parallel diodes. The different choises for the converter is shown in figure 3.5. The configurations in figure 3.5 could be compared to the figure over the three phase converter that is supposed to be modeled, figure 2.15.

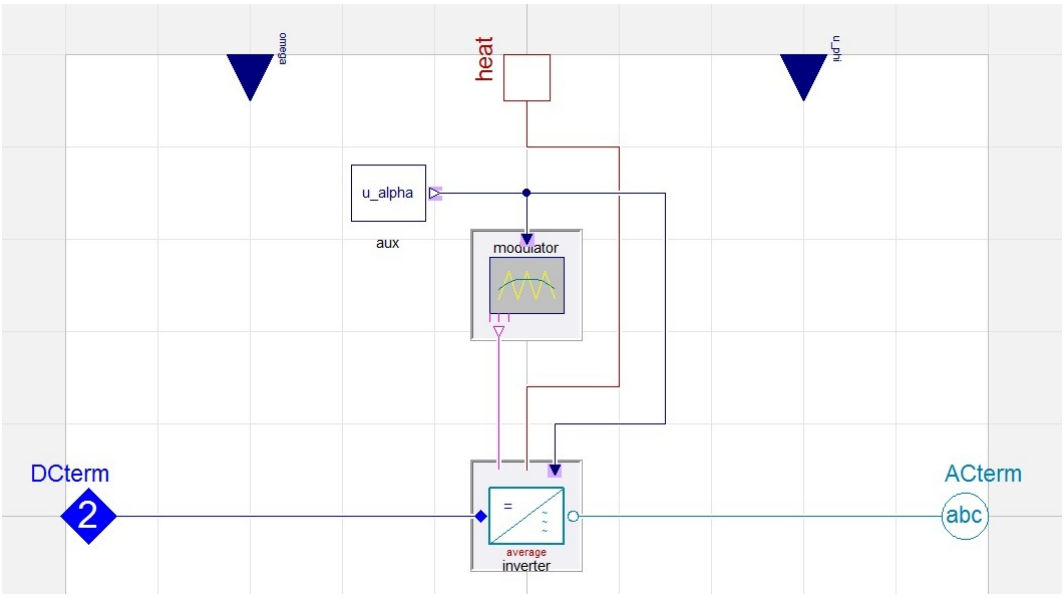

Figure 3.4: The general converter model from EPL. The gray squares around the modulator and inverter indicates that they can be exchanged.

In EPL a slightly different approach is used for the converter. A general converter model is used, by parameter choice the model can then be turned into both the simpler average converter and the more advanced versions. This is shown in figure 3.6 At default no input connectors are used but through parameter choice the same inputs as in SPOT can be activated. A new feature

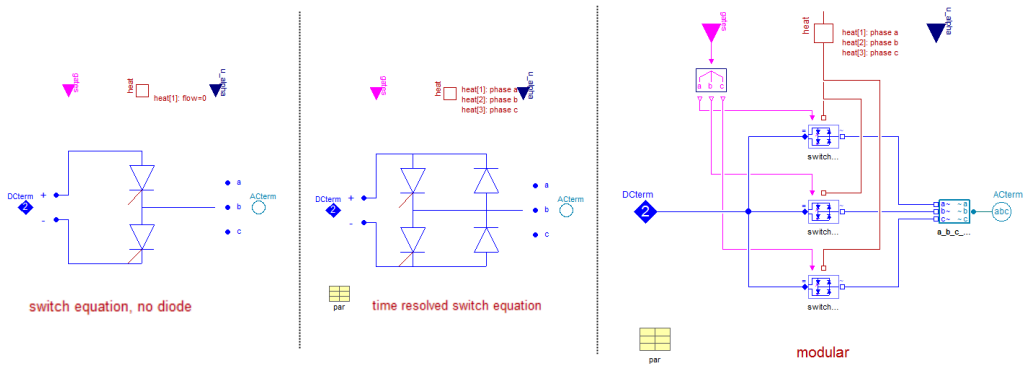

Figure 3.5: Different options for the converter model

is introduced in EPL where the output frequency can be chosen to match the frequency from another AC-voltage source connected as the AC-port.

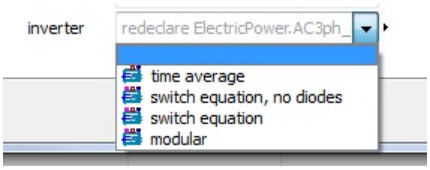

Figure 3.6: Converter choices in EPL

Both in the SPOT and the EPL models the average version results in a sinusoidal signal and requires relatively few computations. The output from the versions using switching will be closer to the real case explained in 2.3.6 but requires a lot more computing time. Since the time average model gives similar or equal results as the other models, it is sufficient to use the time average model in most cases.

Generator

The generator is modeled as a permanent magnet synchronous machine, see section 2.3.5. The SPOT and the EPL models are based on the same equations but the SPOT model uses the electrical angle set by a system component whereas the EPL model uses the derivative of the electrical angle. In the SPOT model of the generator the electrical angle is available as an output from the component, in the EPL model the angle has to be manually extracted. The difference is shown in 3.7.

DC-Link

The DC-link component has been slightly changed between SPOT and EPL. SPOT uses a resistance in series with an inductor and a capacitance in parallel with two capacitances, EPL uses an inductance including resistance in series with a capacitance in parallel with two capacitors as illustrated in figure 3.8.

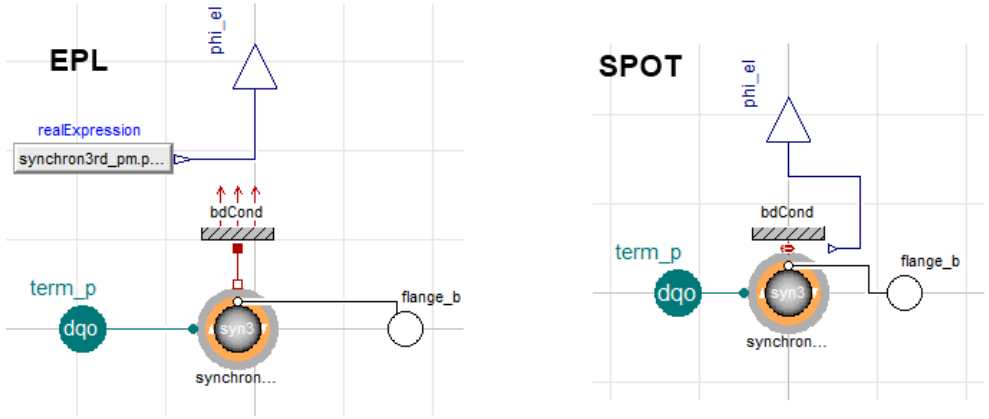

Figure 3.7: PMSM model from EPL version and SPOT version

The parameter values are propagated in different ways between the two versions so it is important to be careful when using the component. In addition heat ports are optional in the EPL version which makes it possible to manage heat losses, which can be useful in detailed modeling.

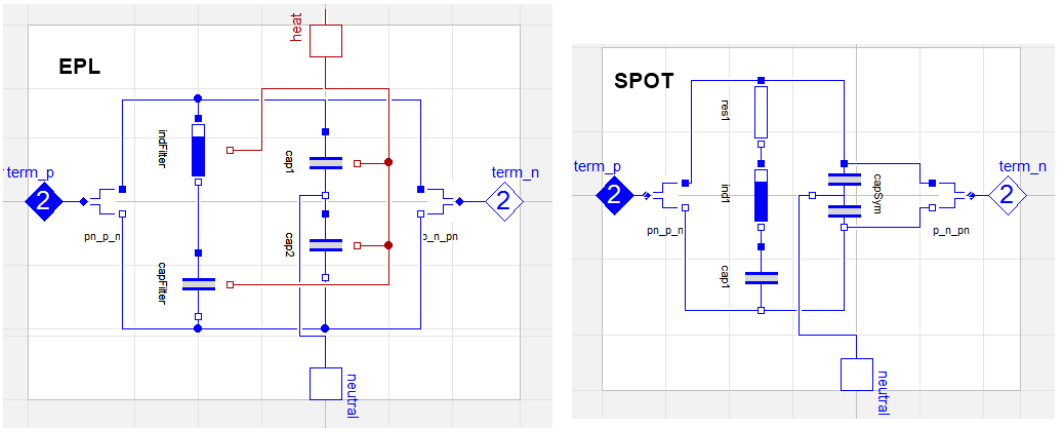

Figure 3.8: DC-link models, left model is from EPL and the right model is from SPOT

3.2.2 Translated tests and experiments

To ensure that the models have been translated in a correct way and that there is a good compliance between the two libraries some test cases and experiments for the two versions are compared.

Generator tests

In a previous thesis[2], a test model of the generator was developed using the SPOT library. A corresponding test model was developed with the EPL components including a generator, an average converter and a DC-link component.

Two EPL versions of the tests were produced to show two different ways of communicating the frequency to the converter. The first version is very similar to the SPOT version, however the electrical angle from the generator has to be derived before connecting it to the converter since the new converters work with the angular frequency instead of the electrical angle. The second option is to use the new synchronize feature of the converter where it "reads" the frequency from its AC port. The test setup for the first EPL case is shown in figure 3.9. A comparison of the test results are shown in figure 3.10.

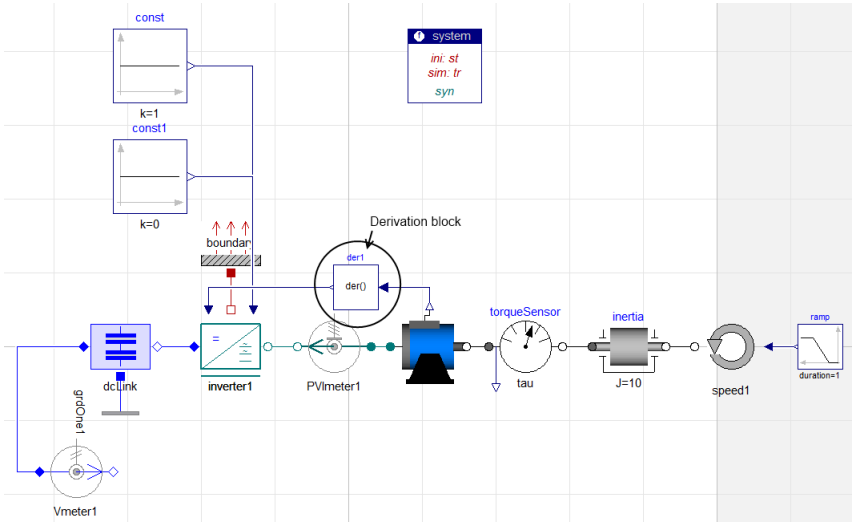

Figure 3.9: The EPL generator test, note the "der() block" handling the electrical angle

The results are shown from 1 sec to 3 sec to give a good resolution. Figure 3.10 indicates that the EPL and the SPOT library test models produce identical results.

Experiment test

The next step is to translate a model where some control functions are used in order to be able to verify that the EPL and SPOT versions work in the same way also when controlled. The translated experiment can be seen in figure 3.11, inputs to the model are wind speed, DC-voltage reference level and power reference. The DC-voltage and power references are inputs to controllers. The DC-controller can be seen in the figure, but the power controller is hidden within the rotor component.

The results from the translated model as well as from the original SPOT model are presented in figure 3.12. In the presented case the wind speed used is varying sinusoidally with an amplitude of two and a frequency of 0.01 Hz. After 20 s a power reference ramp is started and takes the reference value from 700 W to 2000 W over 20 s, the DC-reference is kept at 1000 V throughout the simulation. The most important part here is that both models give the same output, which is shown by the figure 3.12.

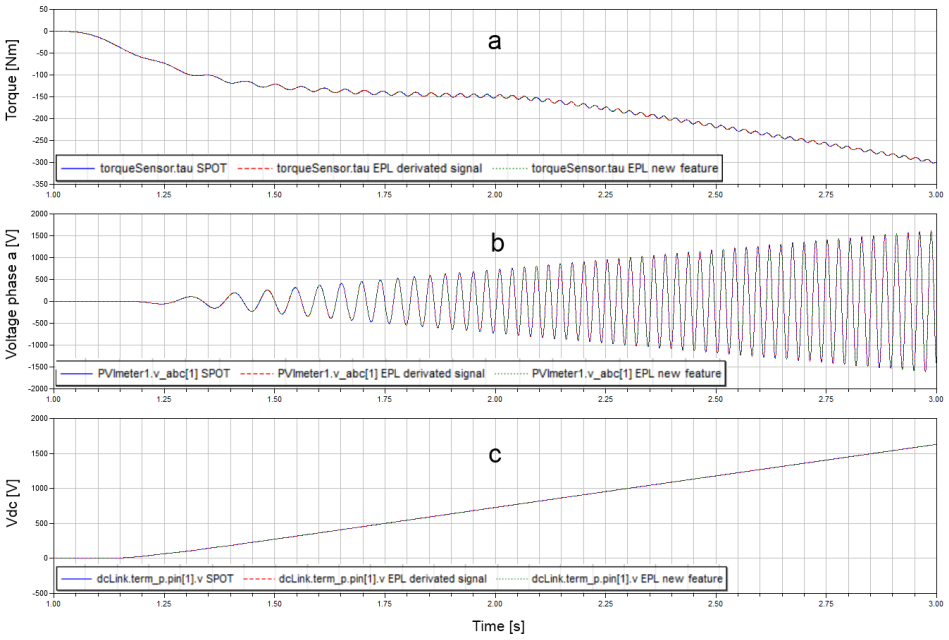

Figure 3.10: Comparative simulation results from EPL and SPOT generator test models.
a) Torque into the generator
b) Voltages for one phase at the generator
c) DC-voltages at the positive pin of the DC-link

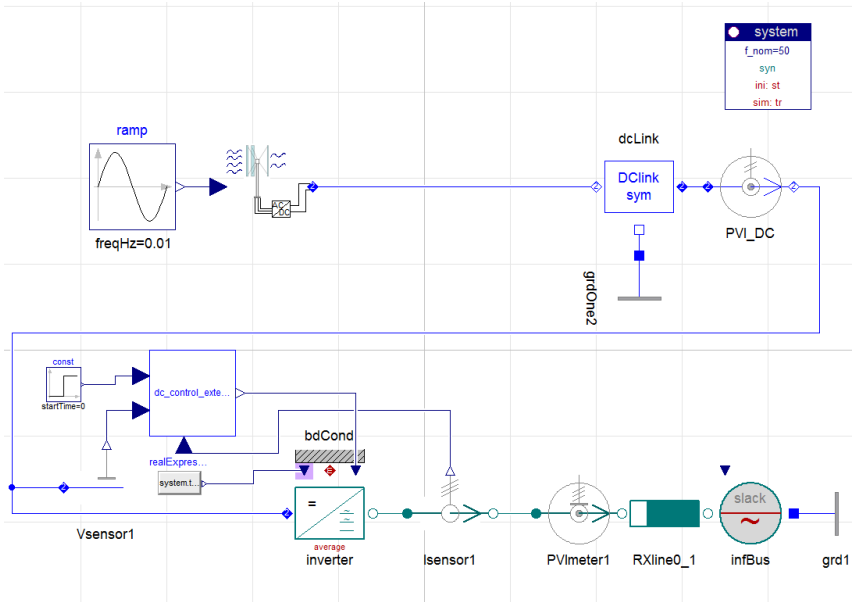

Figure 3.11: Controlled wind power turbine. Power regulation is included in the turbine model and regulation of the DC-voltage level is done by the DC control block.

Some other interesting results from the simulation can be seen at the dotted lines 1-3. At line 1, the power output exceeds the reference value for the first time, resulting in a plateau followed by a negative slope in the reference

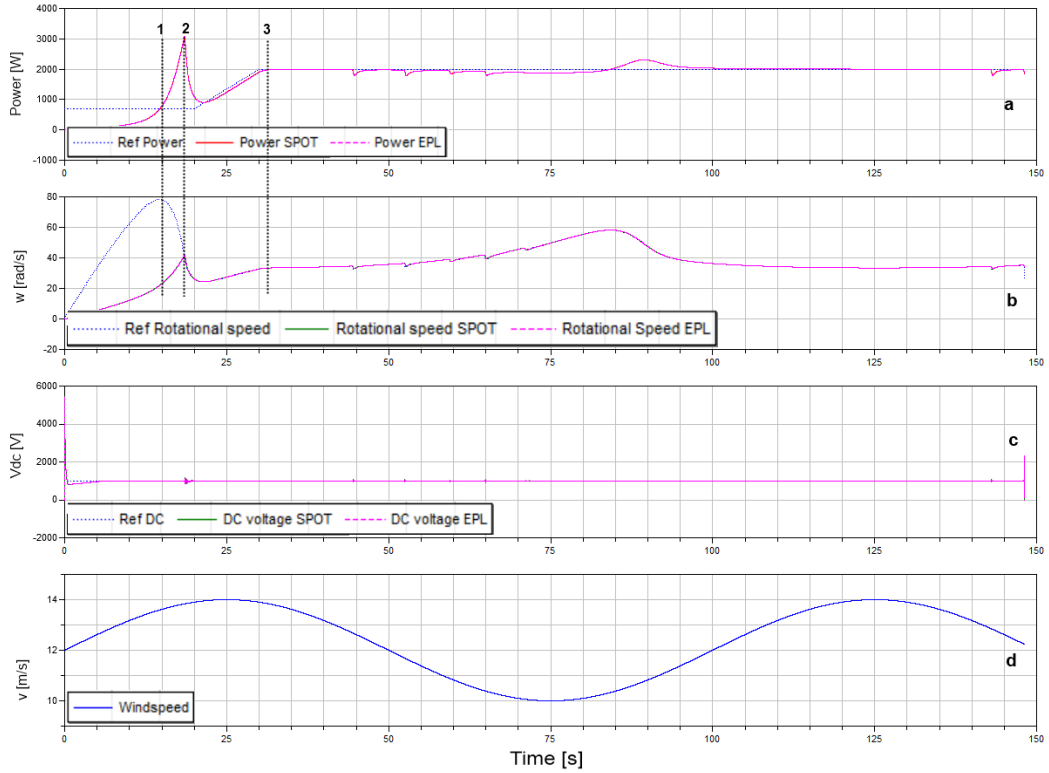

Figure 3.12: Simulation results from the experiment described in figure 3.11 outputs from EPL and SPOT are presented. The bottom plot shows the wind speed. The second plot from below shows the dc voltages. The second plot from the top shows the rotational speed of the rotor as well as the reference rotational speed. The top plot shows the power output at the rotor and the power output reference.

value of the rotational speed. At line 2, the reference rotational speed is reached, however the power output still exceeds the rated value, this results in a continued decrease in reference rotational speed. The increase in the power reference value results in an increase of the rotational speed reference value. The rotational speed value is increased until the reference power is achieved at the third dotted line. Past line 3, the rotational speed is still slightly increased, this is because the wind speed is decreasing and a better operational point is needed to produce the same power. A better operational point can be found by increasing the rotational speed, thereby increasing λ according to equation 2.10. The irregularities seen after line 3 are believed to originate from suboptimal tuning of the control systems.

Chapter 4

Calibration

Models can be created in some different ways. One option is to use well known physical relations such as Kirchhoff´s voltage law, stating that the potential differences around an electrical loop has to be zero and Kirchhoff´s current law stating that the sum of all currents to a node has to be zero to create a model. This is referred to as physical modeling. If the laws of a system are not well known one can use the system identification method that relies solely on measurements of inputs and outputs. A third case, the one focused on in this project, is a combination of the two other. A model is made using known physical relations and measurements are used to estimate unknown parameters in the model[5]. By conducting the calibration procedure in this way, it is possible to identify parameter values that have a real physical meaning.

An aim of this project is to calibrate the parameters of an existing model in order to assure that it in a reliable and accurate way describes the actual wind turbine. In order to do this, a first step is to examine how parameters are affecting the result and in what way. This can be done by generating multiple simulations and varying one or a few parameters in an organized way. However, if two parameters are influencing the output in a similar way it will not be possible to estimate them individually. Therefore it is important to investigate how the system reacts to changes in different tuners. A tuner is a parameter that is to be estimated.

Measurement data can be used as inputs to the model, e.g. wind speed, electrical current or electrical voltages or it can be used to match outputs from the model. This could be a rotational speed as result from the wind speed or an AC-voltage level as a result from a DC-voltage.

In this chapter some basics concerning calibration of object oriented models will be presented.

4.1 Structure of models

Software programs such as Dymola use libraries containing component models containing physical relations. The components are connected together into larger models as seen in e.g. figure 3.8, resulting in a series of coupled equations. In the general case these equations relate a vector of internal variables, $x(t)$ and their derivatives $\dot{x}(t)$ to a input vector $u(t)$. In the equations, there are also some parameters θ which can be unknown, outputs from the system is denoted by $y(t)$. A general system can then be described by the equations 4.1[5].

$$\begin{aligned} F(\dot{x}(t), x(t), u(t), t, \theta) &= 0 \\ y(t) &= h(x(t), \theta) \end{aligned} \tag{4.1}$$

In a small system the estimation and identification can be done manually but this is hard work and requires skill and it is not a valid option if the system is complex[5]. Instead an approach described in the section below can be used.

4.2 Parameter estimation

When a specific model structure M has been created it can be altered by changing the parameter set θ, the parameters are restricted by $\theta \in D_M \subset R^d$. The restriction of θ can be a maximum and a minimum value of a parameter, in special cases it can also be restricted to integer numbers. The set of available models are then defined by

$$M^* = \{M(\theta) | \theta \in D_M\} \tag{4.2}$$

Models in the set will predict the future in its own way, that is, give different outputs. To identify parameters included in a system, measurements have to be done. The dataset can be denoted as Z^N,

$$Z^N = \{u(t_0), y(t_0), ..., u(t_N), y(t_N)\} \tag{4.3}$$

where u are inputs to the system, y are outputs from the system and N is the number of datapoints for each input/output. Apart from the parameters θ, the equations of the model are known and defined by M. The unknown parameters of the system can then be tuned to make the equations produce results which fit the outputs in the measured data as well as possible. Several different methods for finding these parameters exist and there are different views on what is a good fit. One of them is the least square method is described later. The problem to be solved can be expressed by using the information in Z^N to determine the parameter vector θ [27].

To evaluate how well a model with a specific set of parameters estimates the results, an error function, ϵ, is commonly used.

$$\epsilon(t, \theta^*) = y(t) - \hat{y}(t|\theta^*) \tag{4.4}$$

where θ^* is a suggestion for parameter values and $\hat{y}$ is the output from the model using the suggested parameters. When the data set Z^N is known the error at each time step can be computed. A "good" parameter setting is recognized by a small value of the error function. But small can be defined in different ways. As the error function can be seen as a vector of length N, the size of the vector can be measured using any norm in $\mathbb{R}^N$. However the norm is often limited to the norm defined by equation 4.6. The error function is filtered through a linear filter $L(q)$.

$$\epsilon_F(t,\theta) = L(q) \cdot \epsilon(t,\theta), \quad 1 \leq t \leq N \tag{4.5}$$

And the following norm is used:

$$V_N(\theta, Z^N) = \frac{1}{N}\sum_{t=1}^{N} l(\epsilon_F(t,\theta)) \tag{4.6}$$

where $l(\cdot)$ is a scalar-valued, typically positive function. It is introduced, among other reasons, to assure that positive and negative errors are treated equally. V_N is then a scalar-valued function determined by the θ-vector and a specific data serie, Z^N. The parameters θ can then be determined by the minimizing equation 4.6:

$$\hat{\theta}_N = \hat{\theta}_N(Z^N) = arg \;\; min(V_N(\theta, Z^N)) \tag{4.7}$$

where arg min is the minimum value of the function. This general way of determining θ is sometimes referred to as *prediction-error identification methods* (PEM). Special cases of the method can be used by choosing different l, L, model structure and minimizing method. One minimizing method can be seen below.

Least square method

One of the most commonly used special cases of the method described by equation 4.6 is the least square method, in this case $L(q) = 1$ and $l(\epsilon) = \frac{1}{2}\epsilon^2$ resulting in equation 4.8.

$$V_N(\theta, Z^N) = \frac{1}{N}\sum_{t}^{N} \frac{1}{2}[y(t) - \hat{y}(t|\theta)]^2 \tag{4.8}$$

In more complex methods the l and L function can be varied in time, this can be useful if the quality of the measurements are known to change with time. For more methods and details on the subject the reader is referred to[27].

4.3 Calibration using the Design library in Dymola

Dymola includes features to calibrate and assess Modelica models. These features can be found in the Calibration package in the Design library in Dymola.

The calibration function searches for the optimum values of the tuners by varying the tuners and then simulating and evaluating the result, this process is iterated until the simulation result is in good correlation with the measured data. The tuning procedure is an optimizing process to minimize the error between the simulation result and the data. No information regarding which methods used have been found.

The simplex algorithm is a common method used to find optimum solutions to multi variable problems. The method proceeds from one basic feasible solution (one extreme point) of the constraint set of a problem to another to continously decrease the value of the objective function until a minimum value of the objective function 4.6 is reached. This minimum value can be set as a tolerance by the user. The algorithm used in Dymola is not accessible to the user since it is protected software, if more control over the process is desired platform such as JModelica.org can be used.

4.4 Calibration using derivative-free optimization

As an alternative to using Dymola and the Design library, JModelica.org can be used applying derivative-free optimization. However time to do this was not found in our project. The algorithm was developed in the Python programming language and implemented in JModelica.org in a previous master thesis [6]. Derivative-free optimizations are useful when the objective function depends on measurements, when the explicit form of the function is unknown. This is the case in our project, where Dymola models are calibrated to measurement data from the wind turbine. Additionally, sometimes it can be hard, demanding or impossible to find derivatives for a problem.

The algorithm implemented in [6] is the Nelder-Mead simplex method, also known as the downhill simplex method. The method was introduced in 1965 and is one of the most popular derivative-free methods. Its simplicity and ability to adjust to the contours of the objective function have contributed to its popularity. It is a direct-search method, evaluating the objective function at a finite number of points per iteration and acts based on the function values and not on any derivative approximation. In contrary to what the name implies, the method has nothing to do with the simplex algorithm of linear programming[6].

Chapter 5

Experimental Setup and Results

The main purpose of this project is to develop a methodology for calibration, create models to do this and subsequently calibrate the parameters of those models to make them resemble reality as much as possible. In order to be able to do this we have implemented test benches for the most important components. Some data from the real system has been collected and a calibration of the parameters have been done using the Dymola software. Real measurement data have been obtained for calibration of the converter component. Calibrations of the other components have been done using synthetic data.

5.1 Method

The method developed in this project can be described as follows. Firstly, data are collected, either synthetic or real. The synthetic data are collected from a developed wind turbine model (referred to as the main model) including all its components. Submodels (referred to as test benches) of the components are constructed to be used for calibration including signal connectors to be used for inputs, see figures 5.10,5.16 and 5.19. The real or synthetic data are collected, and used as inputs to run the test benches. To verify that the test bench is a correct representation of the component in the main model, the test bench is simulated using the same parameter values as in the whole system and a comparison of the results are done. The difficulty developing the test benches is to make the submodel behave in the same way as the whole system. For example, in the generator test bench (see figure 5.16), the voltage source on the right side in the figure has to behave in a way that it corresponds to the influencing characteristics given by the converter and grid component in the main model. Analyzing the influence of tuning parameters is done using the perturbParameters function of the Design Library, giving an indication of how to use the tuners in the calibration, see figure 5.12. Subsequently the calibration is done using the calibration function of the same library, see section 4.3. Test models (see section 5.3) were developed to show how the method is implemented in practice.

Verification of test benches

The test benches can be verified by simulating them using undisturbed synthetic data and the same parameter values. This is to verify that the test benches are good models for representing the component and that the inputs are used in a correct way. Verification of all three test benches produced results which were very similar to results from the main model, concluding that the test benches are accurately modeled.

5.2 Measurement data

The synthetic data used are collected from simulations of the main model. When generating synthetic data it is important that the data contains the information and dynamics necessary for identifying the tuning parameters when calibrating. In many cases it is a troublesome task, that demands good knowledge about the system. Where the measurements are collected in the main model can be seen in figure 5.1. Data can be saved in a few different file formats in Dymola, it has proven important to save the data in *.mat* format in some cases. This might be because the *.mat* format keeps more significant digits than e.g the *.csv* format.

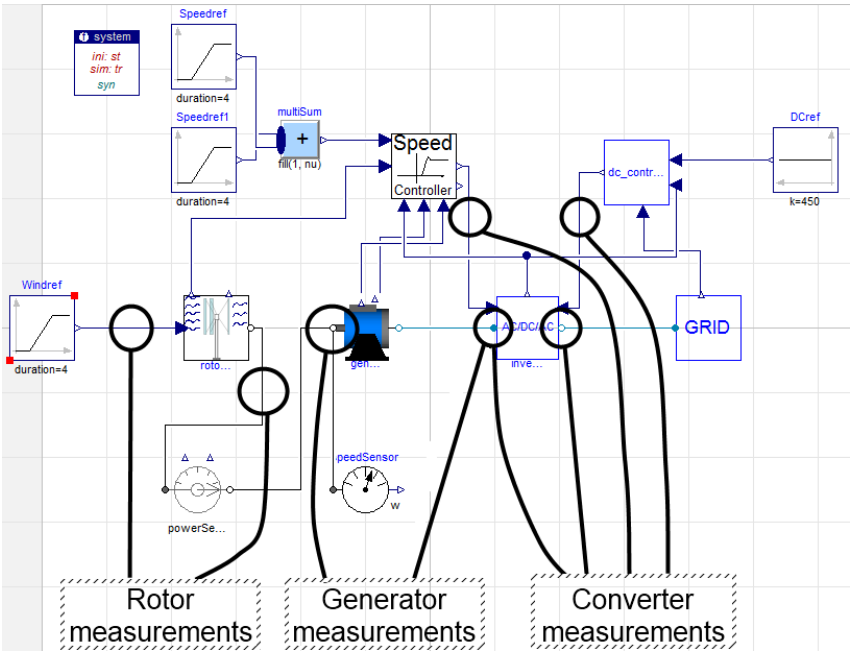

Figure 5.1: Where the synthetic data is collected in the main model

5.2.1 Rotor Dataset

Due to the lack of real measurements a calibration using synthetic data was performed. One important consideration when generating the synthetic data is that it must contain information about what is examined. For the rotor case the parameters of equation 3.1 are analyzed and it is important that the λ-value changes throughout the data. This can be achieved by keeping the rotational speed constant while the wind speed is varied or the other way around, keeping the wind speed constant and changing the rotational speed.

By running the main model shown in figure 5.9 with a constant wind speed of 8 m/s and having the speed controller set to 100 rad/s, a dataset containing wind speed, rotational speed and mechanical power is obtained. This simulation results in a λ-value ranging from 0 to 13 which in this case is the interesting region. By introducing noise to the values the case can be made similar to real measurements. How this is done can be seen in appendix B.1. For this calibration, two sets of noise data is produced, with two different $signal - to - noise - ratios$ or SNR. A lower SNR value means larger disturbances on the measurements.

5.2.2 Generator Dataset

As in the rotor case, no measurement data was available for the generator and synthetic data was used for the calibration of the component. Synthetic data was collected by simulating the main model, shown in figure 5.9. Data was collected from a simulation with varying wind speed and rotor rotational speed to capture some dynamics and get data when the generator is operating with different magnitudes of rotor torque and rotational speed. The generator

test bench (see figure 5.16) has rotational speed, electrical frequency, nominal voltage and voltage phase angle as inputs. The electrical power generated, which is positive when directed from left to right in the figure, is the output used to calibrate the component. These are the variables needed to perform the calibration and are therefore collected to the dataset.

The rotational speed of the rotor and the wind speed is changed throughout the data collection. The inputs wind speed and reference rotational speed as well as the output rotational speed are shown in figure 5.2. The rotational speed is ramped from 20 to 40 rad/s and then back to 20 rad/s, the wind speed is ramped from 8 to 12 m/s. Calibration of the generator is also conducted on data with added noise, as in section 5.2.1, but with different snr.

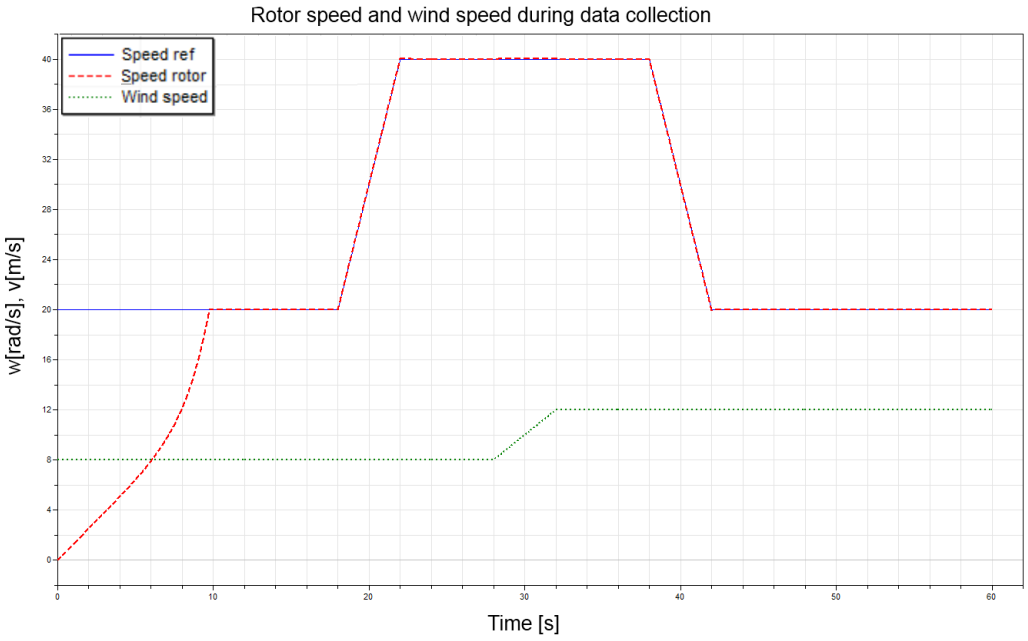

Figure 5.2: Reference rotational speed, rotational speed of rotor and wind speed when simulating the main model for the data collection of the converter and generator experiments

5.2.3 Converter Dataset

The simulation case used for the data collection of the converter is the same as the generator case, see section 5.2.2 and figure 5.2. There are ten inputs for the converter test bench (see figure 5.19), they are the frequency, nominal voltage and the phase on the left and right side of the AC/DC/AC block. Additionally, two control signals for each converter are needed. The electrical power on both sides of the converters are the outputs used to calibrate the component. Datasets with added noise are also generated for the converter case.

5.3 Test Benches and Test Models

One aim of this project is to calibrate and identify the losses that occur in the wind turbine. The components intended are the rotor, the generator and the converter. Calibrating the entire model in one step is too complex since there are too many tunable parameters to work with. In order to get around this, the model can be divided into parts which then can be calibrated individually. Measurements surrounding the subsystems can then be collected and used to drive the submodels.

5.3.1 Mechanical Test Model

A simple mechanical test model was created to examine the calibration approach. The layout of the model is shown in figure 5.3 below. The model describes a series of rotating masses driven by a ramped torque on the left side and a PID-controlled torque on the right side. The submodel, marked by the blue rectangle in figure 5.3, is shown in figure 5.4. By simulating the main mechanical model and storing the values from torqueSensor1, torqueSensor2 as well as the rotational speed and the acceleration of rotor2, (see figure 5.3) a calibration of the subsystem can be done.

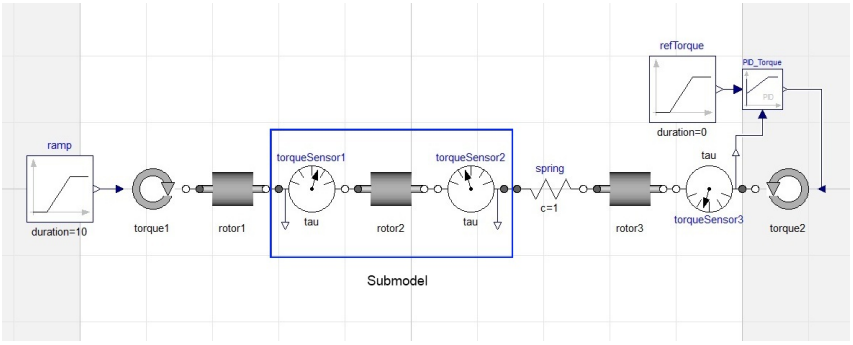

Figure 5.3: Dymola view of the mechanical model

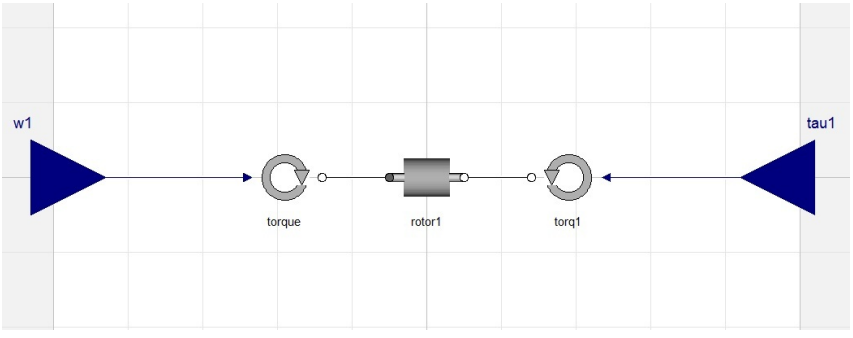

Figure 5.4: Submodel of the mechanical model

Verification

Before attempting to calibrate the submodel it is meaningful to verify the submodel. This is done by using the stored values from the simulation of the mechanical model as inputs to the submodel and leave the rest of the parameters identical to the main model. The velocity and accelleration results of the verification can be seen in figure 5.5.

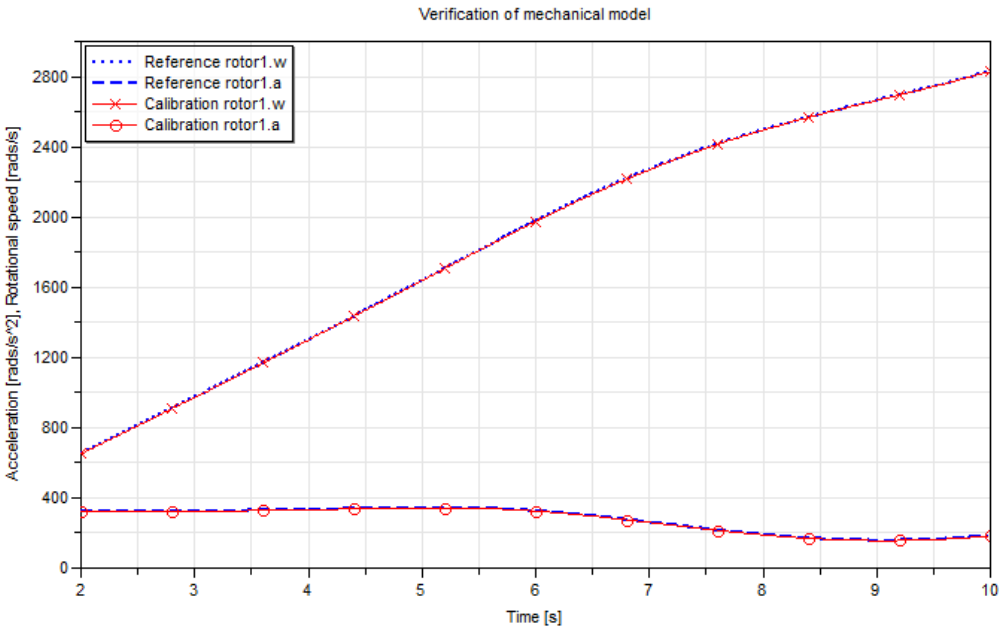

Figure 5.5: Verification of mechanical model, using inputs from the main model. Blue lines show data from the main model and red lines show the results from the submodel using data inputs.

The plot shows that the methodology works, the data taken from the main model simulation can be used as inputs in the verification of the submodel and produce the same results. The plot does not start at time zero since there are transients in the beginning which makes it hard to get accurate results. In order to check the robustness of the method, noise can be added to the measurement data and used for verification. This was done and showed that the submodel produced satisfying results, see appendix A.1.

Calibration

The next step is to calibrate parameters of the model. The first step in this process is to check if the submodel is sensitive to changes of the parameter considered. This can be achieved by varying the parameter and plotting the result as in figure 5.6.

If it is known that the model is sensitive for changes in a parameter, the model can be calibrated to that parameter. The calibration can be done by using the Design Library in Dymola (see section 4.3). In the case of the mechanical model, the inertia, J, is tuned during the calibration.

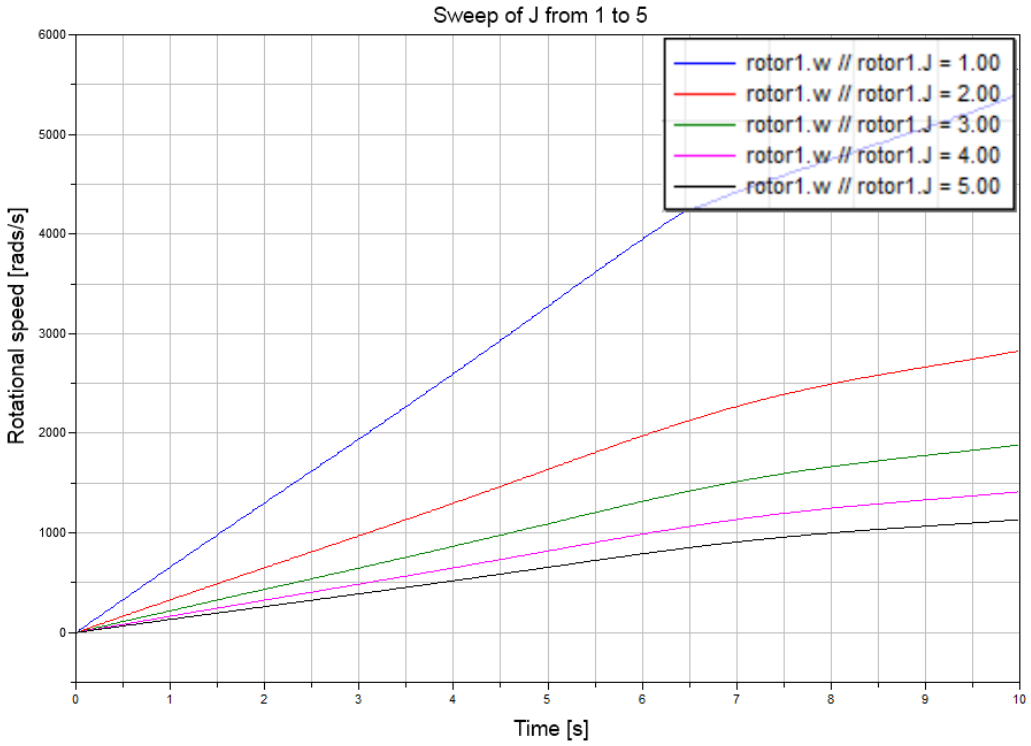

Figure 5.6: The rotational speed of rotor1 in the mecanical submodel depending on time with different values of inertia, J

5.3.2 Electrical Test Model

An electrical model was developed to confront the challanges in the electrical domain which differs from the challanges in the mechanical domain. Three inductor components are connected in series between two voltage sources as shown in figure 5.7. The voltage source to the right is controlled in order to create a scenario similar to the generator and converter case, see section 5.3.5 and 5.3.6. The voltage, the phase and the frequency of the source is varied. In this case the second inductor, ind2, is considered to be the subsystem. The measurements needed in this case are the voltage norm, the electrical frequency before and after the inductor as well as the current. The submodel shown in figure 5.8 has the voltages and the phases as inputs and the resulting current is examined.

Verification and Calibration

When running the submodel with inputs collected from the electrical model, it reproduces the results as shown in figure A.4 in appendix A.2. As in the mechanical case, the parameters of the inductor can be calibrated which is seen in figure A.5 in appendix A.2, where the results after calibration is presented. In the calibration, the parameter default values of the resistance and the self reactance are 2 Ω and the start values are set to 1 Ω and 0.5 Ω. The calibration function tunes the parameters to 1.99983 Ω and 2.00014 Ω for the resistance

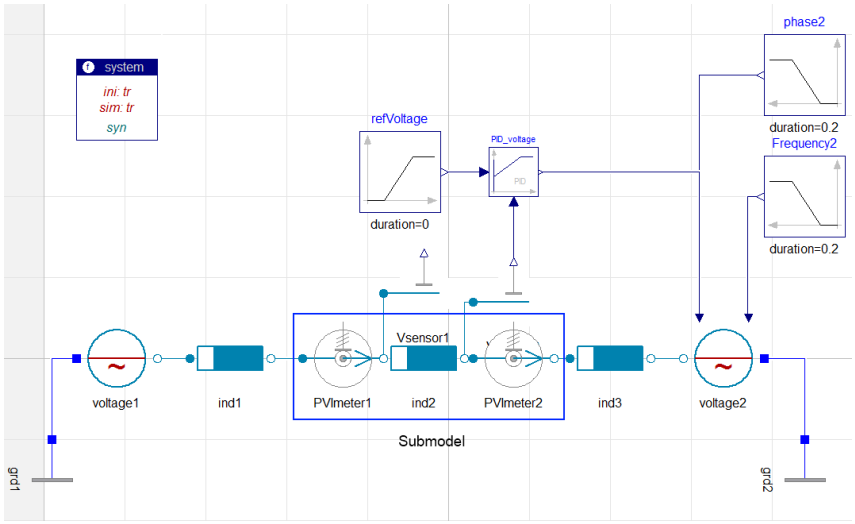

Figure 5.7: The electrical test model

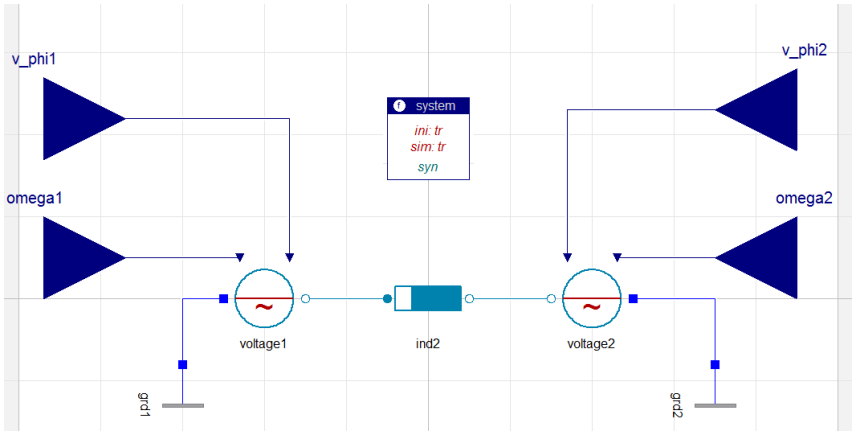

Figure 5.8: The electrical sub model

and reactance respectively. Reactance is a component's opposition to changes in current and voltage.

5.3.3 Wind Turbine

The wind turbine model, referred to as the main model, is shown in figure 5.9. Wind speed is used as input to the rotor component which collects a part of the energy in the wind and transfers the energy to the generator. The generator converts the mechanical energy to electrical energy, the converter block turns the three phase AC to DC and then back to three phase AC which is connected to a simple grid model. The system is controlled by a speed controller that has a reference speed as input, and a DC controller with reference voltage as input which keeps the DC at the requested level. The rotational speed is controlled by changing the power flow to the DC-link and the DC voltage is controlled by changing the power flow to the grid.

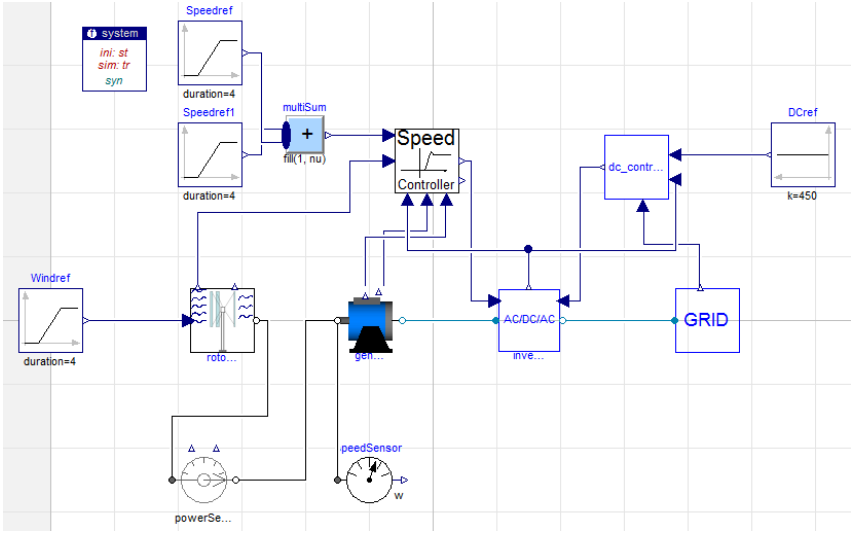

Figure 5.9: The wind turbine main model

5.3.4 Rotor

The test bench for the rotor component is shown in figure 5.10. The test bench uses wind speed and rotational speed as inputs. In the rotor calibration case the resulting power output is used as reference when calibrating. The power is measured as positive when flowing from the wind to the system.

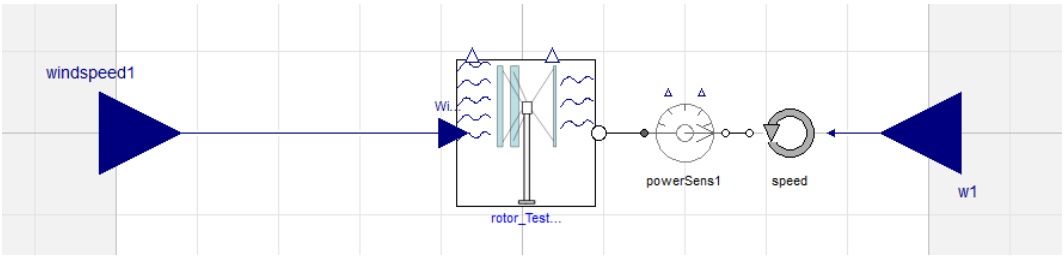

Figure 5.10: Rotor test bench used for calibration of the rotor. The wind speed is set by the input to the left and the rotational speed is set by the input to the right.

The rotor component model can be seen in figure 5.11. The first part of the rotor model is the TSR-component, it calculates the tip speed ratio, denoted λ, according to equation 2.10. The λ-value is sent to the C_p-curve block which determines the percentage of the power in the wind that will be extracted by the rotor, this percentage is dependent on the value of λ and the pitch angle, β, as described by equation 3.1. The shaft of the rotor is modeled with bearing friction and inertia.

Tuners

The parameters which are to be calibrated in the rotor model are the coefficients in equation 3.1. As a first step, a perturbation of the parameters in equation 3.1 is performed to get an idea of which parameters are influencing

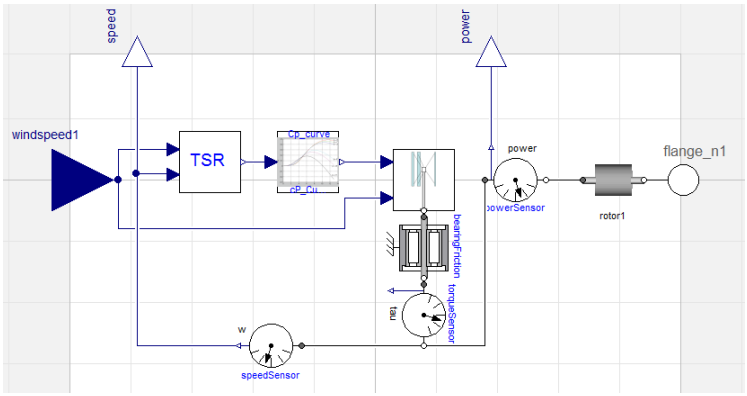

Figure 5.11: Compnents included in the rotor component model used in the rotor test bench

the result the most. The perturbation function increases the value of the parameters with 10% in turns and plots the result. As indicated by figure 5.12, the parameters C_2,C_4 and C_5 are influencing the result the most. They are lumped together to form a parameter group 1. Parameters C_1, C_3 and C_6 are referred to as parameter group 2. The parameters are put into groups of three because the calibration tool can not manage to estimate all six parameters at once. The equation has a variable for the pitch angle, β, which is known and and easy to measure and is thus not treated in the estimation.

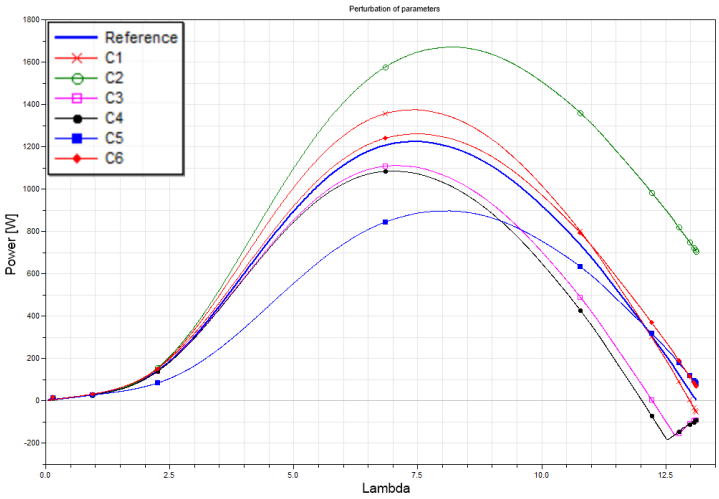

Figure 5.12: The figure shows how the parameters $C_1 - C_6$ affect the power output of the system at different λ values

Calibration

To perform the calibration of the rotor, the values of the parameters $C_1 - C_6$ are all slightly changed from their default values, to resemble initial guesses. The default values and the new start values can be seen in table 5.1. The calibration process is split up into two cases each containing two steps, the

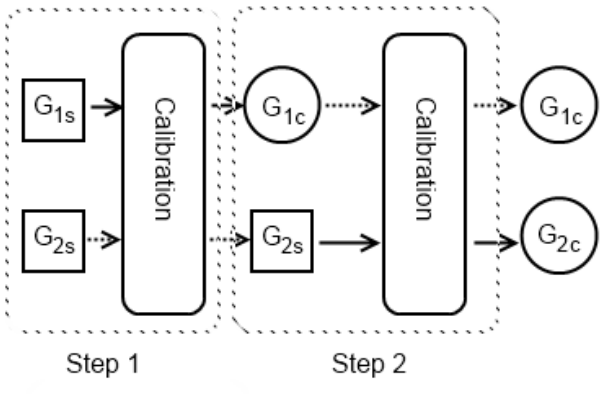

Figure 5.13: Block view of the first calibration case. The subscript s and squares indicate starting values of parameters, subscript c and circles indicate calibrated parameters

first case is illustrated in figure 5.13. The start values of all six parameters are used in the first calibration step where parameters in group 1 are calibrated. In the second calibration step the parameters of group 2 are calibrated using the new values for parameters in group 1. In the second case, the parameters of group 2 are calibrated before the parameters in group 1. The final parameter values from the first and second case are presented in table 5.1 and 5.2. The error sizes in the different cases can be seen in 5.3.How the error is calculated in Dymola is not explicitly accessible. The two cases are run using datasets with different noise levels, referred to as no noise, $snr80$ and $snr60$ in figures and tables. The result from the simulation with start values and values from the final state of the first case, using data with $snr80$ are plotted in figure 5.14 below. The other final simulation results can be seen in appendix A.3.

Table 5.1: Default, start and final values at different noise levels from the first calibration case, group 1 calibrated before group 2

	$C_1(G_2)$	$C_2(G_1)$	$C_3(G_2)$	$C_4(G_1)$	$C_5(G_1)$	$C_6(G_2)$
Default	0.5176	116	0.4	5	21	0.0068
Start	0.3	100	0.5	3	18	0.008
No noise	0.333492	150	0.375928	6.92214	18.854	0.000431302
snr 80	0.333476	150	0.375805	6.92046	18.8552	0.000429775
snr60	0.300093	99.6265	0.500543	3.03951	15.4797	0.00796546

Comments

By studying the tables 5.1 and 5.2, it can be seen that in general the parameter values are closer to the default values after the calibration than before. Since the parameter values in the rotor case have less importance than the actual shape of the curve, the most important result is that the output is closer to the data, as shown in figure 5.14. In figure 5.15, C_p-curves using different parameter values are shown. The values used are from the first and second

Table 5.2: Default, start and final values at different noise levels from the second calibration case, group 2 calibrated before group 1

	$C_1(G_2)$	$C_2(G_1)$	$C_3(G_2)$	$C_4(G_1)$	$C_5(G_1)$	$C_6(G_2)$
Default	0.5176	116	0.4	5	21	0.0068
Start	0.3	100	0.5	3	18	0.008
No noise	0.448172	114.813	0.40501	4.08149	19.0412	0.00001
snr 80	0.448206	114.599	0.405285	4.06875	19.0291	0.00001
snr60	0.402305	100.533	0.507855	3.04209	18.0979	0.00842384

Table 5.3: Error sizes in the two cases with different noises

	Error
Case 1, no noise	1.008 E6
Case 1, snr 80	2.070 E6
Case 1, snr 60	1.629 E8
Case 2, no noise	925937
Case 2, snr 80	1.999 E6
Case 2, snr 60	1.028 E8

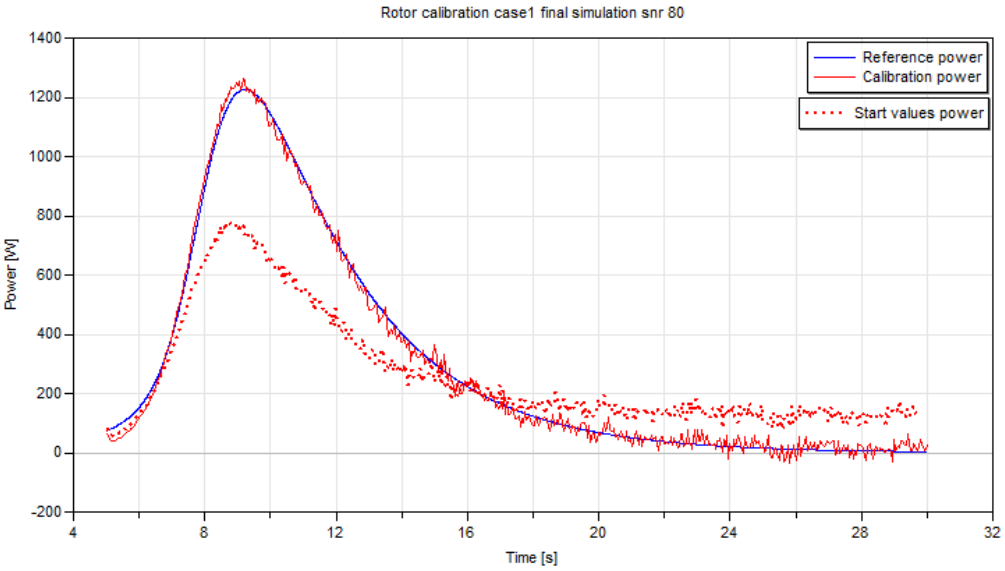

Figure 5.14: Simulation using data with snr 80. Red dotted line is simulated using start parameters, red line is simulated using final valus from the first calibration case at snr 80

case (snr80) as well as using start and default values. It should be noted that there is a small difference between the two cases.

5.3.5 Generator

The generator test bench can be seen in figure 5.16. The rotational speed input determines the rotational speed of the rotor which gives the voltage induced

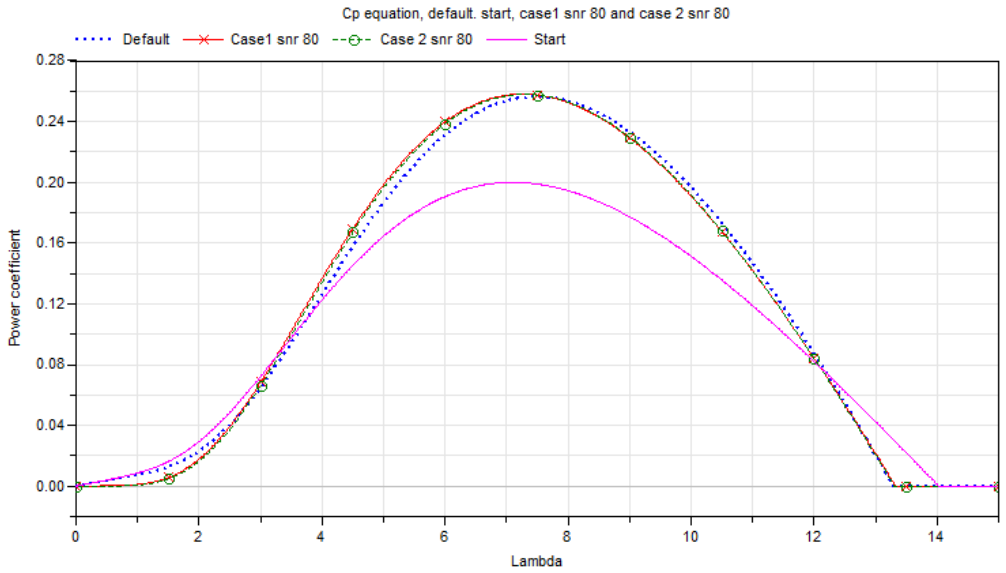

Figure 5.15: The figure show different C_p-curves. The dotted blue curve uses the default calues, the pink curve uses the start values, the red curve with crosses uses values from the first calibration case (snr80) and the green curve with circles uses values from the second case (snr80).

by the generator. The torque of the rotor gives the current, in the test bench the torque is not set and thus allowed to vary. If it would be set, the model would be over specified. Other inputs are the nominal voltage, phase and the electrical frequency.

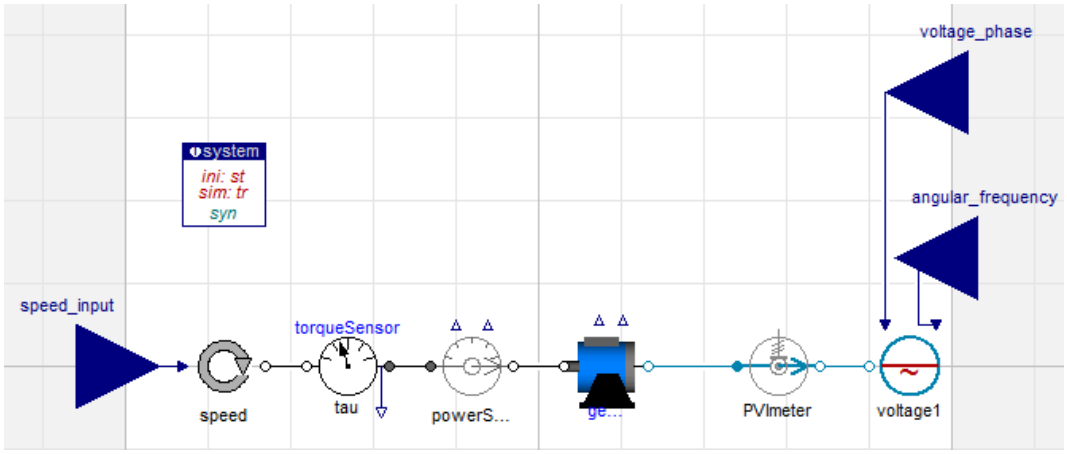

Figure 5.16: Test bench for the generator component

Tuners

The generator component cointains five tunable parameters which affect the power output of the generator. These parameters influence the magnetization, reactance and resistance of the PMSM. A perturbation test was done, the results from the test is shown in figure 5.17. It shows that the parameters psi_{pm},

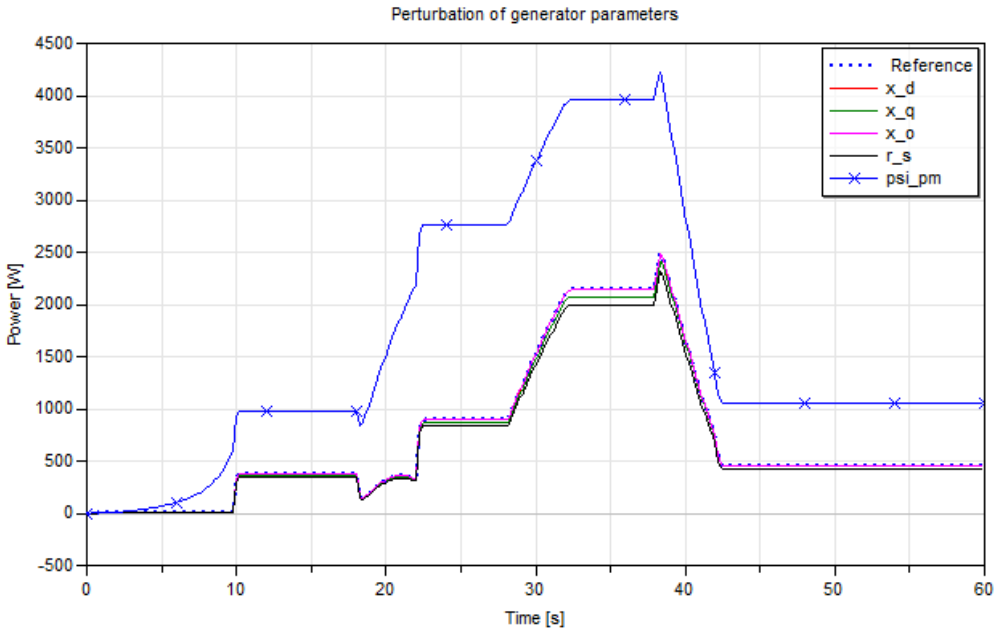

Figure 5.17: Results from the perturbation of the parameters in the generator.

r_s and x_q are the most important and are thus lumped together forming a tuning group. psi_{pm} is the magnetization, r_s is the resistance in the armature and x_q is the reactance in the reactive frame. If calibration of the other parameters, x_d (reactance active frame) and x_o (reactance o frame) are attempted, the values of these parameters tend to go to the upper or lower limit. This is due to that their influence to the output is neglectable. This might not be the case if other dynamics and sizes of the inputs were used in the simulation.

The parameters of the generator can be connected to the losses in the generator by looking in section 2.3.5. r_s in the model corresponds to r_a(winding resistance) in the previous mentioned section. x_q and x_d are correlated to r_m and L in figure 2.9, psi_{pm} is connected to B(magnetic flux density) and the geometry of the generator, also defined in the previously mentioned section.

Calibration

Due to the lack of real measurement data for the generator, the calibration of the generator model was made with synthetic data. The main model (see figure 5.9) was simulated and data were extracted to be used in the generator test bench, with and without added noise. Before the calibration all parameters are slightly changed to be used in the calibration, the changed values are called start values, see table 5.4. In figure 5.18 the resulting electric power curve of the generator test bench can be seen, before and after calibration using the data without noise. The upper black curve is the result when simulating using start values for the parameters. The blue-dotted curve is the reference output from data, the red curve is resulting output after calibration. With the conditions chosen, the calibration function is almost able to tune the parameter values back to the default values. The simulation results after calibration with

disturbed data can be found in appendix A.4.

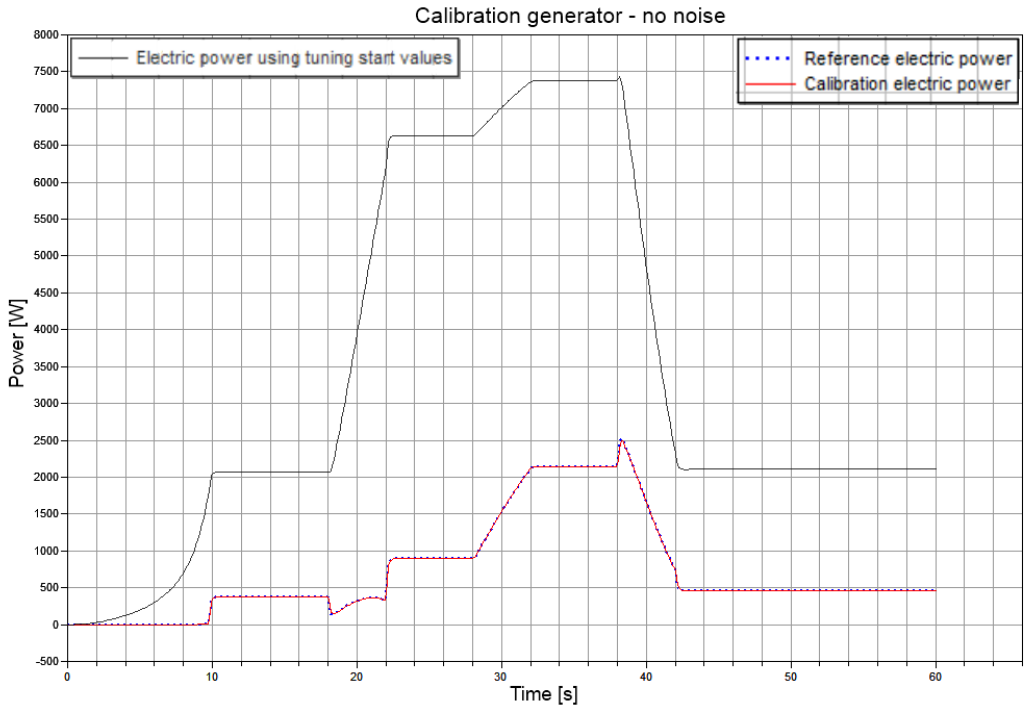

Figure 5.18: Calibration of generator test bench

Table 5.4: Value of parameters after calibration with different levels of noise. The parameters psi_{pm}, x_q and r_s are tuned. Default and start values of the parameters are also listed

	psi_{pm}	x_q	r_s	x_d	x_o
Default	1	0.003	0.5	0.003	0.1
Start value	1.4	0.004	0.7	0.004	0.2
No noise	1.00004	0.00296382	0.502149	0.004	0.2
Snr 120	1.00021	0.00293493	0.499413	0.004	0.2
Snr 100	0.9998151	0.003132	0.567274	0.004	0.2
Snr 80	1.08823	0.000301161	1.2238	0.004	0.2

It should be noted that with a *snr* at 80 or lower the calibration does no longer give accurate results. As can be seen in table 5.4

Comments

When calibrating the generator it was found that the outputs was mainly dependent on three out of five tunable parameters. To be able to determine the other two it might be useful to drive the main model in another way, the parameters might be more important at other speeds or powers. Another comment that should be mentioned about the generator calibration is that the parameters that are tuned has a physical interpretation. It is thus not

meaningful to tune e.g. x_o to an unrealistic value in ordet to slightly reduce the error in the simulation.

5.3.6 Converter

The test bench for the converter is shown in figure 5.19. The left and the right side of the test bench consist of AC-voltage sources which are simulating the dynamics of the generator and the grid respectively. The values of nominal voltage, phase and frequency can be set as input values from a measurement file. Between the AC-voltage sources, an AC/DC/AC converter block is connected, the components of the block is illustrated in figure 5.20. The inputs to the AC/DC/AC block are control signals.

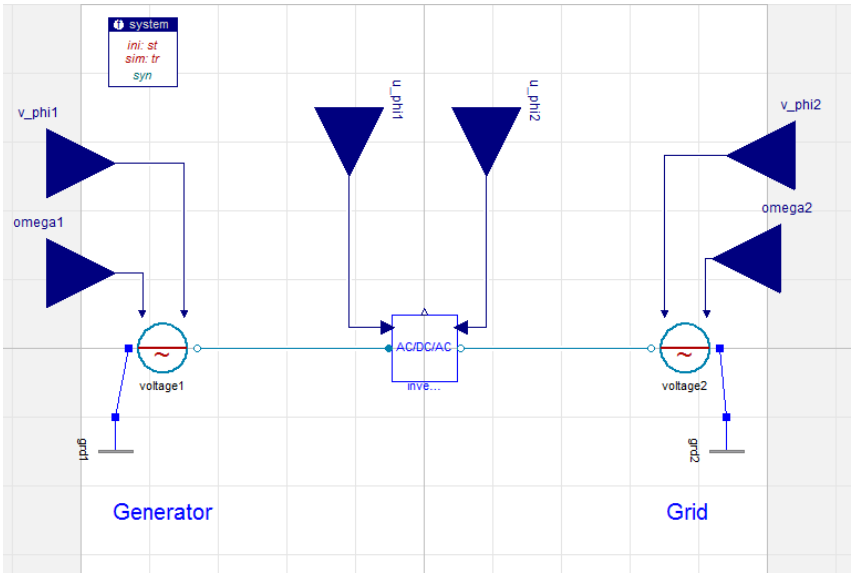

Figure 5.19: Test bench for the converter component

From left to right the AC/DC/AC block consists of an inductance, a converter, a DC-link, a second converter and a second inductance. There are also PVI-meters in order to obtain measurement values. The converters are put together in this way to match the real test set-up. In figure 5.21 the verification of the converter test model can be seen.

Tuners

A parameter perturbation is performed in order to indicate which parameters are affecting the results and in what way. The parameters available for the converter is the forward threshold-voltage, V_f, the switching loss, HSW_{nom} and the switching frequency, f_{switch}. These parameters are described in section 2.3.6. The parameters of the inductors are the resistance, r, and the reactance, r_s, can also be included as tuning parameters. However, the parameter sweep shows that the parameters HSW_{nom} and f_{switch} do not affect the results. This is due to a bug in the structure of the EPL converter component, the mentioned parameters affect the heat loss but the energy lost due to heat is not seen as

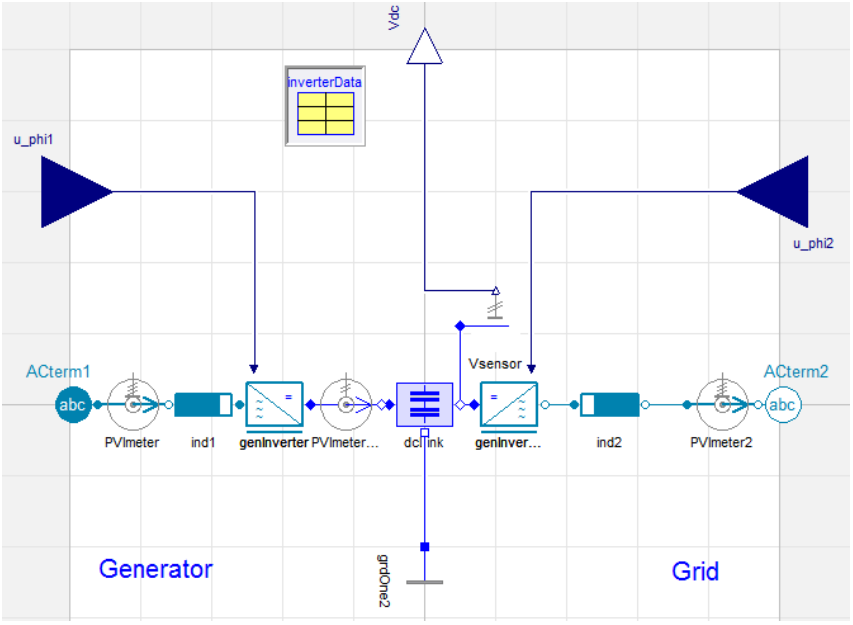

Figure 5.20: AC/DC/AC block

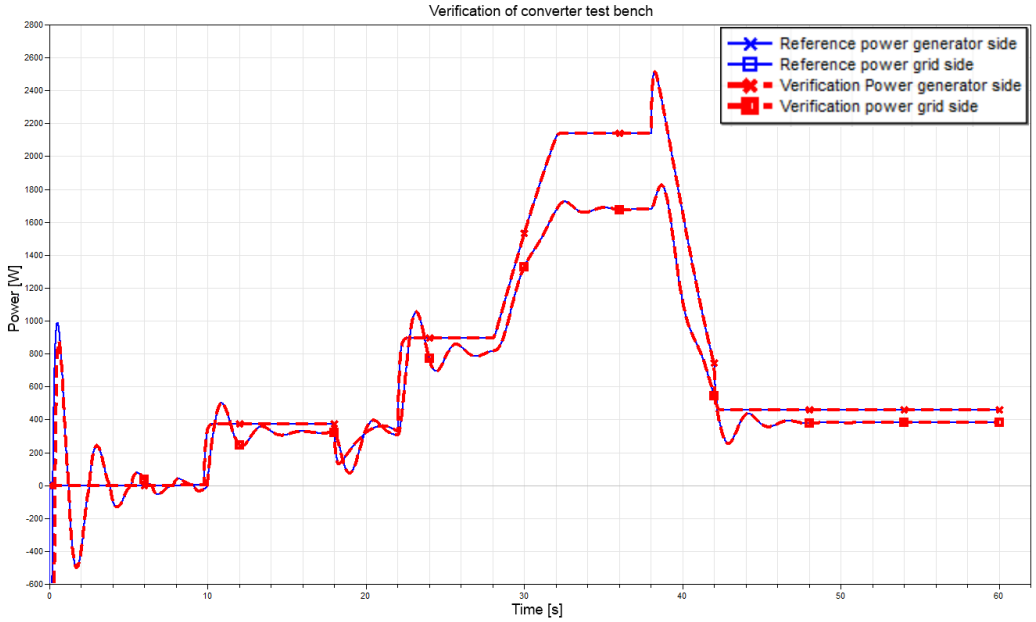

Figure 5.21: Power output before and after the converter block using the main model and the converter test bench

a loss in electrical energy. The power balance is thus not correct. In order to be able to use these parameters as tuners the component has to be modified.

The results from the parameter perturbation (values of the mentioned parameters were changed by 10%) can be seen in figure 5.22. All of the parameters seem to have similar effect on the output but on different scales. This indicates that it will be difficult to tune many parameters at the same time. The figure shows that the parameter with the greatest impact is the resistance of the inductance on the generator side (left) of the converters. The most inter-

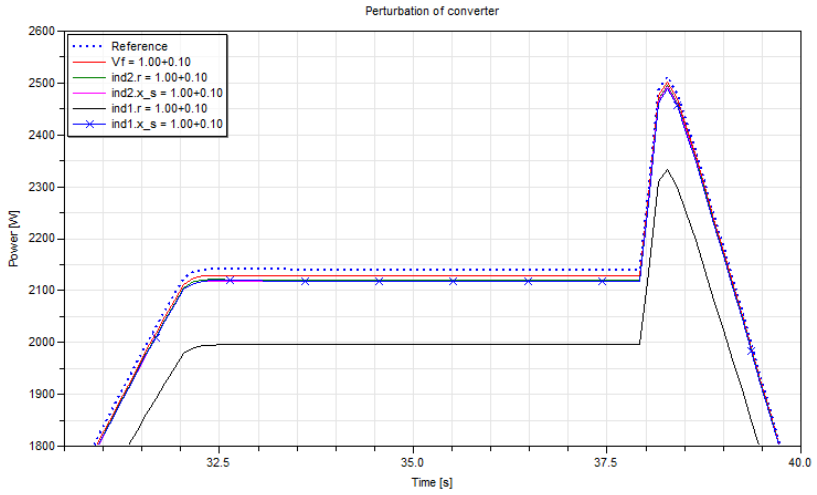

Figure 5.22: How the power on the grid side of the converter test bench is affected by a perturbation of the parameters. The plot is zoomed to the 30-40 seconds interval in order to show the differences.

esting parameter to tune in our case is however the forward threshold-voltage, V_f, since it is a parameter directly connected to the converters. It is however important to have correct values on the other parameters, if a correct value of V_f should be found in a real case.

Calibration using synthetic data

The calibration of the converter is done with V_f as the only tuner. This is because the other parameters mentioned affects the results in a similar way as V_f and make the results unreliable. A demonstration of this effect can be done by calibrating the test bench using undisturbed data. The start values of the parameters V_f, r_{ind1} and r_{ind2} are set according to table 5.5. The resulting parameters from the calibration are seen in table 5.6.

Table 5.5: Starting values for calibration of converter parameters

	V_f	r_{ind1}	r_{ind2}
Case 1	2	2	2
Case 2	0.5	0.5	0.5
Case 3	3	0.5	0.5

Table 5.6: Final values after calibration to undisturbed data

	V_f	r_{ind1}	r_{ind2}
Default	1	1	1
Result case 1	1.3e-10	4.99	0.00147
Result case 2	0.5488	0.000504	0.971
Result case 3	1.34405	0.0479	1.025

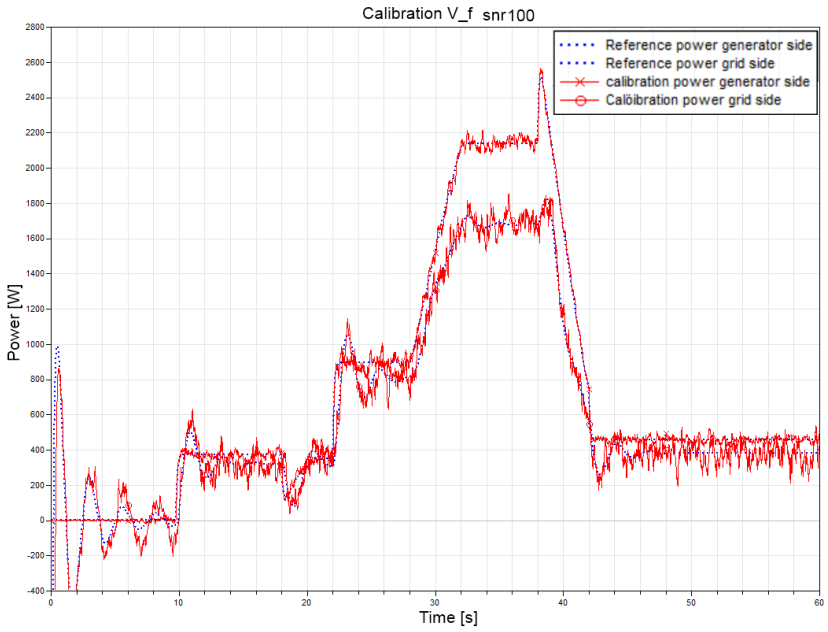

Figure 5.23: Simulation from converter testbench using data with $snr100$ and the calibrated value on V_f

A calibration of the converter was conducted by introducing noise to the same synthetic measurement signals as before and using the default values on all parameters except V_f. The start value of V_f is set to 6 V and the default value of V_f is 1 V. The snr values used for this calibration was 80, 100 and 120, as well as one calibration where no noise was added. The result from the calibration using snr 100 is shown below in figure 5.23. The results from the other cases can be seen in figures A.16 and A.17 in appendix A.5. The parameter values that were obtained for the different cases are summarized in table 5.7.

Table 5.7: Shows the results from calibration of the V_f parameter using different signal to noise ratios. The start value of V_f is set to 6 V in all cases, the default value of V_f is 1 V

snr	V_f final
No noise	0.952484
120	0.96999
100	0.960513
80	4.10364

In figure 5.23 the calibration result is seen. The calibration and simulation are done using data with noise value snr 100. The blue dotted lines is reference power from data nad the red line with crosses is the power on the generator side from the simulation. The red line with circles are the power output at the grid side. It should be noted that the power on the generator side is higher than the power on the grid side most of the time, during those periods the difference can be seen as a loss. During short periods the power on the grid

side is higher than on the generator side. More power is taken from the DC-line than is added to DC-line during those periods.

Calibration using real data

Data collection Real data was collected from a laboratory set-up of the back to back AC/DC/AC converter, the device will later be used in the LTH test unit. Since the test unit was not operating at the time of this project, the converter data collection was done in the laboratory. A three phase generator was used and the generator rotor was driven by a DC-motor. The generator was connected to the converter which on the other side was connected to the grid. By having access to the control system of the converter and with help from staff at the university, data could be collected. 26 different values were collected with a sampling frequency of 10 kHz. What type of data collected are presented in appendix B.2. During the data collection the reference voltage level between the two converters was set to 400 V, the power to the DC-motor was controlled in order to get data at different power levels. Measurements where conducted during approximately 230 s resulting in a data file size of 1 Gb. To reduce the file size, a sparser version of the data set is produced by choosing every tenth value from the original dataset, thereby reducing the sampling frequency to 1kHz. It is necessary to reduce the sampling frequency since the large file size makes the complete dataset unsuitable to work with, it is important to be careful when doing this since a too low sampling frequency will not capture the events in an accurate way. A comparison between complete data and sparse data can be done in figure 5.24 and 5.25.

Filtration Filtration of some of the data is performed in order to reduce the noise. Two different MatLab filters are used, the *sGolay*-filter, (Savitzky-Golay) used for signals that does not oscillate around zero, and the *FiltFilt*-function which was used for signals that oscillate around zero, e.g. the instantaneous AC voltage values. The two filters used do not shift the data in time which is important when the signals are used in calibration, this since they have to match the other inputs in time. Two examples of filtered data can be seen in figure 5.24 and figure 5.25. The data in figure 5.24 is filtered with the *FiltFilt*-function and the data in figure 5.25 is filtered using *sGolay*. Other important signals are presented in appendix C.

Managing the data for use in Dymola The data differ slightly from the synthetic data taken from the Dymola model. In Dymola it is possible to access the parameter V_{norm} directly. V_{norm} is expressed with equation 5.1.

$$V_{norm} = \sqrt{{V_a}^2 + {V_b}^2 + {V_c}^2} \tag{5.1}$$

The data collected in the laboratory did not contain V_{norm}, however, it can be calculated since the data included the phase voltages V_a, V_b and V_c.

Other inputs to the converter test bench are the voltage phase angles (one phase angle is needed for each side of the converter test bench), but these

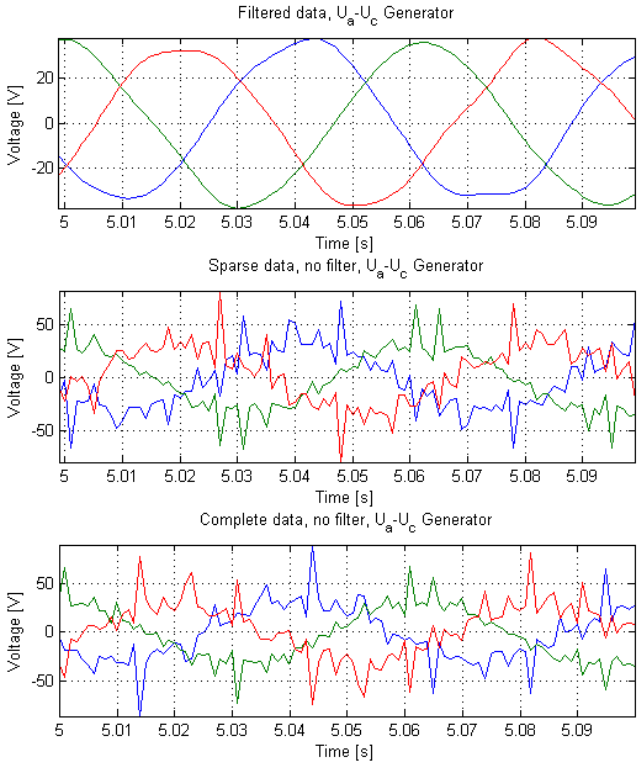

Figure 5.24: Voltage measurements from the generator side. Top: filtered sparse data, middle:sparse data, bottom: complete data

values were not possible to collect in the laboratory. If the electrical angle, θ_e, and the voltage phases are known, the voltage phase angles can be calculated using Dymola. No direct measurement of $theta_e$ is done but it can also be calculated from other measurements.

An analogy can be done to motion, the θ_e-value can be seen as the position of the electrical voltage. The position of a wheel with radius equal to one can be calculated by knowing the frequency at every time point by taking the time integral of frequency and multiplying with two times π. The electrical angle θ_e can then be calculated from the measurements of frequency as

$$\int_0^T f(t) \cdot 2\pi \, \mathrm{d}t \tag{5.2}$$

When using the synthetic data the control signals are taken directly at the input to the converter, as shown in figure 5.26. These values were not available from the real measurements but instead data from parts in the speed and DC controller are available, see figure 5.27.

Since the available values differ from the values sampled from Dymola, the testbench is altered slightly. The version used for real measurements is shown in figure 5.28.

Some effort has been put into filtrating the measurement data and inserting

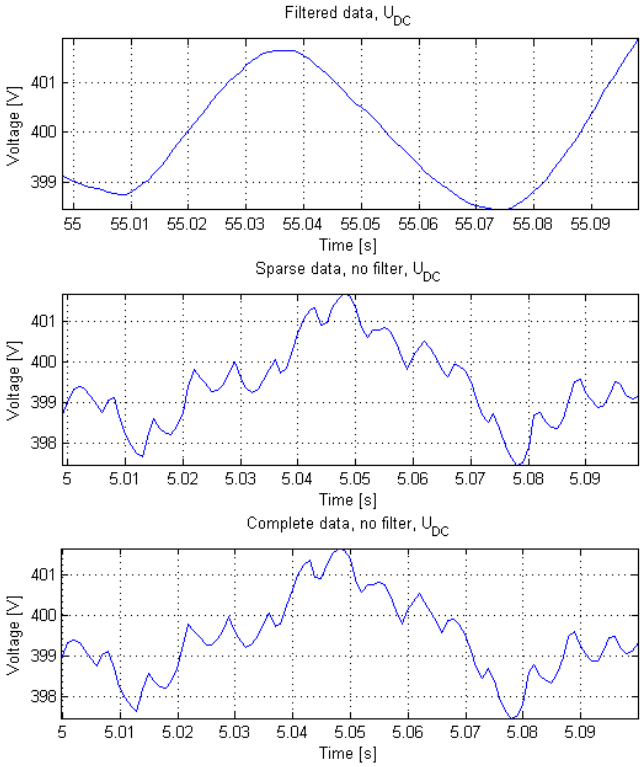

Figure 5.25: Voltage measurements from the DC-link between the two converters. Top: filtered sparse data, middle: sparse data, bottom: complete data

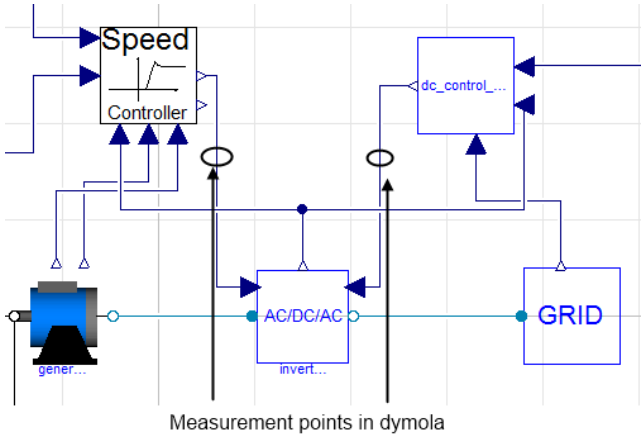

Figure 5.26: Where the control signals are measured in Dymola

it into the test model described in figure 5.28. However, no realistic results have been achieved when doing this. A possible reason for this can be that the model structure is too far from the real system. Other possible sources of error can be that the data have been filtered in an incorrect way or that the inputs are treated in the wrong way. Some effort has been put to check these possibilites but no solution has been found and no source of error has

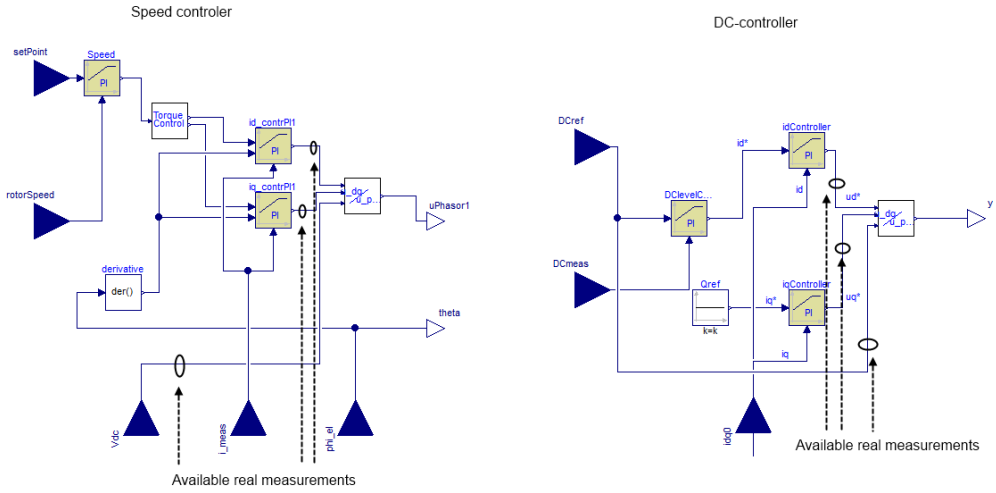

Figure 5.27: Available control data from laboratory collection

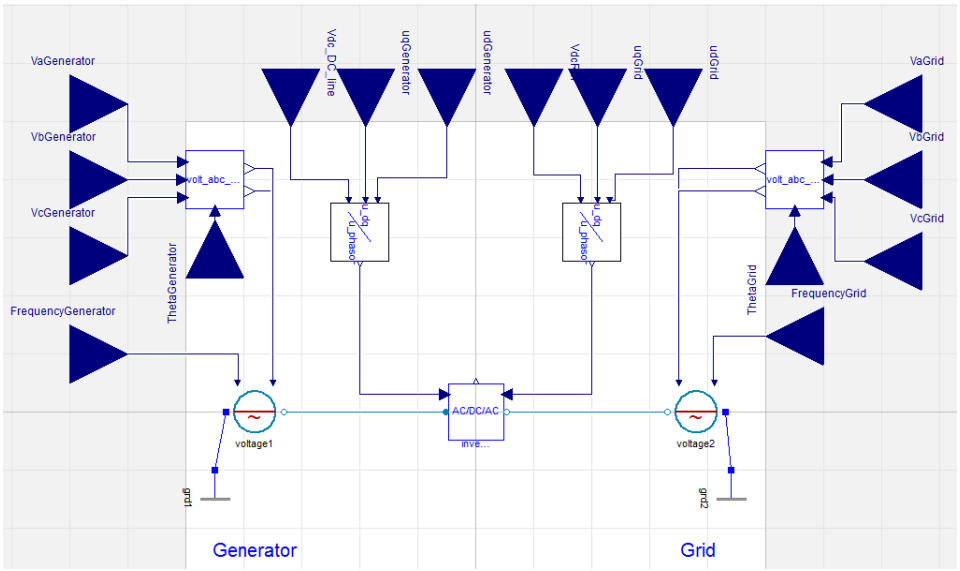

Figure 5.28: Test bench used for the real data set. The u_{dq} block converts measurements into signals compatible with the converter models. The $volt_{abc}$ block converts the phase measurements and theta measurements to signals compatible for the voltage source components

been ruled out. Another more fundamental problem with the testbench is that many inputs are needed and that a small error in one or two of the signals can result in a large error.

5.4 Discarded approach

Before we arrived to the method described above in section 5.3 an alternative set of test benches were created. These will be described below followed by some reasoning to why they were discarded. There are of course a lot of similarities between the two approaches. The discarded approach as well as the final approach include the split up of the large system into the smaller components; rotor, generator and converter for reasons mentioned in 5.3.

Rotor

The rotor model is very similar to the version in the final approach. The wind speed and the torque are used as inputs and the speed or the power of the rotor component in figure 5.29 could then be used as a result to calibrate against. In this version the torque is a linear speed dependent torque that increases linearly with the rotational speed of the shaft. This resembles the actual case of having the shaft connected to a generator which in turn is connected to the grid at the shaft, although not with any high accuracy.

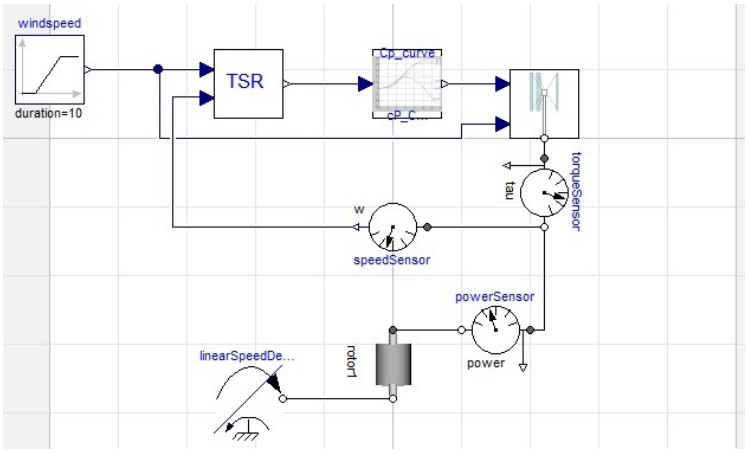

Figure 5.29: The discarded setup for calibration of the rotor where the rotor is connected to a linear speed dependent torque.

Generator

The discarded generator test bench includes a torque which is used as input and a resistance is used as load. The speed of the generator is controlled with a speed controller which alters the signals to the converter, controllinng the voltage and the phase of the voltage in the three phase line. The torque from the rotor can be used as input, and the grid connection can to some degree be estimated by the resistance, although not with any high accuracy. The parameters of the generator could be calibrated against measurements of the power in the three phase line.

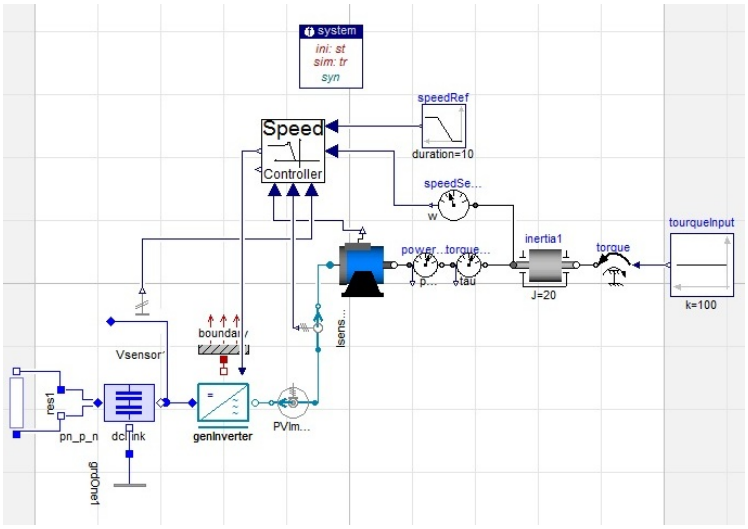

Figure 5.30: The discarded set-up for generator calibration using torque as input and a resistance and a DC-link as load

Converter

The discarded converter test bench can be seen in figure 5.31. The test bench is controlled by PID-controllers and contains two voltage sources, one DC and one three phase AC. An inductance is introduced on the AC-line to smoothen the signal from the converter. If the values of current and voltage are known at both sides of the inverter as well as the parameters of the controls, the set-up could be calibrated against power.

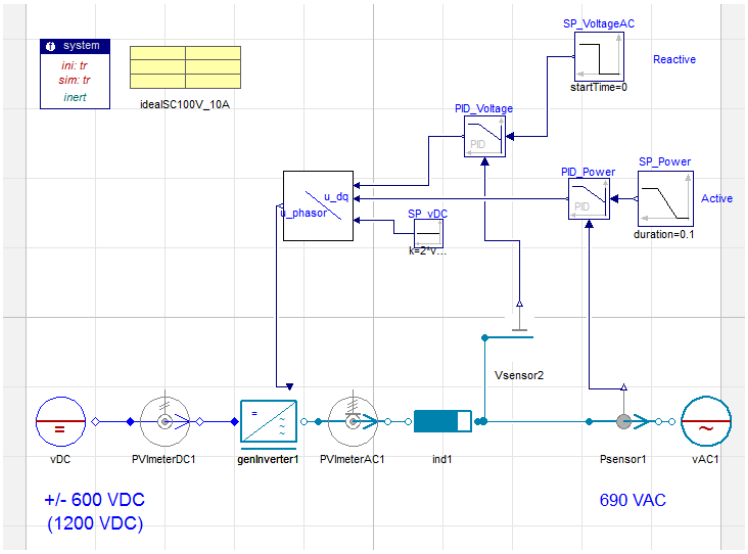

Figure 5.31: The discarded converter test bench with voltage sources as input and controllers for the inverter

Comments

The major difference between the two approaches is that in the discarded versions the control systems are included in the test benches. However, using an approach including control systems to calibrate parameters in the model requires the controls of the model and the actual plant to be identical. Apart from the requirement that the control system should be the same, the reference signals to the control system have to be known. In the chosen approach there is instead the signals are required to be known. This can be regarded as being closer to the actual parameters that we want to determine.

Chapter 6

Discussion

6.1 Evaluation of the Project

The purpose of this project was to calibrate a model of a vertical axis wind turbine to data collected from a prototype turbine located at Lund University. In order to do this, a previously developed wind turbine model [2] based on the SPOT-library was converted to the EPL. This were followed by the development of test benches for the calibration of the rotor, the generator and the converter. The calibration against real data were preceded by a calibration against synthetic data. The limitations of the project are listed in section 1.2.1.

Translation of models and components from SPOT to EPL was successfully performed. Many but not all tests developed using SPOT were translated. Simulations of those translated are shown in section 3.2.2, the figures indicate that the models manage to produce the same results.

Two sets of test benches were developed, the one developed first was discarded as not being a good approach. The second set needed more inputs but did not include any controls which made it a feasible approach. The second set of test benches were calibrated against data collected from a model of the entire turbine, referred to as the main model. Calibrations were performed, using both disturbed (with added noise) and undisturbed data. The rotor model and the generator model contained several parameters suitable for tuning and the calibration against synthetic data can be regarded as successful. For the converter model, only one parameter was found suitable for tuning. To be satisfied with the converter calibration, at least one or two more parameters should be tunable.

Real measurement data were taken from the AC/DC/AC-converter. The data have been examined and filtered in order to prepare for calibration. Examples of the data before and after filtration can be seen in appendix C. Calibration using the real data turned out to be complicated. The issue is believed to be in the number of inputs necessary for the converter calibration model, there are as many as 16 inputs. This means that there are many sources of error and the model seems to be unable to handle small disturbances in only a few inputs. Unfortunately, data from other components of the wind

turbine were not available in time to be used for calibration. It would have been interesting to see if the models could be correctly calibrated to the real measurement data, for example if the used C_p-equation would be able to fit the C_p-curve from the LTH test unit.

Since calibration against real measurement data has not been succeeded, the origin of the energy losses have not been identified. This is partially due to the non-availability of measurements from other components other than the converter. The other components should be easier to use for calibration against real measurement data since they do not have control signals as inputs. However, the experience from the converter case shows that even if data from other parts of the plant are collected, a considerable amount of work is needed before calibration using real measurement data can be finalized.

6.2 Experiences and Difficulties

During the course of the working process, several obstacles have been encountered. Especially setting up test benches for the different components and translating existing models from the SPOT Library to EPL was shown to be more troublesome than expected. How a test bench should be designed for use in calibration was unclear. Different set-ups were developed with the purpose of finding one which could be used to calibrate against measurement data. This is time consuming work, where often the trial and error approach was used. A considerable amount of time was spent on trying to get the converter test bench to work in switched mode. After some significant work had been put down, we concluded that the difficulties were to be found in the structure of the EPL converter and the sensitivity of modeling using EPL. Concerning the converter case, the power balance connection between the electrical and the thermal domain is nonfunctional. As a consequence, parameters which should have influenced electrical losses by emitting them as thermal losses, did not have any effect on the electrical domain.

Before collecting data for a calibration process a lot has to be known about how the calibration is going to be performed. When the first data collections during this project were conducted, too little about the calibration process was known. This resulted in putting time and effort into collecting data which were not useful.

6.3 Future Work

Calibration

When performing the rotor calibration the parameters were put into two groups, one that has a large effect on the outputs and one that has small effect on the outputs. If further work would be done, it would be interesting to see how arranging the parameters in other ways would affect the results. When examining the generator it was found that two out of five parameters

hardly affected the outputs. It is believed that to calibrate those two parameters, the main model has to be driven in another way giving more information of the influence of those parameters.

Real measurement data

When real measurement data from the entire system are available, the test benches developed should be useful to utilize for the calibration of the components. Measurement data should be collected so that the number of inputs in the test benches are minimized.

Some work has been put into filtering the collected data, but more can be done in this region.

Models

- The converter models in EPL needs additional work for solving the power balance problem. Several parameters which influence the power loss in the EPL converter do not give a result in output power loss.
- Calibration can be done using a more advanced converter, such as the switch converter.
- The C_p-equation used in the rotor model can be modified to better correspond to the characteristics of the LTH test unit
- The model of the rotor is now based on a C_p equation according to equation 3.1. It would be interesting to investigate the fluid dynamics of the LTH test unit´s rotor and create an aerodynamic model of the component. This would facilitate rotor improvements.

Bibliography

[1] I. E. Agency, "World energy outlook 2011," tech. rep., International Energy Agency, 2011.

[2] J. Petersson and P. Isaksson, "Modeling and simulation of a vertical wind power plant in dymola/modelica," Master's thesis, Lund University, 2012.

[3] H. Riegler, "Hawt versus vawt: Small vawts find a clear niche," Refocus, vol. 4, no. 4, pp. 44 – 46, 2003.

[4] D. S. AB, Dymola - Dynamic Modeling Laboratory User Manual. Dassault Systèmes AB, 12 ed., May 2012.

[5] M. Gerdin, Identification and Estimation for Models Described by Diferential-Algebraic Equations. PhD thesis, Linköpings Univertsitet, 2006.

[6] S. Gedda, "Calibration of modelica models using derivative-free optimization," Master's thesis, Lund University, Faculty of Engineering, 2011.

[7] A. R. J.F. Manwell, J.G. McGowan, Wind Energy Explained - Theory, Design and Application. John Wiley & Sons Ltd, 2009.

[8] R. I. Argatov, "Energy conversion efficiency of the pumping kite wind generator," Renewable Energy, vol. 35, pp. 1052–1060, 2010.

[9] H. v. R. Erich Hau, "Basic concepts of wind energy converters," in Wind Turbines, pp. 67–80, Springer Berlin Heidelberg, 2006.

[10] H. v. R. Erich Hau, "Rotor aerodynamics," in Wind Turbines, pp. 91–160, Springer Berlin Heidelberg, 2006.

[11] K. Pope, G. F. Naterer, I. Dincer, and E. Tsang, "Power correlation for vertical axis wind turbines with varying geometries," International Journal of Energy Research, vol. 35, no. 5, pp. 423–435, 2011.

[12] E. B. Marco Raciti Castelli, "Comparison between lift and drag-driven vawt concepts on low-wind site aeo," World Academy of Science, Engineering and Technology, vol. 59, pp. 1677–1682, 2011.

[13] A. F. Mazharul Islam, David S.-K Ting, "Aerodynamic models for darrieus-type straight-bladed vertical axis wind turbines," Renewable and Sustainable Energy Reviews, vol. 12, pp. 1087–1109, 2008.

[14] S. Eriksson, H. Bernhoff, and M. Leijon, "Evaluation of different turbine concepts for wind power," Renewable and Sustainable Energy Reviews, vol. 12, no. 5, pp. 1419 – 1434, 2008.

[15] J. L. Loth, "Aerodynamic tower shake force analysis for vawt," Journal of Solar Energy Engineering, vol. 107, no. 1, pp. 45–49, 1985.

[16] T. M. S.M. Muyeen, Juinji Tamura, "Wind turbine modeling," in Stability Augmentation of a Grid-connected Wind Farm, Green Energy and Technology, pp. 23–65, Springer London, 2009.

[17] M. Alaküla and P. Karlsson, Power Electronics, Devices, Converters, Control and Applications. Department of Industrial Electrical Enginering and Automation, Lund Institute of Technology, 2010.

[18] C. Bhende, S. Mishra, and S. Malla, "Permanent magnet synchronous generator-based standalone wind energy supply system," Sustainable Energy, IEEE Transactions on, vol. 2, pp. 361 –373, oct. 2011.

[19] A. de Almeida, F. Ferreira, and J. Fong, "Standards for efficiency of electric motors," Industry Applications Magazine, IEEE, vol. 17, pp. 12 –19, jan.-feb. 2011.

[20] A. D. Hansen and G. Michalke, "Modelling and control of variable-speed multi-pole permanent magnet synchronous generator wind turbine," Wind Energy, vol. 11, no. 5, pp. 537–554, 2008.

[21] J. Tamura, "Calculation method of losses and efficiency of wind generators," in Wind Energy Conversion Systems (S. Muyeen, ed.), Green Energy and Technology, pp. 25–51, Springer London, 2012.

[22] "Chapter 11 - unified power quality conditioner (upqc)," in Power Quality in Power Systems and Electrical Machines (E. F. Fuchs and M. A. Masoum, eds.), pp. 443 – 468, Burlington: Academic Press, 2008.

[23] S. Bacha, J. De La Ree, C. Heyde, A. Lindemann, A. Orths, Z. Styczynski, and J. Wankowicz, "Electrical engineering," in Springer Handbook of Mechanical Engineering (K.-H. Grote and E. K. Antonsson, eds.), pp. 1421–1510, Springer Berlin Heidelberg, 2009.

[24] S. Krauter, "Inverters," in Solar Electric Power Generation, pp. 49–60, Springer Berlin Heidelberg, 2006.

[25] S. Maniktala, "Chapter 8 - conduction and switching losses," in Power Sources and Supplies (M. Brown, ed.), pp. 247 – 278, Burlington: Newnes, 2008.

[26] V. Petitfils, "Setup and performance test of a small-scale vertical axis wind turbine," Master's thesis, Lund University, 2011.

[27] L. Ljung, System Identification, Theory for the User. Prentice Hall, 1999.

Appendix A

Figures

A.1 Mechanical model

The plots in this section are from the simulations of the mechanical test model. The simulations are done using data as inputs to the submodel. The blue lines are reference values from data, and the red lines are verification values from the submodel.

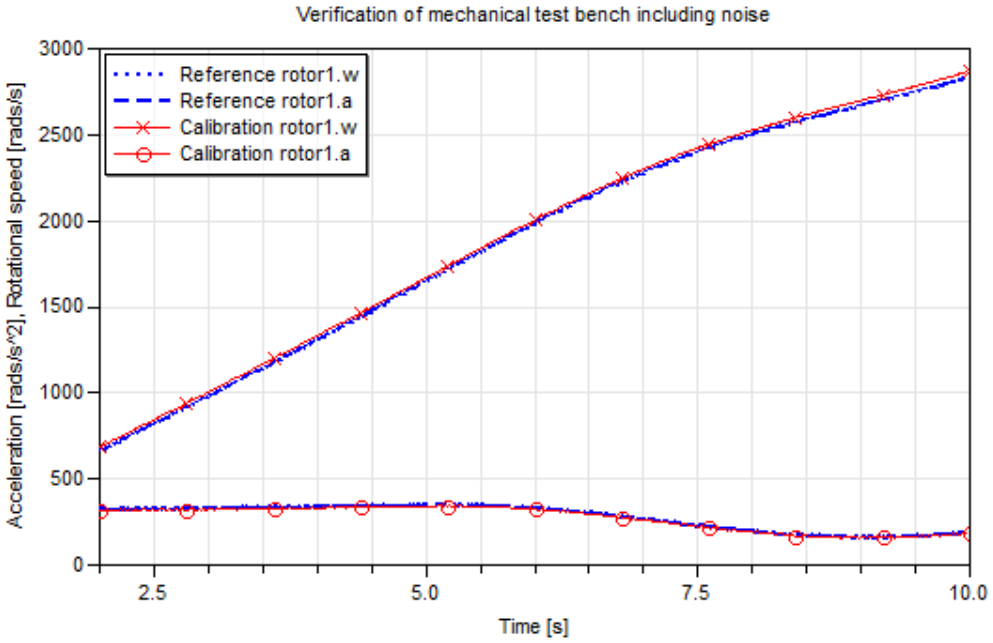

Figure A.1: Verification of mechanical model, using disturbed inputs from the main model. Blue lines show disturbed data from the main model and red lines show the results from the sub model.

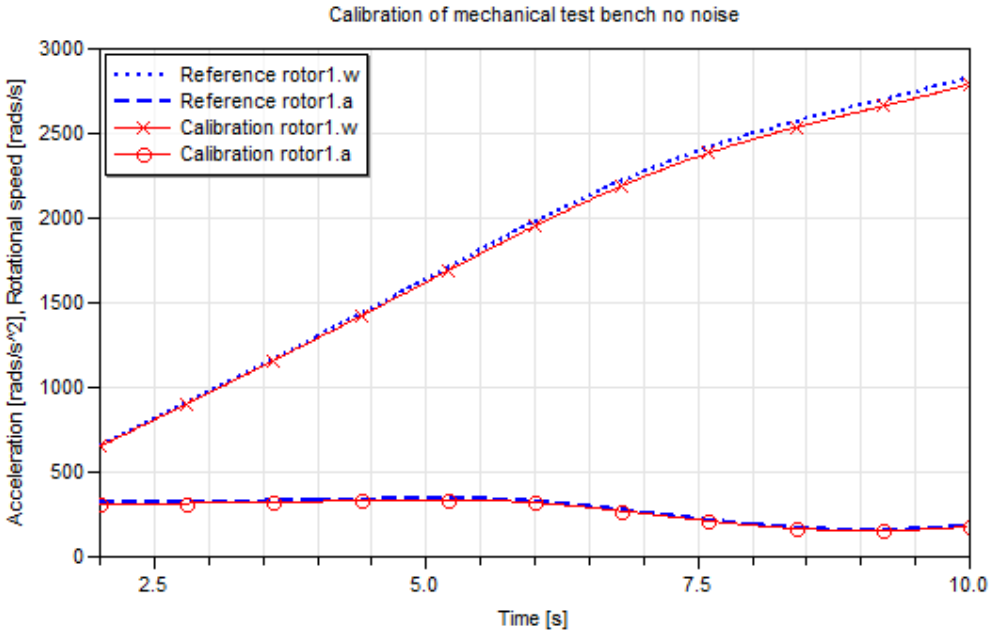

Figure A.2: Calibration of mechanical model, using data whitout noise. Blue lines show reference data and red lines show simulated values after calibration

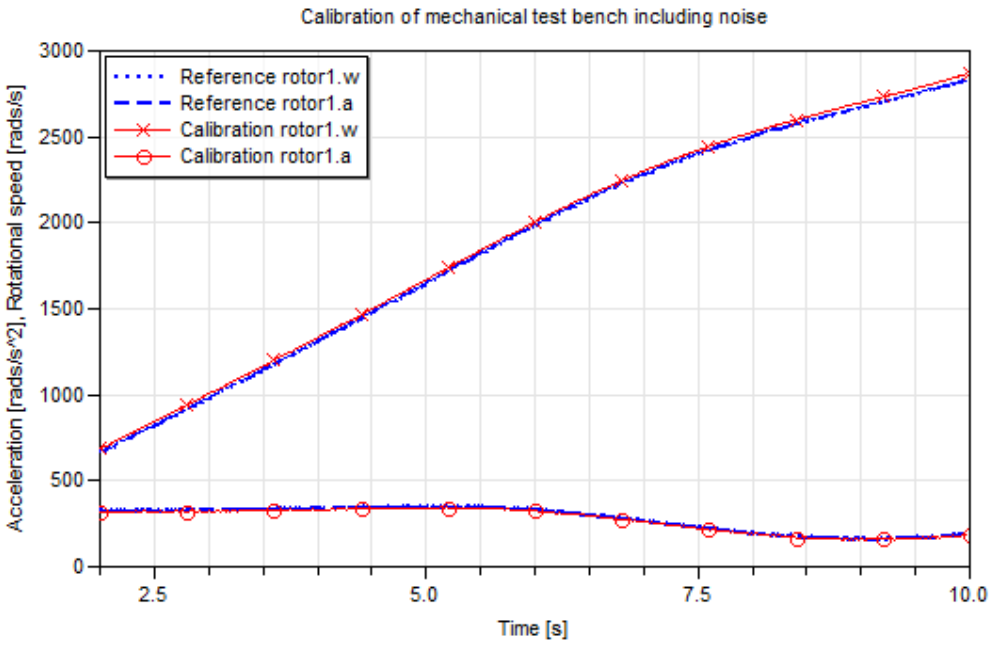

Figure A.3: Calibration of mechanical model, using data whit noise. Blue lines show reference data and red lines show simulated values after calibration

A.2 Electrical model

The plots in this section are from the simulations of the mechanical test model. The simulations are done using data as inputs to the submodel. The blue lines are reference values from data, and the red lines are verification values from the submodel.

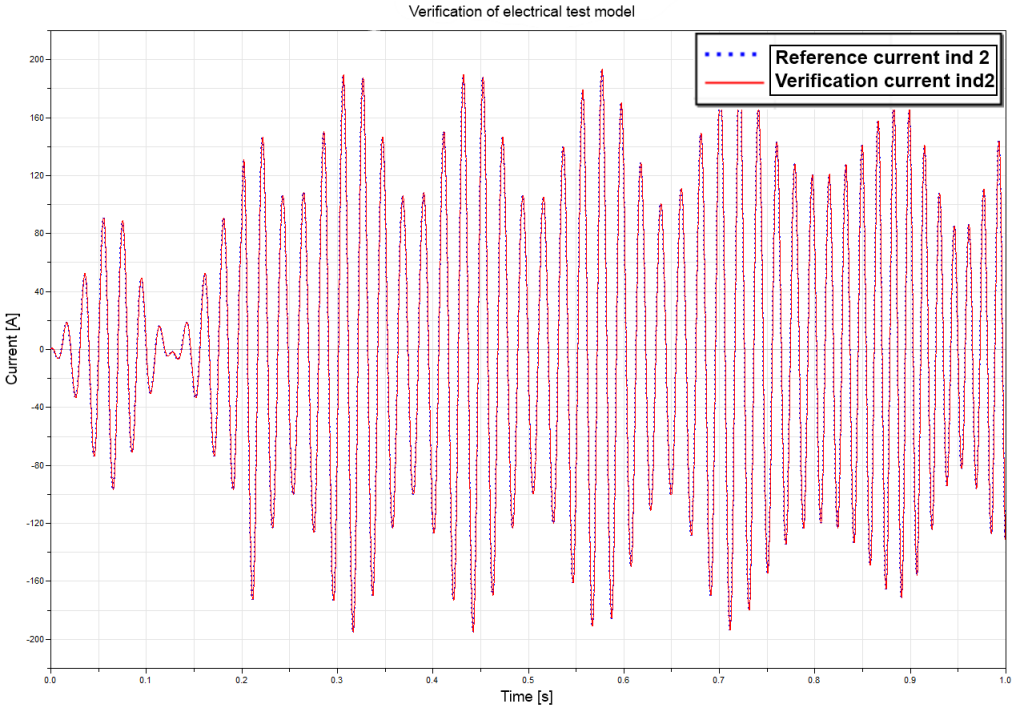

Figure A.4: Verification of electrical test bench. Shows one of the phase currents through ind2, the blue dotted line is from the reference data and the red line is from the verification where the sub model is simulated with data.

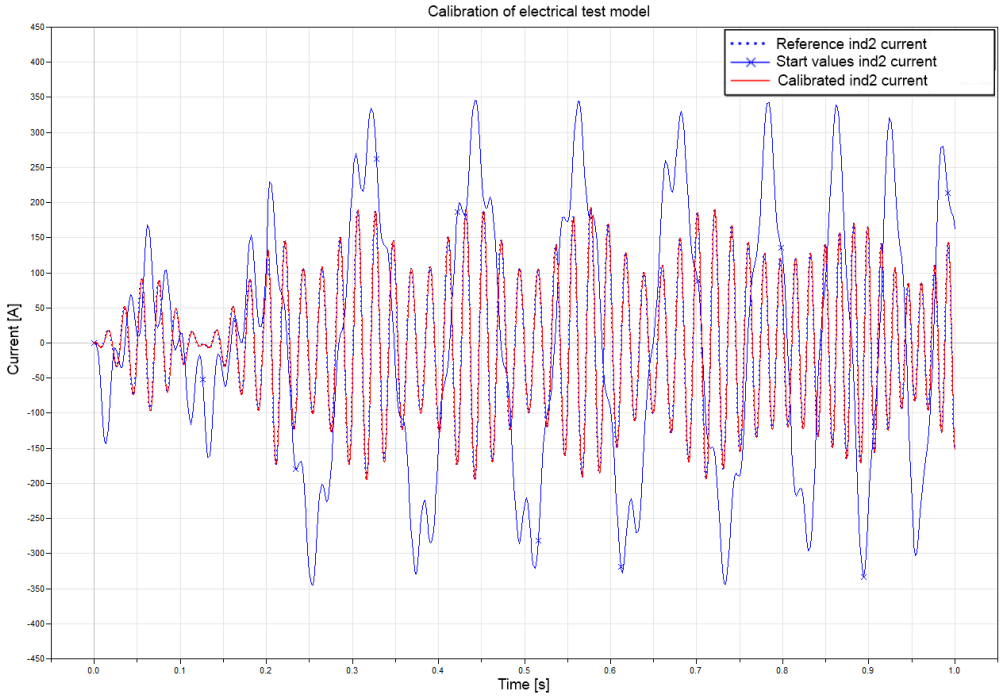

Figure A.5: Calibration of electrical test bench. Shows one of the phase currents through ind2, the blue dotted line is from the reference data, the red line is fro the calibration case where parameters have been changed to make the output fit the reference data. The blue line with crosses are from the simulation before the parameters where calibrated.

A.3 Rotor

The plots in this section are from the simulations of the rotor when a calibration has been done. The calibrations and simulations are done using data with different noise levels. The noise level associated to each simulation is to be found in the figure texts. The blue lines are reference power from data. The red lines are power form the simulations.

Final simulations from the first case

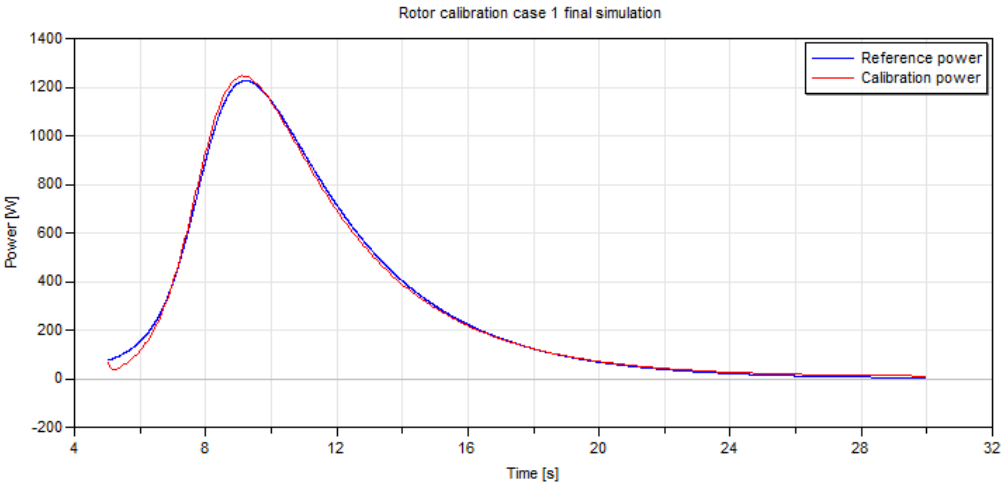

Figure A.6: Simulation of the rotor using parameters from the first calibration case and data whitout noise. The blue lines are reference power from data. The red lines are power form the simulations when calibration has been done.

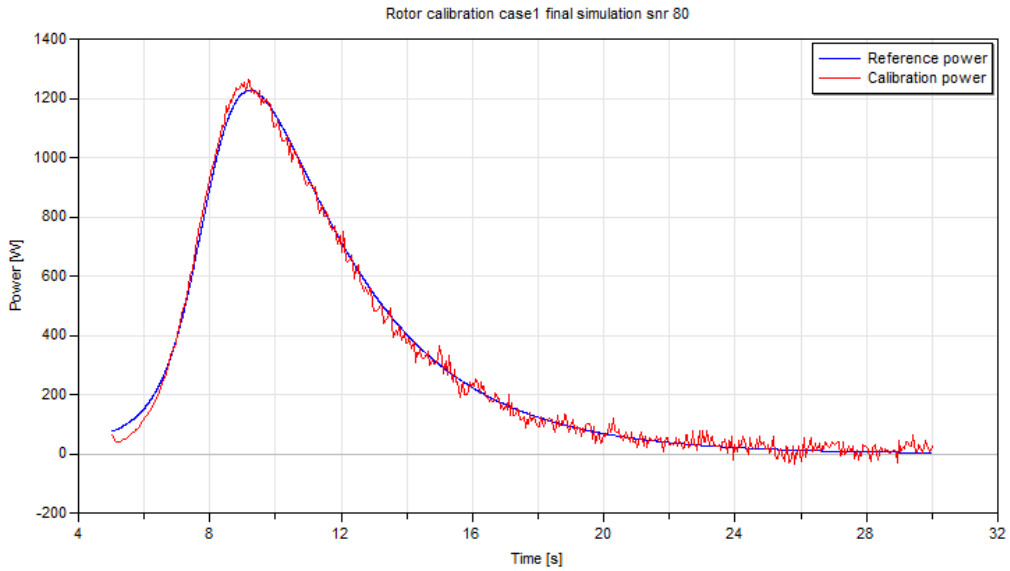

Figure A.7: Simulation of the rotor using parameters from the first calibration case and data with noise snr = 80. The blue lines are reference power from data. The red lines are power form the simulations when calibration has been done.

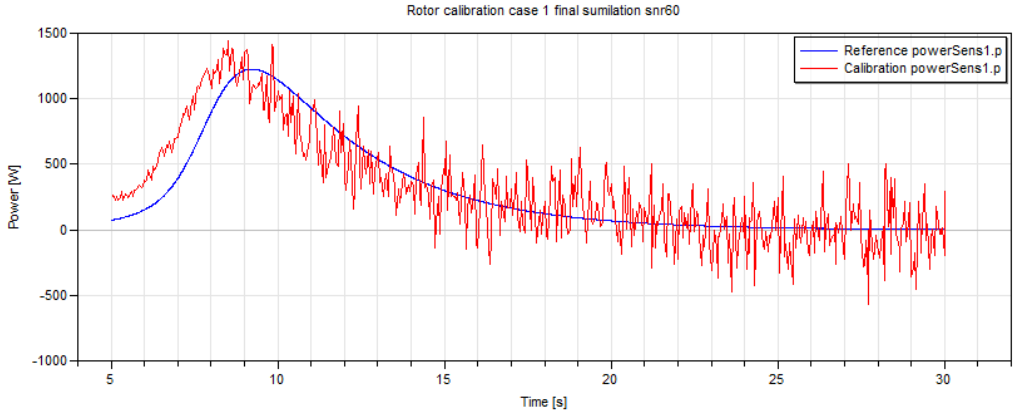

Figure A.8: Simulation of the rotor using parameters from the first calibration case and data with noise snr = 60. The blue lines are reference power from data. The red lines are power form the simulations when calibration has been done.

Final simulations from the second case

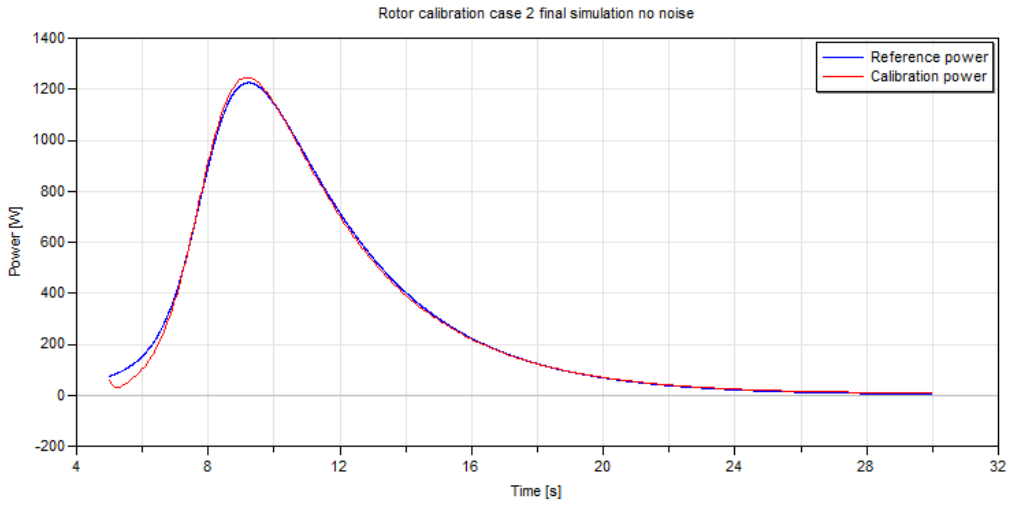

Figure A.9: Simulation of the rotor using parameters from the second calibration case and data without noise. The blue lines are reference power from data. The red lines are power form the simulations when calibration has been done.

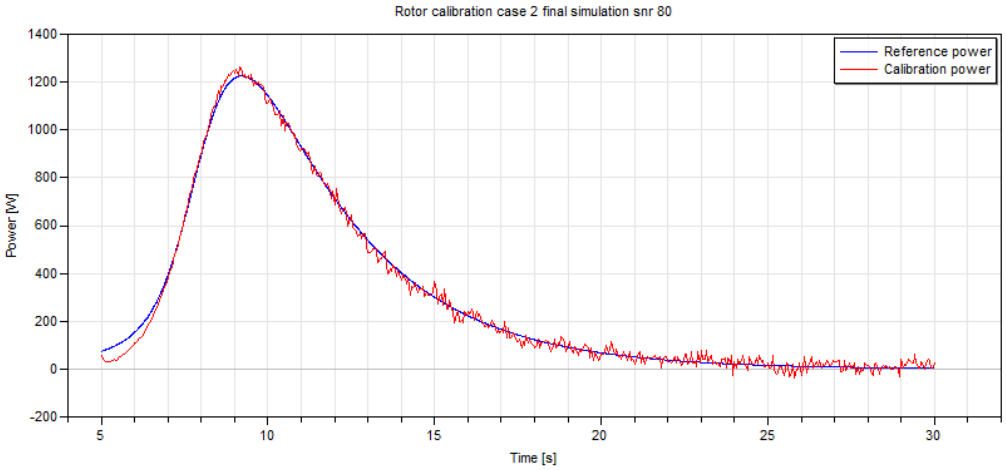

Figure A.10: Simulation of the rotor using parameters from the second calibration case and data with noise snr = 80. The blue lines are reference power from data. The red lines are power form the simulations when calibration has been done.

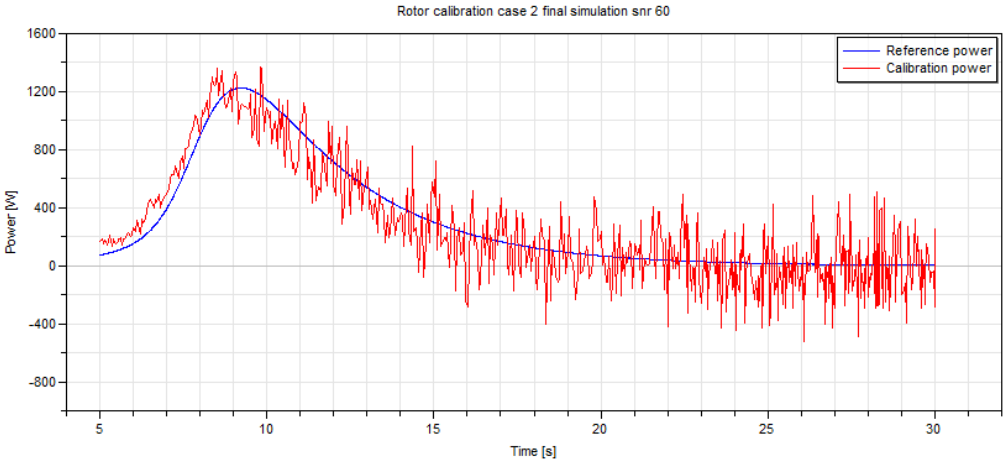

Figure A.11: Simulation of the rotor using parameters from the second calibration case and data with noise snr = 60. The blue lines are reference power from data. The red lines are power form the simulations when calibration has been done.

A.4 Generator

The plots in this section are from the simulations of the generator when a calibration has been done. The calibrations and simulations are done using data with different noise levels. The noise level associated to each simulation is to be found in the figure texts. The blue lines are reference power from data. The red lines are power form the simulations.

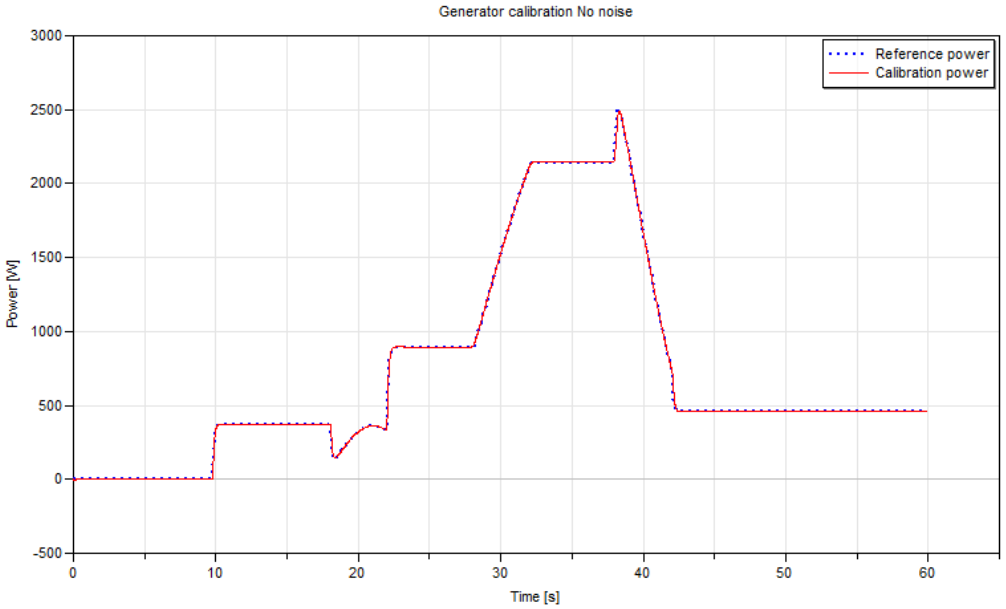

Figure A.12: Simulation of the generator test bench when the parameters have been tuned using data without noise.The blue lines are reference power from data. The red lines are power form the simulations.

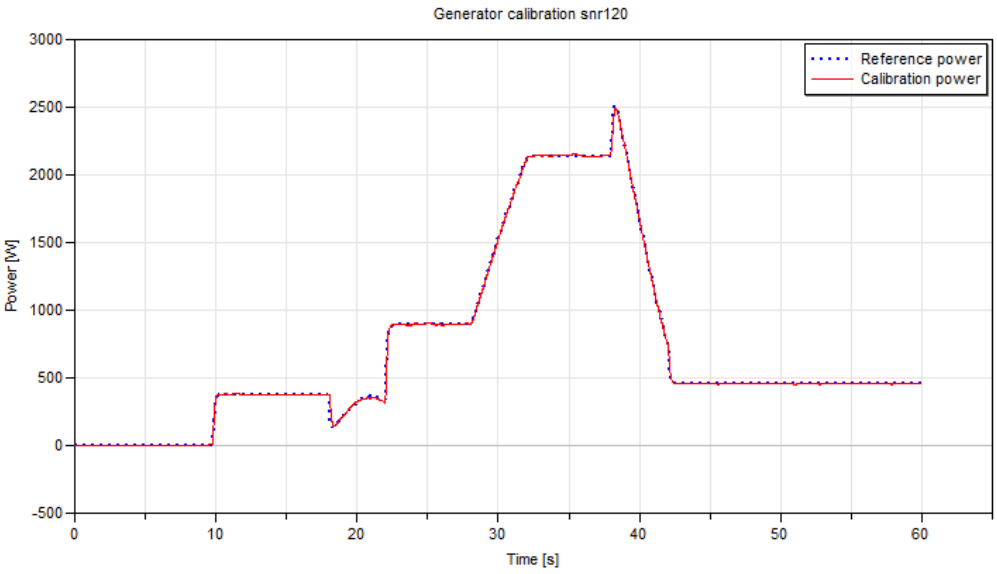

Figure A.13: Simulation of the generator test bench when the parameters have been tuned using data with snr = 120.The blue lines are reference power from data. The red lines are power form the simulations.

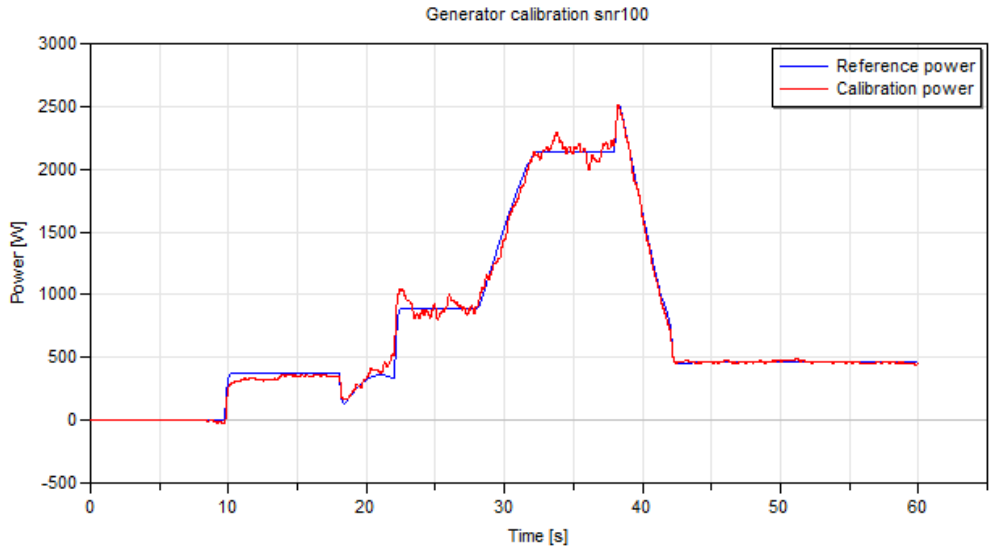

Figure A.14: Simulation of the generator test bench when the parameters have been tuned using data with snr = 100.The blue lines are reference power from data. The red lines are power form the simulations.

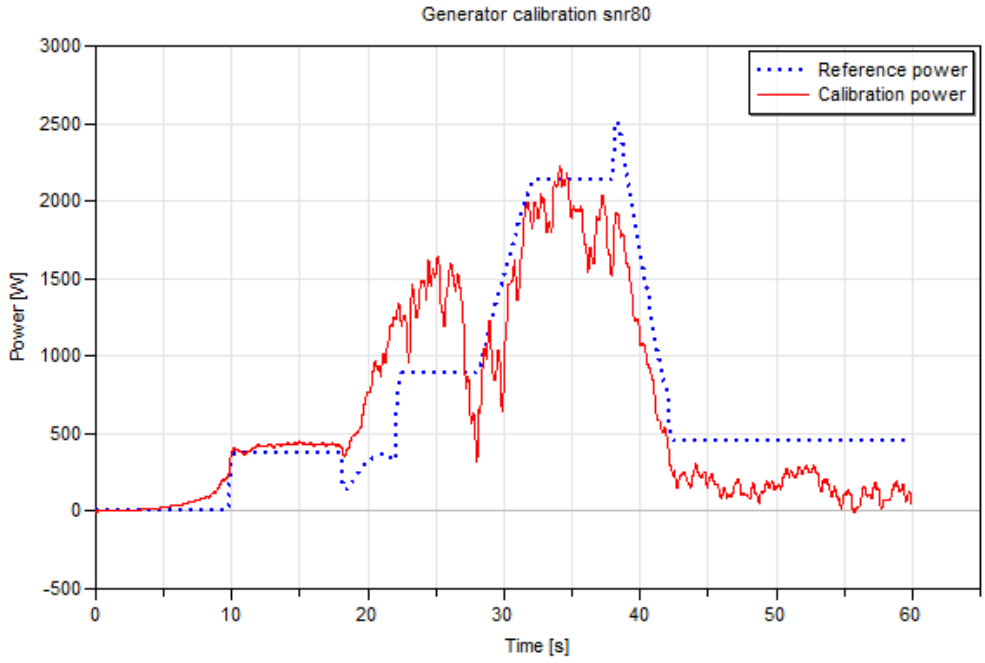

Figure A.15: Simulation of the generator test bench when the parameters have been tuned using data with snr = 80.The blue lines are reference power from data. The red lines are power form the simulations.

A.5 Converter

The plots in this section are from the simulations of the converter when a calibration has been done. The calibrations and simulations are done using data with different noise levels. The noise level associated to each simulation is to be found in the figure texts. The blue dotted lines are reference power from data. The red line with crosses is the power on the generator side form the simulation. And the red lines with circles are the power output at the grid side.

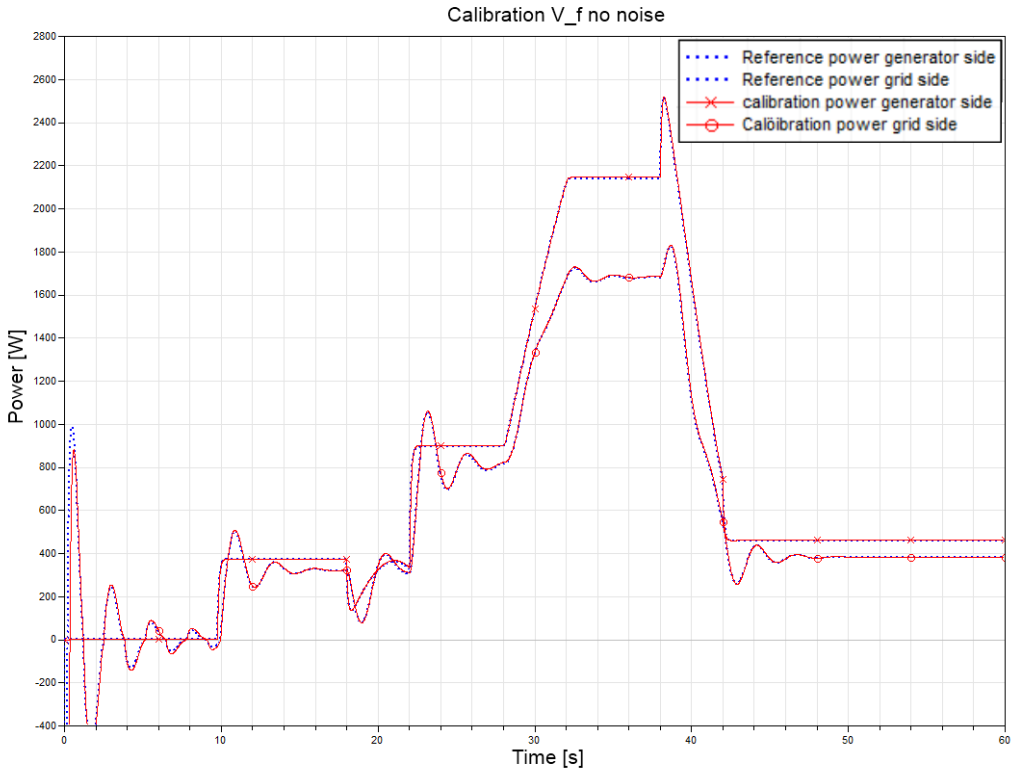

Figure A.16: Simulation from converter testbench using data with *nonoise* and the calibrated value on V_f

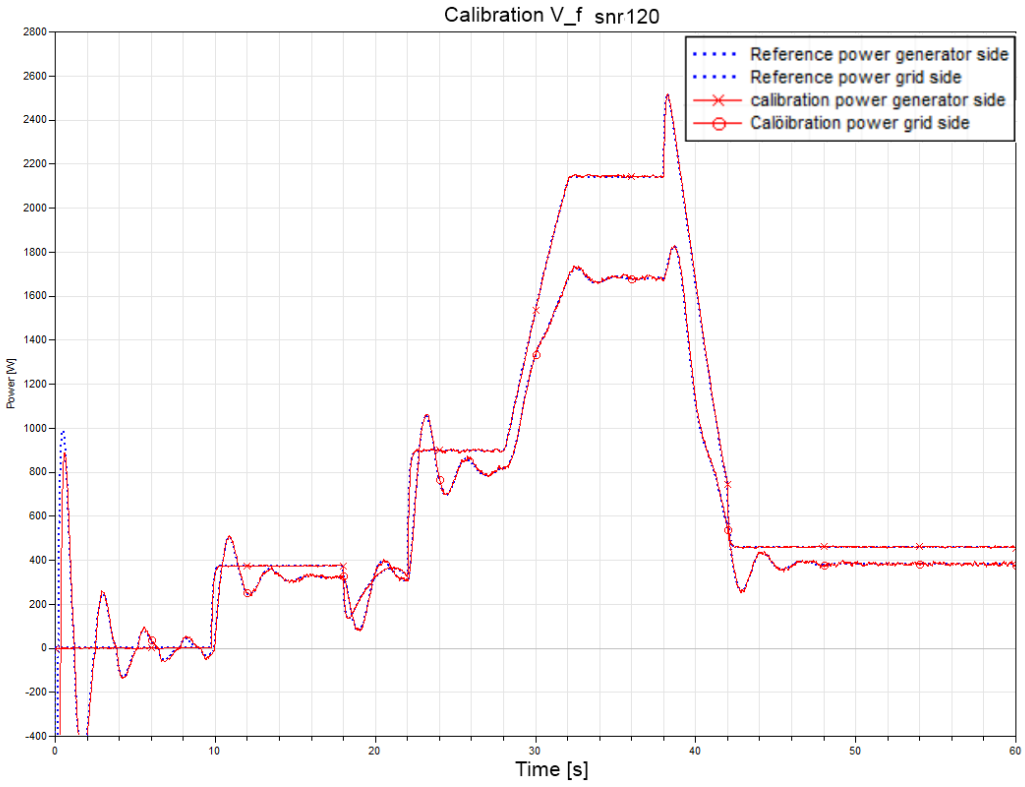

Figure A.17: Simulation from converter testbench using data with $snr120$ and the calibrated value on V_f

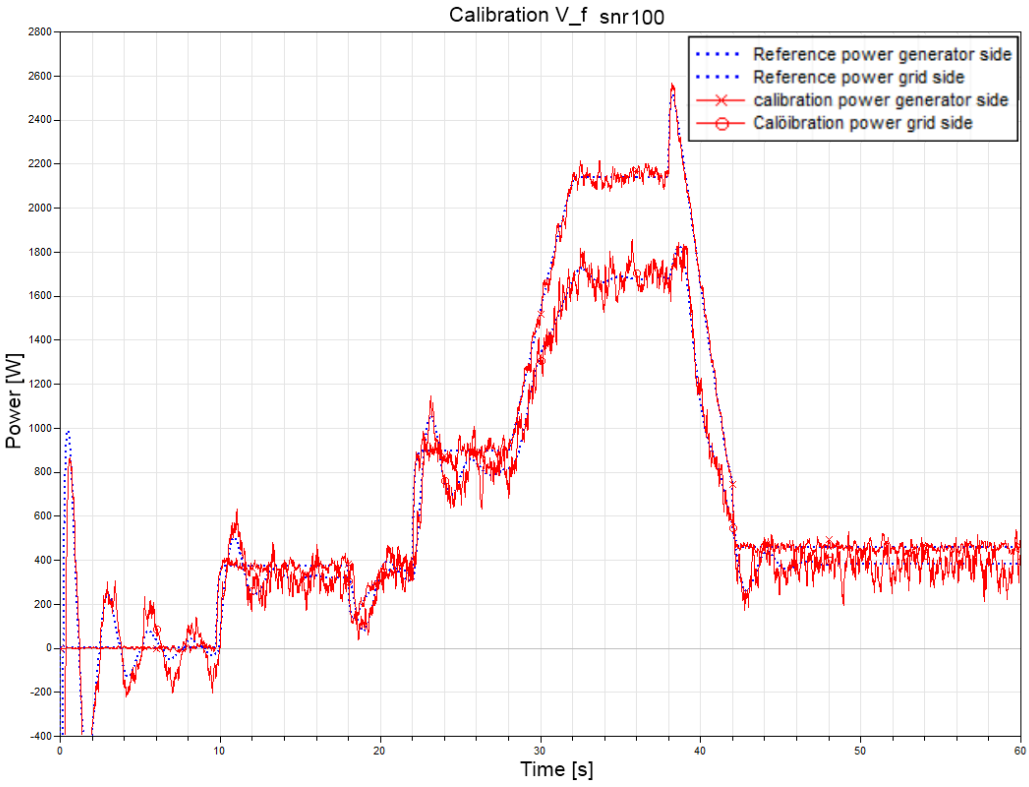

Figure A.18: Simulation from converter test bench using data with $snr100$ and the calibrated value on V_f

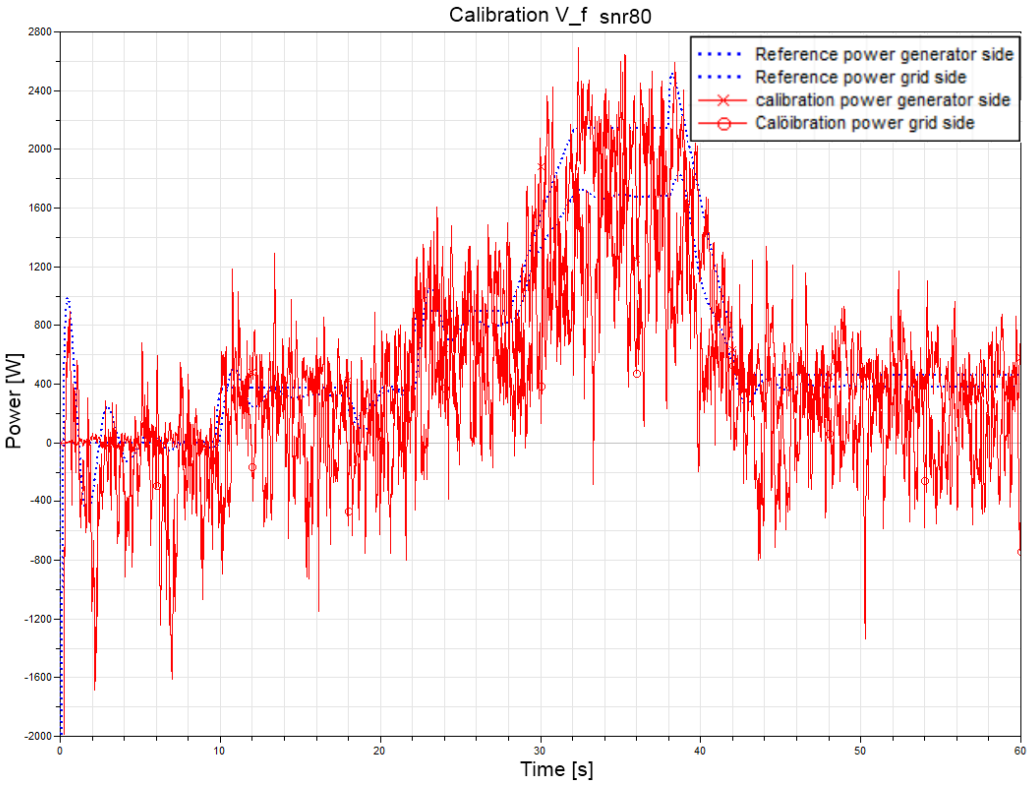

Figure A.19: Simulation from converter test bench using data with $snr80$ and the calibrated value on V_f

Appendix B

Code

B.1 Noise to data

```
close all

%Matrix "data" containing measurements have to be open in working dirr
%Measurement names has to be open in vector "names"
%First column in "data" is asumed to contain time

%Columns in data matrix substracting the time column
col=size(data,2);
rows=size(data,1);

%Adds noise to entire data matrix
noiseData=awgn(data(:,2:col),100,'measured');
noiseData= [data(:,1) noiseData];   %Removes noise from time vector

noise=noiseData-data;
data=noiseData;

%option to save as .csv
%csvwrite('Rotor_testbench_2013-01-02_noise_srn60.csv',noiseData);

%option to save as .mat version 4 needed to work in Dymola
save('Rotor_test_bench_2013-01-11_snr100','Aclass','data','names','-v4')

%Plots the data including noise against time
figure(1)
plot(noiseData(:,1), noiseData(:,2))

%plots the noise level of all measurements as function of time
figure(2)
plot(noiseData(:,1), noise);
```

B.2 Data management and Filtration

Declaration of indexes from data collection

```
Gridside
_____________________
MatL    Collection
2    0. Udc          DC-level
3    1. Udc*         Requested DC-level
```

```
4    2. ia              Real current pahse a
5    3. ib              Real current pahse b
6    4. ix              Reactive current (all phases)
7    5. iy              Active current (all phases)
8    6.  ix*            Requested current ractive, from P regulator
                  (set to zero)
9    7. iy*             Requested current active, from
                  P regulator (set in order to keep dc-level constant)
10   8. frequency          Electrical frequency
11   9.  ux*            Requested reactive voltage from regulator
12   10. uy*            Requested active voltage from regulator
13   11. ux             Reactive current towards netside
14   12. uy             Active current towards netside
15   13. theta          Theta value, the electrical angle
                  represented as a sawtooth between -1 and 1
16   14. u_alfa         Voltage in two pase representation, rotating dqo
17   15. u_beta         Voltage in two pase representation, rotating dqo
                  separated by 90 degrees
18   16. ua             Real voltage phase a
19   17. ub             Real voltage phase b
20   18. uc             Real voltage phase c
21   19. duty usx          Requested reactive voltage form regulator
22   20. duty usy          Requested active voltage form regulator
23   21. duty ualfa        Voltage in two phase system, rotating dqo
24   22. duty ubeta        Voltage in two phase system, rotating dqo
                   separated by 90 degreesr
25-27   23-25. duty a, b, c Reference signals in A, B, C
28   26. power          Active effekt, (positive towards the grid)

In the matlab file the indexes are puched up by two, one for the added
time and one because matlab starts index at one.

Generatorside
-------------------

29   0. Udc             Not active
30   1. Udc*            Not active
31   2. ia              Following as above but grid is replaced by gerator
32   3. ib
33   4. ix
34   5. iy
35   6.  ix*
36   7. iy*
37   8. frekvens
38   9.  ux*
39   10. uy*
40   11. ux
41   12. uy
42   13.  theta
43   14. u_alfa
44   15. u_beta
45   16. ua
46   17. ub
47   18. uc
48   19. duty usx
49   20. duty usy
50   21. duty ualfa
51   22. duty ubeta
52-54   23-25. duty a, b, c
55   26. power

56   Theta net calculated in matlab from MatL index 15
57   Theta grid calculated in matlab from MatL index 42
```

Matlabcode to filter collected data

```
clear all
close all
% To read the file
net = fopen('2012dec19_0837_dataloggNetside.bin','r','l');
netsideData = fread(net, [27,inf],'*double')'; % Matris med 27 kolumner och ↩
    många rader
fclose(net);
generator = fopen('2012dec19_0837_dataloggGenerator.bin','r','l');
generatorData = fread(generator, [27,inf],'*double')';
fclose(generator);
%netsideData(1:10,:);            % Läser ut första tio raderna
%plot(netsideData(:, 17:19))

%% Syncronize data sets
difference=length(netsideData)-length(generatorData)+1; %difference in ↩
    length of the data sets
netsideData=netsideData([difference:length(netsideData)],:); %Delites the ↩
    first part of the gridside data to syncronize the data set

%% Time vector

sampFreq=10000;        %sampling frequency
timeStep=1/sampFreq;
t=[0:timeStep:(length(netsideData)-1)/sampFreq]'; %Creates time vector in ↩
    secounds

%% Calculation of theta from frequency

thetaNetFreq=cumsum(netsideData(:,9)*2*pi/sampFreq); %Vector of the ↩
    electrical accumulative angle at every samplingpoint. The length of the ↩
    vector will be one shorter than the "original"
thetaGenFreq=cumsum(generatorData(:,9)*2*pi/sampFreq); %Vector of the ↩
    electrical accumulative angle at every samplingpoint. The length of the ↩
    vector will be one shorter than the "original"


 %% Calculation of theta using measured theta

D_theta_grid=diff(netsideData(:,14));            %Takes the difference to ↩
    the next theta value
D_theta_generator=diff(generatorData(:,14));      %Takes the difference to ↩
    the next theta value

for i = 1:length(D_theta_grid)

    if abs(D_theta_grid(i))>1;
    D_theta_grid(i)=0;
    end

    if abs(D_theta_generator(i))>1
    D_theta_generator(i)=0;
    end

end

thetaNetTheta=pi*[0 ; cumsum(D_theta_grid)];
thetaGenTheta=pi*[0 ; cumsum(D_theta_generator)];

thetadiffnet=thetaNetTheta-thetaNetFreq;
thetadiffgen=thetaGenTheta-thetaGenFreq;

% figure(5)
% plot(t,thetadiffgen)    %Difference between the two methods of calculating↩
     theta generator side
% figure(6)
% plot(t,thetadiffnet);   %Difference between the two methods of calculating↩
     theta generator side
```

```
%% Merging all data to one matrix

net_gen_tot=[t netsideData generatorData thetaNetTheta thetaGenTheta];

%% Selecting part of data

ps=106*sampFreq;        %First datapoint
pf=ps+5000;             %Final datapoint
dataPoints=pf-ps;       %Number of datapoints

net_gen_short=net_gen_tot(ps:pf,:); %Merges the time vector and the data ↩
    from generatorside and gridside
t_short=net_gen_short(:,1);


%% Sparce values Selects a sub set form the original data matrix e.g every ↩
    tenth value

sc=10; % Selection constant
net_gen_sparce=net_gen_tot(1:sc:end,:);
%generatorDataSparce=generatorData(1:sc:end,:);    %Selects every tenth ↩
    value from the matrix

%% Filtration of data

FilterData=sgolayfilt(net_gen_sparce,2,41); %filtration of data

%Filtfilt is used to filtrate the data on voltage since it will other ways
%loose in aplitude

h=fdesign.lowpass('Fp,Fst,Ap,Ast',0.15,0.25,1,60);
d1 = design(h,'butter');
FilterDataVoltage=filtfilt(d1.sosMatrix,d1.ScaleValues,net_gen_sparce);

%% Choose data filteted and non filtered

MixData=net_gen_sparce;

changeSGolay=[2 11 12 10 56 37 38 39 57 55]; %columns to change
MixData(:,[changeSGolay])=FilterData(:,[changeSGolay]);
changeFiltFilt=[18 19 20 45 46 47];     %Columns to exchange to filtfilt ↩
    data
MixData(:,[changeFiltFilt])=FilterDataVoltage(:,[changeFiltFilt]);

MixDataShort=MixData(1:10000,:);

%% Write to file
%csvwrite('Net_Gen_short2012-12-21-1441.csv',net_gen_short)
%csvwrite('Net_Gen_Sparce2012-12-21-1441.csv',net_gen_sparce)

%save('Converter_test_bench_2013-01-08_short_106s','net_gen_short','-v4');
%save('Converter_test_bench_2013-01-08_sparce','net_gen_sparce','-v4');
save('Converter_test_bench_2013-01-09↩
    _sparce_SelectedVariables_Filtered_short', 'MixDataShort', '-v4');

%% Matlab version of V_nom För att jämföra mot Dymola

% v_a=netsideData(:,17);
% v_b=netsideData(:,18);
% v_c=netsideData(:,19);
%
% V_abc=[v_a v_b v_c];
%
% V_nom=sqrt(V_abc.^2);
% %figure(1)
% %plot(t,V_nom)
t_sparce=net_gen_sparce(:,1);
```

Appendix C

Data

The figures below show the most important input and output values. The bottom plots are a selection of the complete sets. The middle plots are sparse sets where every tenth data point of the original data is used. The top plots are sets where the chosen points have been filtered.

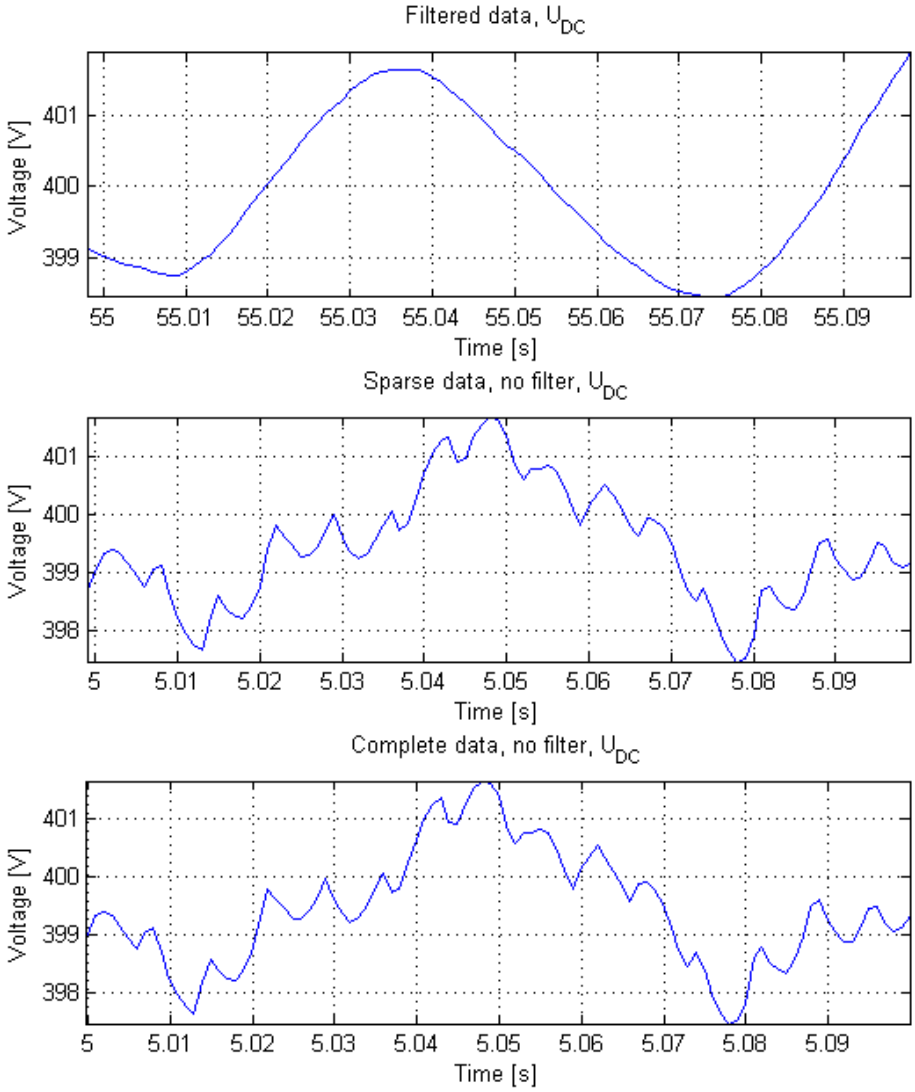

Figure C.1: Selection of voltage data from the DC-link, filtered, sparse and complete

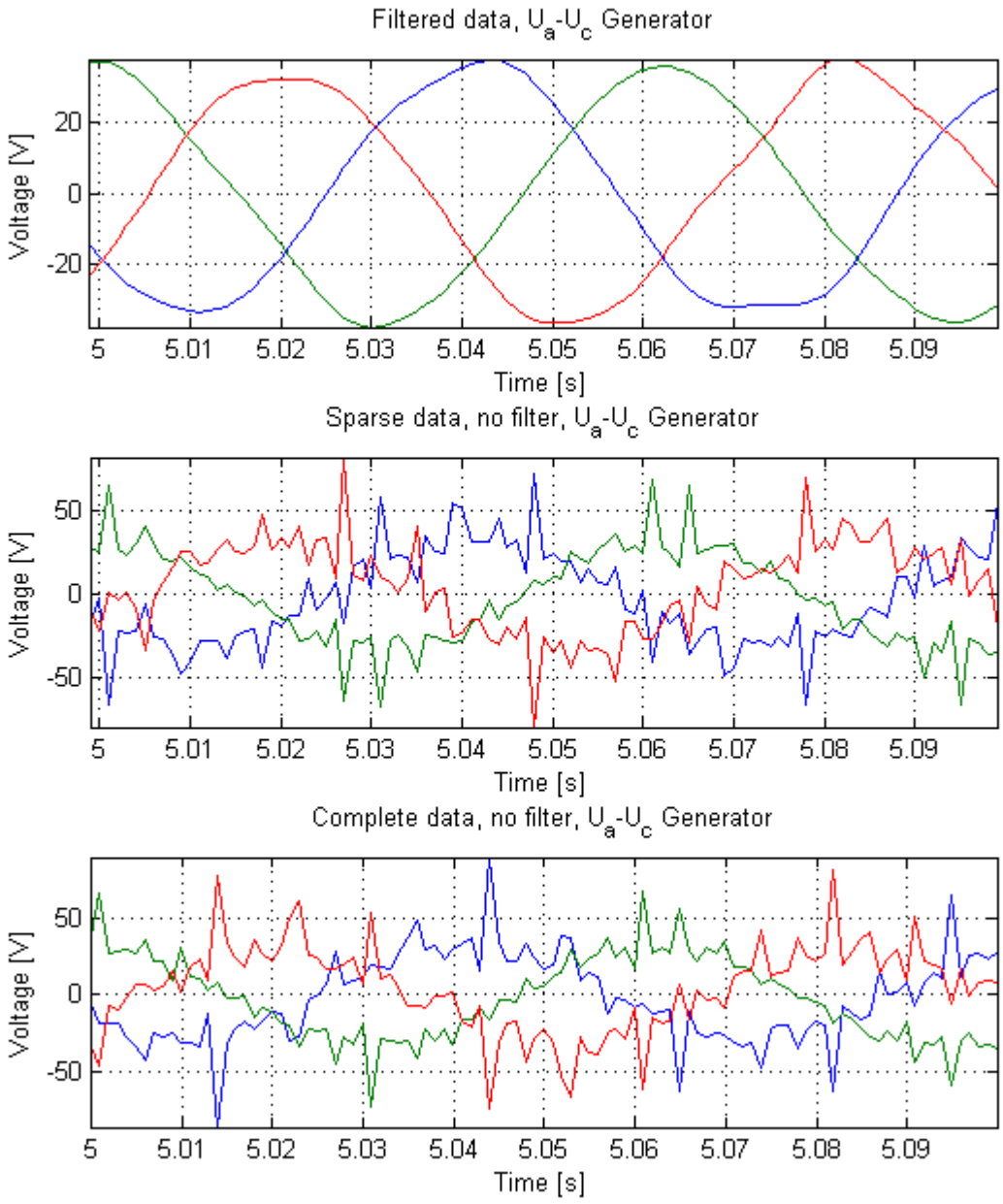

Figure C.2: Selection of voltage data from generator side of the converter, filtered, sparse and complete

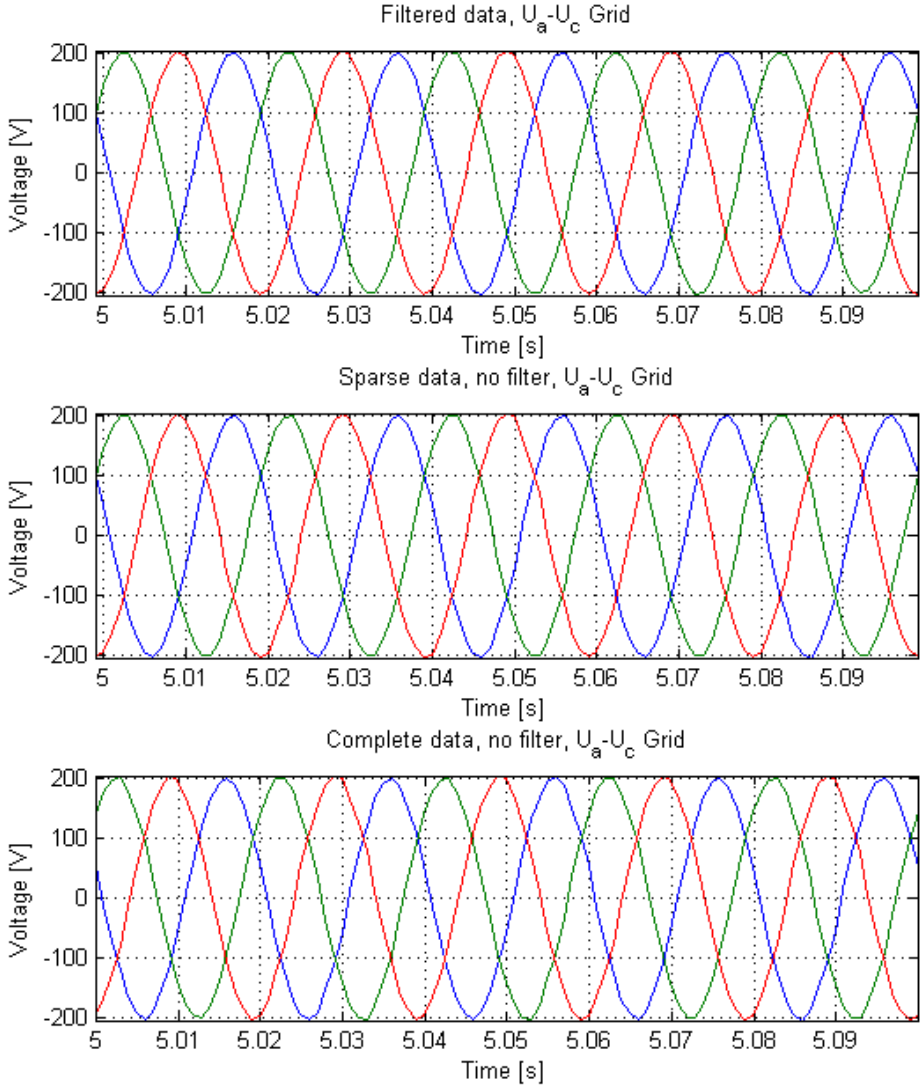

Figure C.3: Selection of voltage data from grid side of the converter, filtered, sparse and complete

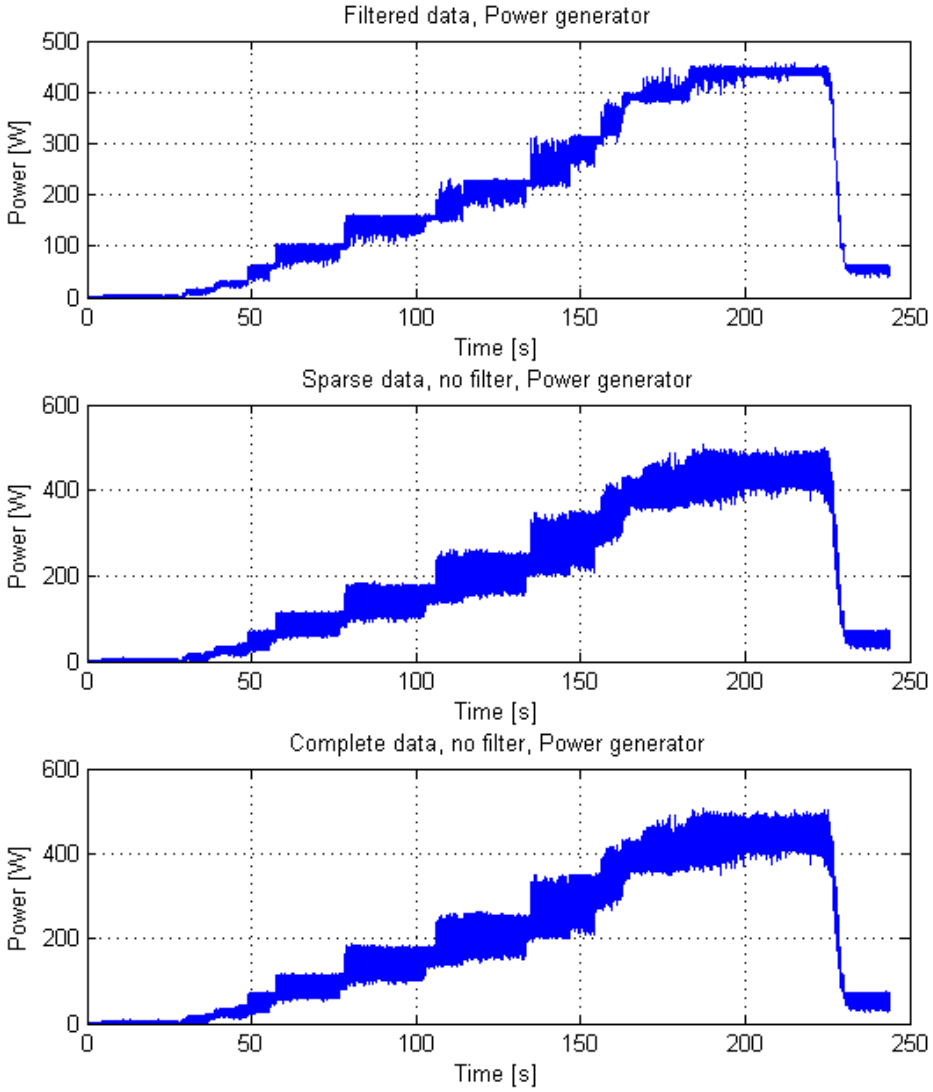

Figure C.4: Selection of power data from generator side of the converter, filtered, sparse and complete

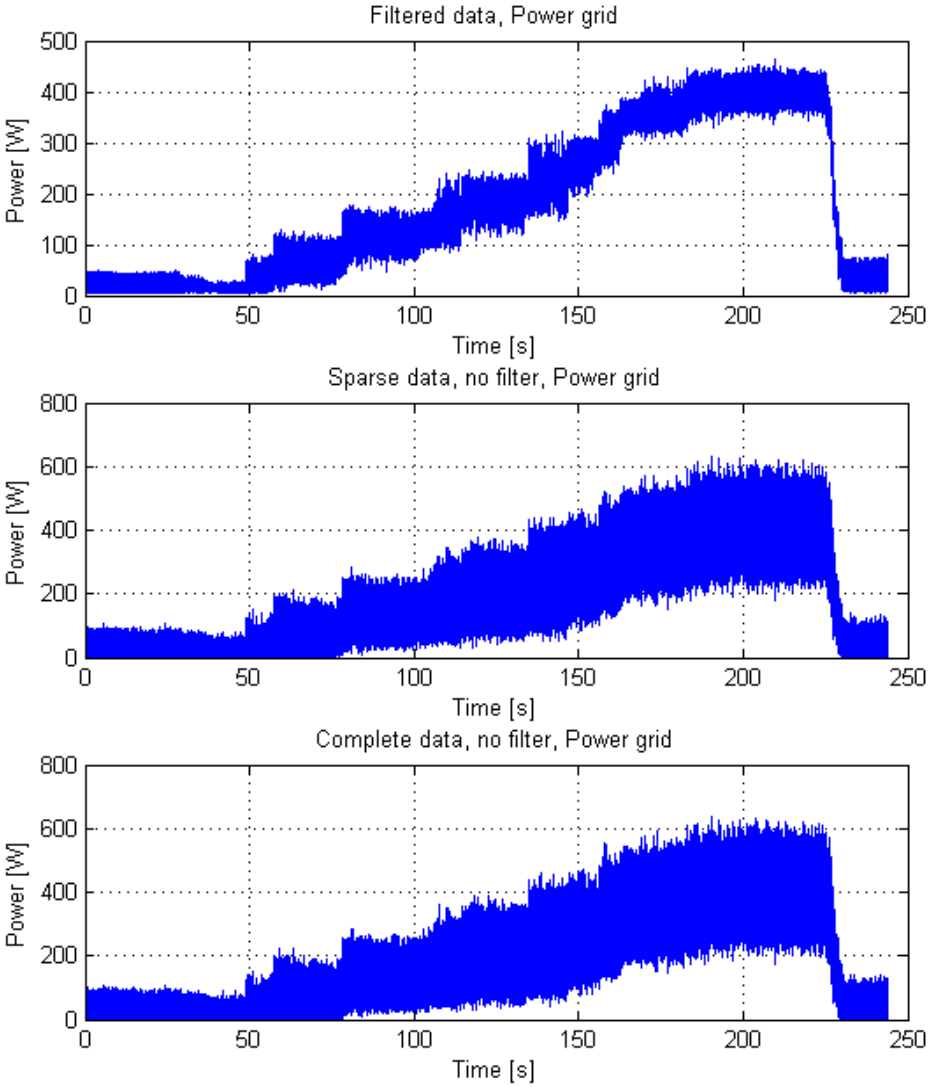

Figure C.5: Selection of power data from grid side of the converter, filtered, sparse and complete

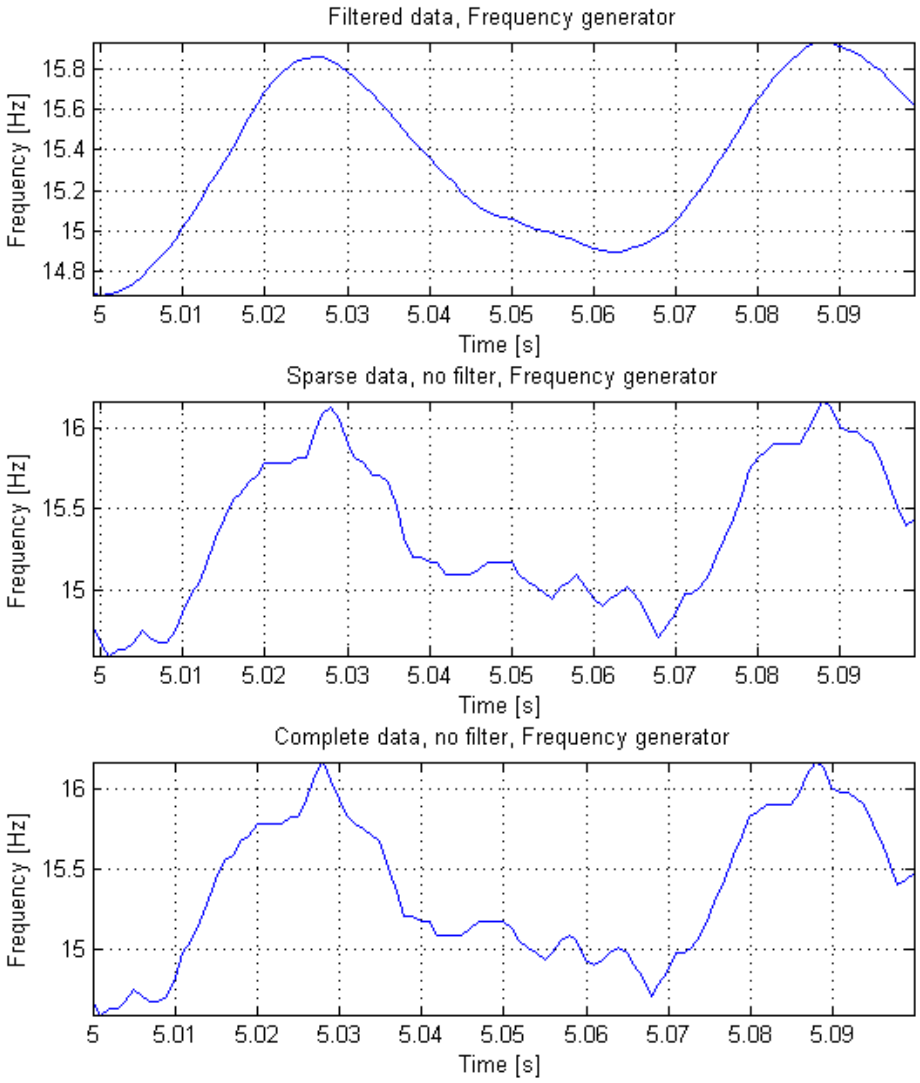

Figure C.6: Selection of frequency data from generator side of the converter, filtered, sparse and complete

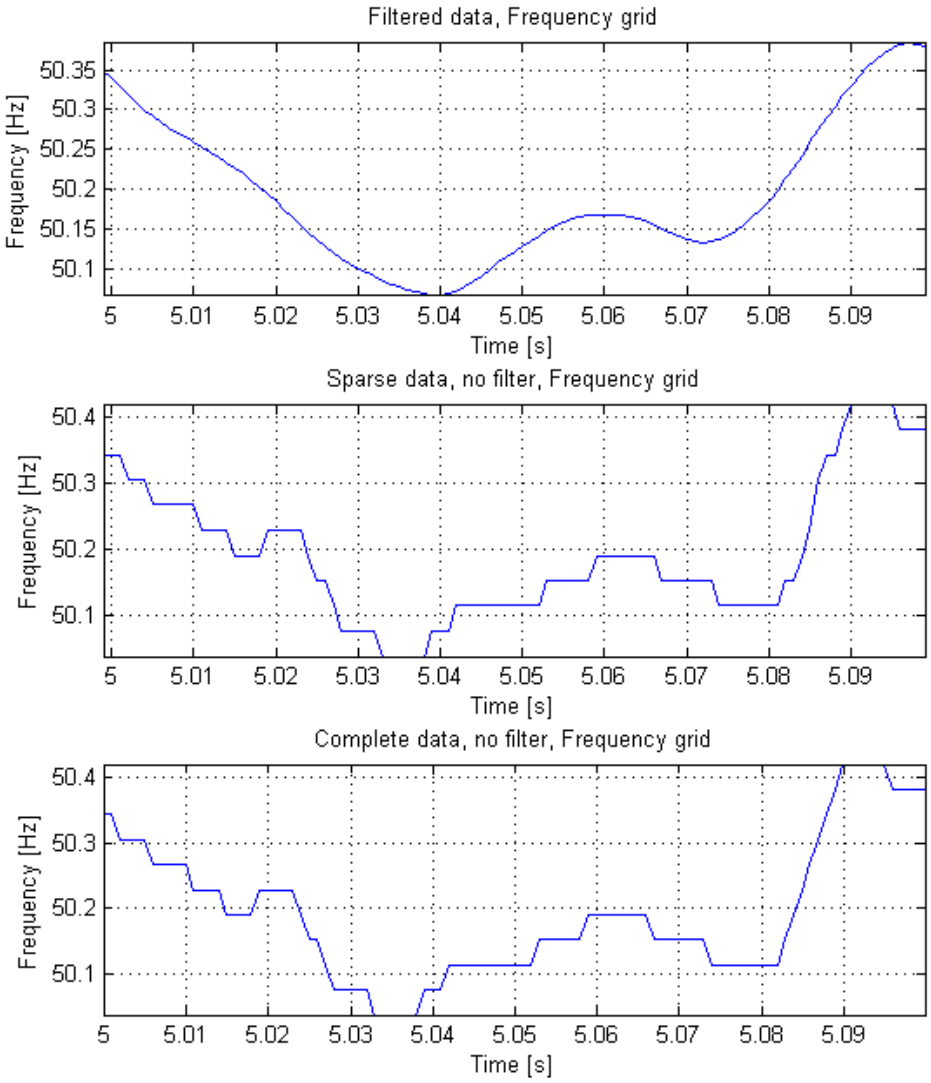

Figure C.7: Selection of frequency data from grid side of the converter, filtered, sparse and complete